ABSTRACT

Title of Dissertation: THE RIBOSOME AND BEYOND: UNDERSTANDING THE ROLE OF TRANSLATIONAL FIDELITY IN RARE GENETIC DISORDERS

Alexandra Olson, Doctor of Philosophy, 2022

Dissertation directed by: Professor and Chair, Dr. Jonathan D. Dinman, Department of Cellular Biology and Molecular Genetics

With the increasing accessibility of patient genome sequencing, causative mutations for rare genetic diseases are being uncovered at an unprecedented rate. Among these are disorders resulting from mutations in protein synthesis machinery, including the ribosome and translation factors. Originally described in 1999, the accumulation of new information brings new questions regarding their tissue-specific and otherwise paradoxical nature. Described here are investigations into two classes of genetic disorders, describing several novel diseases that illustrate the commonalities and differences between their classes. Specifically, two variants of *RPL9* are shown to cause disparate clinical presentations despite both causing pre-rRNA processing defects, including Diamond Blackfan anemia (DBA) from a 5'UTR variant and

multiple cancer incidences from a missense mutation. The 5'UTR variant is shown to result in haploinsufficiency and p53 activation, while the missense variant impairs translational fidelity because of defective stop codon recognition. Additionally, evidence is presented that correlates several *de novo* missense mutations in *EEF2* to neurodevelopmental disorders, building on research connecting eEF2 dysfunction to neurological disease. These mutations are shown to also cause translational fidelity loss and implicate eEF2-ribosome interactions in reading frame maintenance. All of the disease-causing mutants of eEF2 were found to map to sites of interaction with critical features of ribosomal RNA. These eEF2 sites of ribosome contact were further investigated using a panel of rationally designed mutations intended to probe the relationships between biophysical interactions of eEF2 and the ribosome, and biological function. These mutants exhibited translational fidelity defects and were demonstrated to have lower catalytic activity *in vitro*. Overall, this work highlights salient points about ribosomopathies and translationopathies, their molecular mechanisms, and the relevance of translational fidelity to human health.

THE RIBOSOME AND BEYOND: UNDERSTANDING THE ROLE OF TRANSLATIONAL FIDELITY IN RARE GENETIC DISORDERS

by

Alexandra Olson

Dissertation submitted to the Faculty of the Graduate School of the
University of Maryland, College Park, in partial fulfillment
of the requirements for the degree of
Doctor of Philosophy
2022

Advisory Committee:
Professor Jonathan D. Dinman, Co-chair
Professor Douglas Julin, Co-chair
Professor Kwaku Dayie
Assistant Professor Nicole LaRonde
Professor Leslie Pick, Dean's Representative

Foreword

This thesis includes works that were previously published in Nucleic Acids Research and Human Molecular Genetics. These articles were published in collaboration with clinicians and other researchers; therefore, authorship of the experimental research has been indicated in figure legends where appropriate. I confirm that, as an author on both, I made substantial and relevant contributions to these jointly authored works.

Dedication

This work is dedicated to my (roommate's) cat, Sox. Thank you for sticking around long enough (21 years and counting!) so that we could be friends and for choosing to spend your golden years with me. I couldn't imagine a better writing companion and sentient alarm clock.

Acknowledgements

I would like to thank my advisor Dr. Jonathan Dinman for his support and guidance during my time here. Thank you for seeing something in me back in my first year and giving me room to learn and grow in all the years since. Thank you for your patience and encouragement, I couldn't have done this without the support you've provided.

To my committee members, Dr. Douglas Julin, Dr. Kwaku Dayie, Dr. Nicole LaRonde, and Dr. Leslie Pick, thank you for being here throughout this process and giving me helpful feedback and advice. I have greatly appreciated your expert perspectives during this endeavor.

I would also like to thank the current and former members of the Dinman lab, especially Dr. Carol Vieira and Dr. Jamie Kelly for the invaluable emotional (and technical!) support you have given me. Also, to the undergraduate students I have had the pleasure of mentoring, including Lexie Schneider, Tanya Ghosh, and Serena Song, this work would have been impossible without your contributions and thank you for giving me the opportunity to pass on what I have learned.

I am indebted to Dr. Jiaqiang Ling and Dr. Zhihui Lyu, as well as Dr. Jason Kahn and Ian Ferencz for kindly allowing me to use their facilities and being accommodating and helpful. Many of the experiments here would not have been possible without your assistance.

Lastly, I would be remiss to not thank my friends and family for their encouragement and understanding, even when my voicemail inbox was full and I didn't unload the dishwasher.

Table of Contents

List of Tables

List of Figures

List of Abbreviations

5-FOA	5-fluoroorotic acid
5'UTR	5' untranslated region
aaRS	Aminoacyl-tRNA synthetase
ABCE1	ATP-binding cassette sub-family E member 1
ADP	Adenosine diphosphate
AML	Acute myeloid leukemia
ANOVA	Analysis of variance
ATP	Adenosine triphosphate
CD	Circular dichroism
cDNA	Complementary DNA
CNS	Central nervous system
DBA	Diamond Blackfan Anemia
DC	Decoding center
DMSO	Dimethylsulfoxide
DNA	Deoxyribonucleic acid
Dpf	Days post fertilization
DTT	Dithiothreitol
EBV	Epstein-Barr virus
EDTA	Ethylenediaminetetraacetic acid
eEF	Eukaryotic elongation factor
EF-G	Elongation factor G
EF-Tu	Elongation factor thermo unstable
eIF	Eukaryotic initation factor
ER	Endoplasmic reticulum
eRF	Eukaryotic release factor
ETS	External transcribed spacer
FACS	Fluorescence-activated cell sorting
FC	Fold change
FPLC	Fast protein liquid chromatography
GAC	GTPase-associated center

GDP	Guanosine diphosphate
GTP	Guanosine triphosphate
HSR	Heat shock response
ISR	Integrated stress response
ITS	Internal transcribed spacer
LCL	Lymphoblastoid cell line
LSU	Large subunit
mRNA	Messenger RNA
NDD	Neurodevelopmental disorder
NGD	No-go decay
NMD	Nonsense mediated decay
NSD	Nonstop decay
PAGE	Polyacrylamide gel electrophoresis
PCR	Polymerase chain reaction
Pi	Inorganic phosphate
PRF	Programmed ribosomal frameshifting
PTC	Peptidyl transferase center
qPRF	Quantitative PCR
RNA	ribonucleic acid
RP	Ribosomal protein
rRNA	Ribosomal RNA
SCA26	Spinocerebellar ataxia 26
siRNA	Silencing RNA
SRL	Sarcin-ricin loop
SSU	Small subunit
T-ALL	T-cell acute lymphoblastic leukemia
TCR	Termination codon readthrough
TP53	Tumor protein p53
tRNA	Transfer RNA
UPR	Unfolded protein response
VUS	Variant of unknown significance
WT	Wild-type

Chapter 1: Introduction

Translation

Synthesizing new proteins is central to cellular life; from single-celled bacteria to vertebrate animals, all organisms produce and reproduce thanks to the ability to translate information contained in their genetic codes into new proteins. This process, called 'protein synthesis' or 'translation', represents the final step of the "sequence hypothesis" of molecular biology: DNA is transcribed into RNA, which is translated into protein. Therefore, translation sits at the nexus of biological information flow and is life's way of following the instructions set forth in its genetic code. Underscoring the central relevance of translation is the conservation of components of the translational apparatus encoded by the genes shared by all living systems. Of the <100 genes that unite the biological world, more than half are genes that encode ribosomal proteins, translation factors, and other auxiliary components[1,2]. Furthermore, it has been shown that, at a minimum, cells devote between 20-50% of energy resources on translation alone and up to 60-80% in rapidly dividing cells[3,4]. As such, it is a tightly regulated process that serves as one of the pivotal steps of gene expression.

The ribosome

The central actor of translation is the ribosome, a complex molecular machine that consists of ribosomal RNA (rRNA) and proteins (RPs) that acts to decode messenger RNAs (mRNA) and synthesize the corresponding polypeptides. All ribosomes contain a large subunit (LSU) and a small subunit (SSU) that associate together during protein synthesis. In prokaryotic ribosomes, the LSU is composed of two rRNA molecules and 33 RPs while the SSU has a one

rRNA molecule and 21 RPs[5]. Eukaryotic ribosomes are larger and more complex than their bacterial counterparts. The LSU of the eukaryotic ribosome contains three rRNAs and 46 RPs while its SSU has one rRNA molecule and 33 RPs[5]. In addition to the increase of RPs, the rRNA of eukaryotic ribosomes contain expansion segments, which are nucleotide insertions on the periphery of the prokaryotic rRNA[6].

Ribosomes from all kingdoms of life have a conserved core that houses the main functional centers (**Figure 1**)[7]. Within the ribosome are three transfer RNA (tRNA) binding sites: the Amino-acyl (A) site, the Peptidyl (P) site, and the Exit (E) site, each named for the type of tRNA bound within these sites during translation. It also contains functional centers for catalysis of peptidyl transfer (peptidyltransferase center), recognizing mRNA-tRNA base pairing (decoding center), and activation of *trans*-acting translational GTPase factors (GTPase associated center)[8]. Unlike the majority of proteinaceous cellular machinery, each of these functional sites were found to be comprised of rRNA rather than protein[9,10]. Conversely, within the ribosome RPs tend to have auxiliary roles, acting as scaffolding for rRNA and stabilizing ribosome structure[11,12]. Additionally, RPs are vital for ribosome biogenesis where they are involved in rRNA processing, stabilizing rRNA secondary structure, pre-ribosome transport, and recruitment of ribosome biogenesis factors[13]. They can also have secondary roles outside the ribosome in cell cycle regulation, cell signaling, and DNA repair[14].

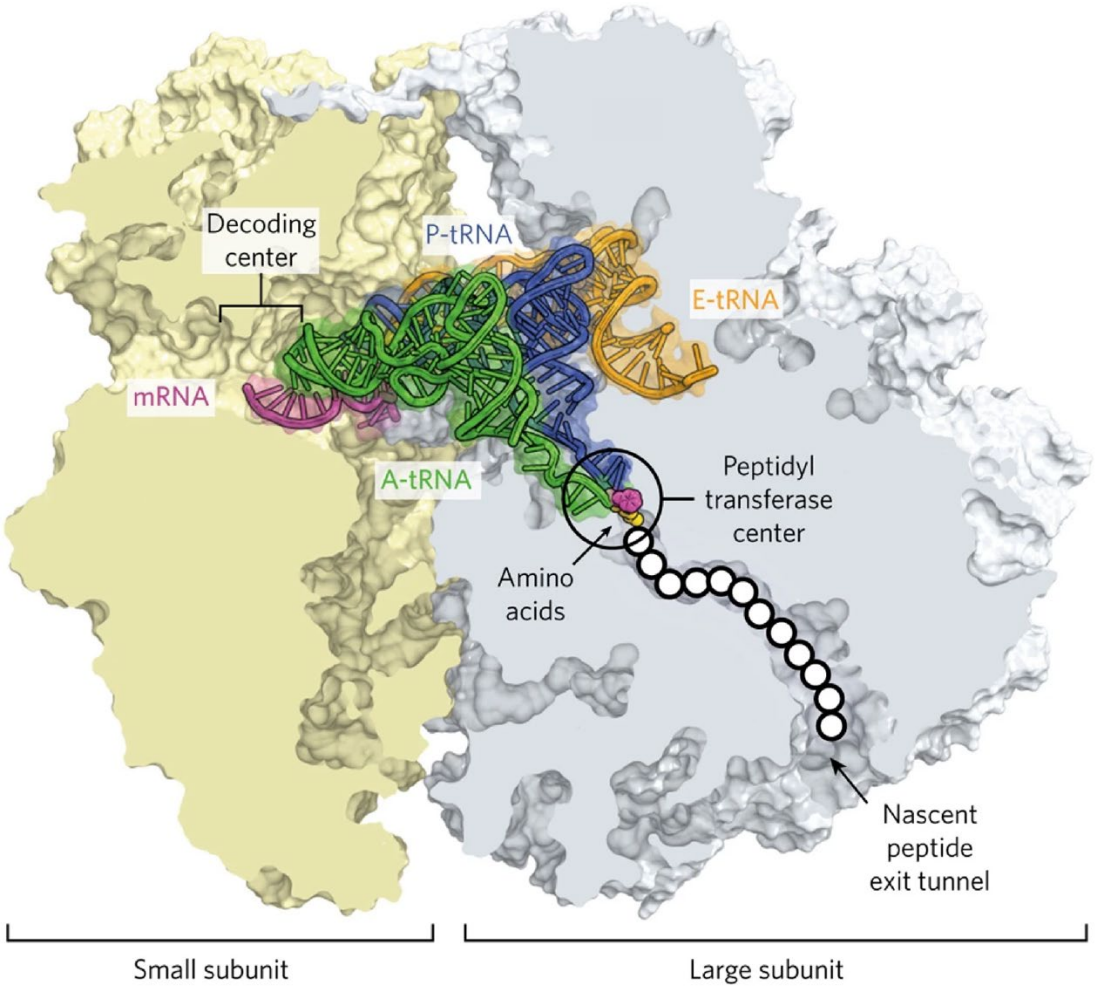

Figure 1: The functional centers of the ribosome

The large subunit is shown in grey and the small subunit in yellow. The decoding center of the small subunit and the peptidyl transferase center of the large subunit are highlighted. Also shown are the mRNA and peptide tunnels as well as the A, P, and E site tRNAs in their corresponding binding sites. Image adapted from[15].

Stages of translation

The process of synthesizing proteins from mRNA follows three stages: initiation, elongation, and termination (**Figure 2**). In eukaryotes, initiation begins with formation of the 43S preinitiation complex where the eIF2 ternary complex delivers the initiator Met-tRNA^{Met} to the SSU in complex with eIF3 and eIF5[16]. The preinitiation complex is recruited to the mRNA by the eIF4F complex whereupon the SSU and associated factors scans the mRNA in the 5' to 3'

direction until it encounters a start codon which base pairs with the intiator tRNA anti-codon[17]. The LSU is then recruited and displaces the initiation factors on the SSU to form the 80S ribosome[16]. The ribosome then enters the elongation phase where it decodes the mRNA one codon at a time and synthesizes amide bonds between their cognate amino acids (**Figure 2B**). Termination begins with recognition of a stop codon in the A site. Here, the eRF1-eRF3 ternary complex binds to the ribosome where it catalyzes the release of the nascent polypeptide from the peptidyl-tRNA in the P site (**Figure 2C**)[18,19]. Finally, during ribosome release/recycling, the ribosomal subunits are split from one another by ABCE1 and the deacylated tRNA and mRNA bound to the SSU are released, allowing the free subunits to then participate in another round of translation[19].

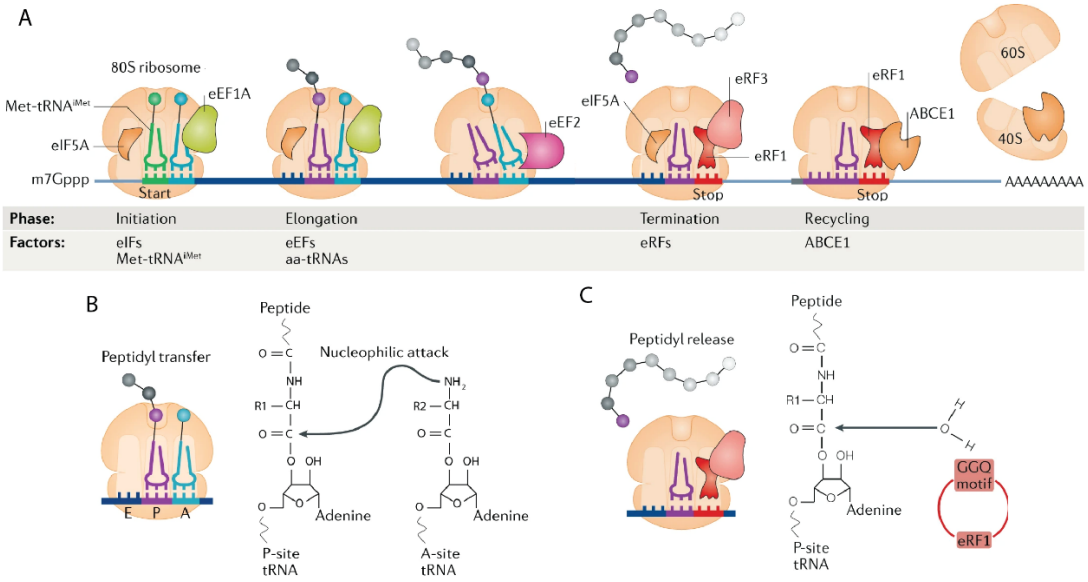

Figure 2: The steps of translation

A) Translation begins with initiation where the 80S ribosome is ultimately assembled by eIFs at start codon. Elongation consists of iteratively adding corresponding amino acids to the growing peptide chain, facilitated by elongation factors eEF1A and eEF2. Termination is initiated by the presence of a stop codon in the A site, where eRFs release the nascent polypeptide. Finally, ribosome recycling occurs via the help of ABCE1 to release the subunits and allow them to begin a new cycle of translation. B) The peptidyl transfer reaction. C) Peptidyl release hydrolysis. Image adapted from[20].

Elongation

The research described in this document occurs during the elongation stage of translation. Thus, this step merits deeper examination. Elongation encompasses the bulk of time and energy expended during protein synthesis and proceeds through a cycle of its own (**Figure 3**): iteratively decoding the mRNA, adding a new amino acid to the nascent peptide, and advancing on to the next codon.

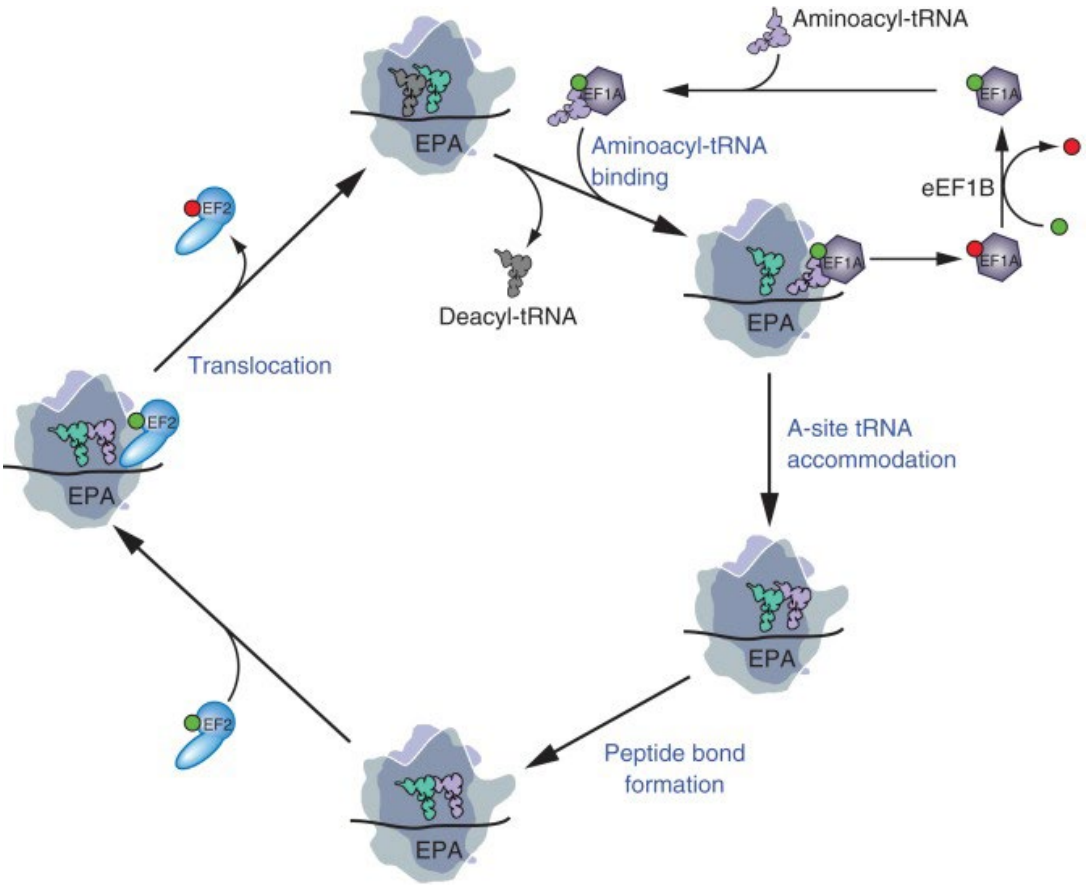

Figure 3: Translation elongation cycle in eukaryotes

The eEF1A ternary complex delivers aa-tRNA to the A site of the ribosome. Green circles represent GTP and red circles represent GDP. Upon GTP hydrolysis, eEF1A is released and the aa-tRNA is accommodated into the A site. Then, the ribosome catalyzes transfer of the nascent chain to the A-site tRNA, forming a new peptide bond and lengthening the growing polypeptide. eEF2 then binds to the ribosome and catalyzes translocation by GTP hydrolysis, moving the tRNA from the A and P sites to the P and E sites, respectively. The E-site tRNA then exits the ribosome and a new round of elongation begins. Image from[21].

tRNA accommodation

The first step in the cycle of elongation is the recruitment of the aminoacyl-tRNA (aa-tRNA) containing the anticodon of the mRNA situated in the A site. This cognate aa-tRNA is delivered to the ribosome by eukaryotic elongation factor 1A (eEF1A), the homolog of the bacterial EF-Tu. eEF1A is a GTPase which, by hydrolyzing GTP to GDP, expends energy to dissociate from the ribosome and tRNA once the anticodon of the tRNA has formed canonical base pairing interactions with the mRNA codon. This GTP hydrolysis is activated by the ribosome, which recognizes the Watson-Crick geometry of the first two nucleotides of the codon-anticodon interaction via the decoding center of the SSU[22,23]. Conformational changes then transmit this information to the GTPase activating center (GAC), inducing eEF1 dissociation and accommodation of the tRNA into the A site[24].

Peptide bond formation

Upon accommodation into the A site, the aminoacyl end of the tRNA is positioned in the peptidyl-transferase center (PTC) of the LSU. Here, a bond is created between the amino acid in the A site and the elongating peptide of the peptidyl-tRNA in the P site. Specifically, the amino group of the A site amino acid attacks the carbonyl carbon of the ester bond linking the peptide to the P site tRNA (**Figure 2B**)[25]. This forms a tetrahedral intermediate that decomposes by severing the ester linkage between the peptide and its tRNA, yielding the reaction products of a deacylated tRNA in the P site and an amide bond between the peptide and the new amino acid, functionally adding to the length of the nascent chain. This is an enthalpically favorable reaction which, when not catalyzed, occurs at a rate of 10^{-4} $M^{-1}s^{-1}$. However, the ribosome is able to catalytically accelerate the reaction 10^6-10^7 fold largely due to the precise positioning of the substrates, thereby lowering the entropic barrier[26].

eEF2 binding

The ribosome must then shift the tRNA from the P and A sites to the E and P sites, respectively, in order to position the next codon in the A site to accept its cognate tRNA. This "translocation" step is catalyzed by eEF2, the homolog to the prokaryotic EF-G. While the ribosome is able to translocate without catalysis, it is extremely slow and the presence of eEF2 increases the rate by 10^4-fold[27]. eEF2 (**Figure 4B**) is an 858 amino acid protein that is highly conserved among eukaryotes, with 66% sequence identity between the yeast and human homologs. It is divided into 5 structural domains, including the G-domain which is responsible for GTP binding and hydrolysis and Domain IV which acts as a molecular mimic of the anti-codon loop of tRNA to facilitate accommodation in the A site of the ribosome[28] (**Figure 4A**). eEF2 can be inactivated by phosphorylation of Thr-57 by the regulatory factor eEF2 kinase[29] (eEF2K) and also bears a unique diphthamide modification on residue His-715, which is the target for ADP-ribosylation by diphtheria toxin[30].

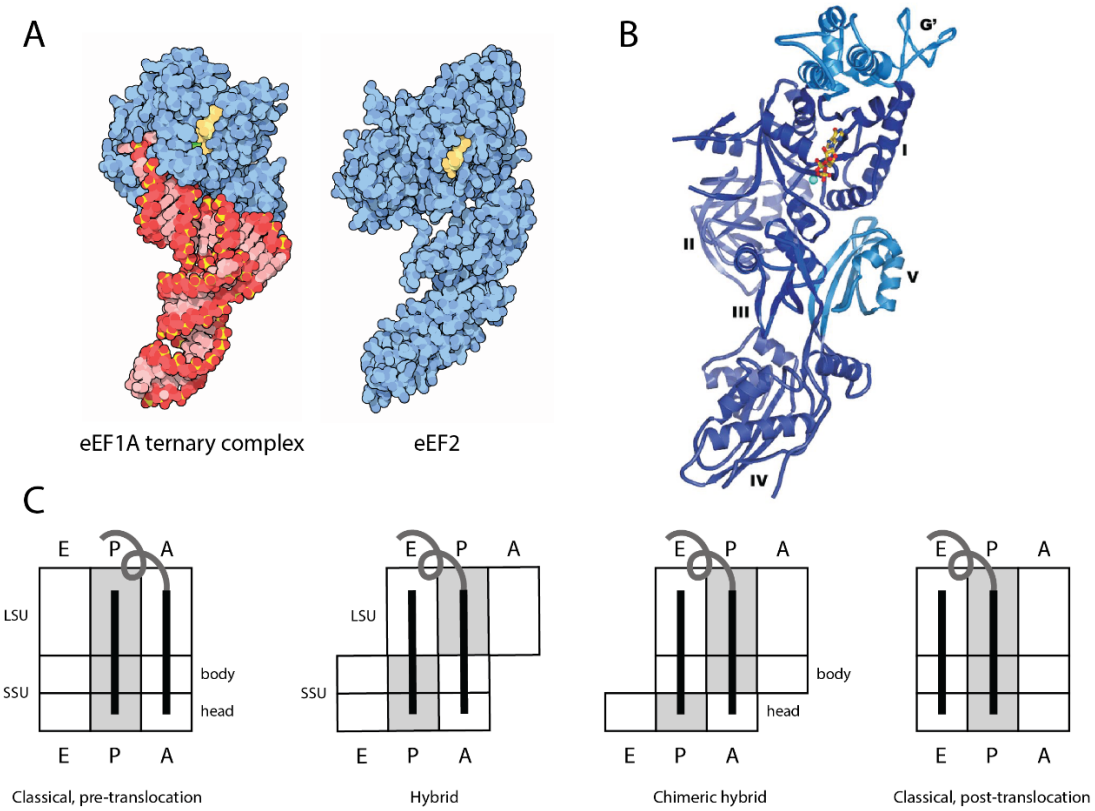

Figure 4: eEF2 and translocation

A) Molecular mimicry of eEF2 shown by structural comparison of the eEF1A ternary complex and eEF2. Image adapted from[31]. B) Crystal structure of eEF2 with domains labeled. Image from[32]. C) tRNA positions on the ribosome during translocation. Image adapted from[33].

Translocation

The first step in translocation occurs prior to eEF2 binding. It occurs immediately after peptidyltransfer, when the acceptor end of the tRNAs on the LSU shift to the E- and P-sites while the anticodon loops remain hybridized to the mRNA in the SSU P- and A-sites respectively[34]. The tRNA are thus straddled between two different sites: the deacylated tRNA in the P/E sites and the peptidyl tRNA in the A/P sites (**Figure 4C**). This is referred to as the "hybrid state" because it describes the status of the tRNAs in the ribosome. This shift also involves the counterclockwise rotation of the small subunit relative to the large subunit into the

pre-translocation complex[27,28] . This is called the "rotated state" (as contrasted to the "non-rotated state") because it refers to the status of the ribosome as a whole. Notably, in the absence of eEF2-GTP, the elongation complex can dynamically shift between the rotated and non-rotated states[35], while eEF2-GTP preferentially binds to and stabilizes the rotated state, sterically inhibiting the A/P tRNA from returning to its canonical A/A position.[36,37]

The next intermediate state occurs when the small subunit partially swivels back and the head of the subunit rotates in the direction of translocation relative to the body: this is referred to as the "head swivel". [37,38]. The tRNAs now contact separate binding sites on the body and head of the small subunit in ap/P and pe/E positions, called the "chimeric hybrid"[33] (**Figure 4C**). Finally, the small subunit rotates clockwise, undoing the rotation into the hybrid state and returning the elongation complex to the classical, post-translation state. The movement of the small subunit has been likened to a ratchet that twists to deliver the tRNA/mRNA to the next sites on the large subunit, then breaks its contacts with the tRNA/mRNA and returns to its prior position, having transported the tRNA/mRNA to the next position.

The role of eEF2 in these later stages of translocation is currently under debate; two models have been proposed to understand how it contributes to ribosome movement. The first is that eEF2 harnesses the energy from GTP hydrolysis to drive the movement of the tRNA-mRNA complex through the ribosome, similar to molecular motors such as kinesin and myosin[39]. This "power-stroke" theory was proposed when studies in bacterial systems showed that GTP hydrolysis precedes tRNA movement[40,41] and EF-G undergoes large conformational changes upon ribosome binding[42,43]. Alternatively, in the "Brownian rachet" model it has been suggested that eEF2 acts as a pawl or doorstop, while the actual translocation event is driven by spontaneous movement of the ribosome. This is supported by the ability of the ribosome to

complete translocation in the absence of eEF2 and that non-hydrolyzable analogs of GTP[40,44,45] as well as GTPase inactive EF-G mutants[46,47] are still able to promote translocation, albeit at up to a 50-fold reduced rate. Here, the role of GTP hydrolysis would be to modulate the binding of eEF2 to the ribosome, thereby promoting its dissociation upon the completion of translocation. While the early hydrolysis of GTP may appear to contradict this model, it has been shown that Pi release is delayed and is rate limiting for eEF2 release. Consistent with this, a recent structural study of translocation intermediates indicates Pi release is regulated by the reverse rotation of the SSU and leads to stepwise dissociation of EF-G from the ribosome, beginning with the GTPase domain losing contact with the SRL[48].

Translational fidelity

Because of its necessity for translocation, eEF2 may play a role in translational fidelity, or the accuracy of decoding an mRNA message into a protein. There are several ways translational fidelity can go awry during elongation, including utilization of the wrong tRNA at a codon (missense incorporation), utilization of a tRNA at a termination codon (nonsense suppression), premature termination, and slippage of ribosomes on an mRNA during elongation (ribosomal frameshifting). Each of these error types can have disastrous impacts on cellular fitness due to a decrease in functional proteins and an accumulation of potentially harmful products.

Translational fidelity errors

Missense incorporation refers to an error where the incorrect amino acid is incorporated into the elongating peptide. There are several ways in which this type of error can occur, including mischarging of aa-tRNA and misincorporation of a non- or near-cognate aa-tRNA.

Mischarging is when an amino acid is attached to the acceptor end of an incorrect tRNA by its aminoacyl-tRNA synthetase (aaRS). tRNA charging is a two-step process where the aaRS first binds and activates its corresponding amino acid, then selects the corresponding tRNA and esterifies the activated amino acid to its 3' end[49]. This is typically a highly accurate process due to the binding specificity of the aaRS, which can discriminate between amino acids that differ by only a methyl group[50]. Furthermore, some aaRSs have editing abilities to target and hydrolyze mischarged aa-tRNA, decreasing the error rate from one in 10^4 events to one in 10^6 [50,51].

Besides mischarging, missense incorporation is can also be caused by accommodation of a non- or near-cognate tRNA by the ribosome. Misincorporation accounts for the majority of missense errors and is highly dependent on the specific codon, as some are more error prone than others. This is a result of differential stability of codon-anticodon interactions and the relatively low concentration of certain tRNAs, leading to their cognate codons being called "rare codons"[52]. Typically, the ribosome utilizes a kinetic partitioning model to ensure accommodation of the correct tRNA, where the initial selection step is separated from accommodation by irreversible GTP hydrolysis[53]. During selection, cognate tRNA are more likely to activate GTP hydrolysis while non-cognate tRNA have a higher chance of dissociation. The fidelity of this initial step is also enhanced by an "induced fit" mechanism, where cognate tRNA binding induces conformational changes in the ribosome that increase the rate of GTP hydrolysis[54]. After selection, the codon-anticodon interaction is sampled again, allowing for the discrimination between cognate and near-cognate tRNA. Cognate tRNA are again more likely to be fully accommodated into the A-site for peptide transfer, while near-cognate tRNA are more often rejected. However, in the case of rare codons, the likelihood of misincorporation increases due to the relatively low concentration available of the cognate tRNA[52]. Overall, missense errors tend to

be more tolerated than other types of translation errors, due to their relatively minor effect on the final product. In fact, it is estimated that 15% of protein molecules in *E. coli* will contain missense errors[55].

Translation errors can also occur by inaccurate termination, either by terminating too soon or not terminating at all. Premature termination results in truncated proteins, which can have deleterious *trans*-dominant negative effects. Thus, an entire molecular machinery devoted entirely to "mRNA surveillance" has evolved, in which such events promote degradation of mRNAs in a process called nonsense mediated decay (NMD)[56,57]. In addition, given the enormous amount of energy devoted to synthesizing ribosomes and protein synthesis, terminally stalled ribosomes represent a potentially deleterious energy drain on cellular metabolism. Accordingly, molecular processes have evolved to identify and release ribosomes that become trapped on ribosomes. These are divided into no-go decay (NGD) which occurs on ribosomes arrested during elongation of open reading frames[58], and non-stop decay (NSD) which occurs on ribosomes that have bypassed bona fide termination codons and which have progressed into polyA tails of mRNAs[59]. Importantly, there is some degree of mechanistic overlap between these three processes[60].

Premature termination occurs at background levels around 0.1% in the cell due to competition of aa-tRNA and eRF1 for certain codons, specifically sense codons that differ from a stop codon in the wobble position[61,62]. This can be exacerbated by excess eRF1 or a lower abundance of the cognate aa-tRNA. The NGD pathway also enables premature termination of ribosomes stalled on mRNA due to rare codons, amino acid depletion, the presence of thermodynamically stable mRNA structural elements, and damaged mRNA[57]. On the other hand, termination codons can be bypassed (genetically called "nonsense suppression") when near-

cognate tRNA outcompetes eRF1 for the decoding of a stop codon[63], or due to a prion-like change in eRF1 conformation called Ψ (Psi)[64]. This leads to continued elongation into the 3' UTR and either a C-terminally extended peptide or activation of the NSD pathway.

Frameshifting errors are those that result in the ribosome slipping into an aberrant reading frame along the mRNA message. As nucleotides are decoded one codon at a time, any movement of the ribosome more or less than three nucleotides results in a shift in translational reading frame. Frameshifting errors are thought to occur at a very low background frequency of less than 10^{-5} per codon[10] and typically result in premature termination at (previously) out-of-frame stop codons. In this way, frameshifting can be subject to the same mRNA surveillance as termination errors[60]. Reading frame maintenance is the ability of the translation apparatus to avoid erroneous frameshifting and is facilitated by accurate translocation. As the ribosome contacts with the tRNA-mRNA complex are reoriented during translocation, it presents the most vulnerable state for frameshifting. eEF2 is thought to not only enhance the speed of translocation, but it's accuracy as well. Indeed, structural studies have suggested that the diphthamide moiety acts as a "pawl" that prevents the ribosome from slipping out of frame during translocation[65]. Analogous to the role of domain IV in EF-G, diphthamide is likely involved in "unlocking" the codon-anticodon complex from the decoding center, thereby breaking the hold the ribosome has on the tRNA-mRNA complex[66]. Additionally, the recent elucidation of a chimeric elongation complex without EF-G demonstrated that in its absence, tRNA and mRNA movement become uncoupled[67], further supporting the role of EF-G/eEF2 in maintaining codon-anticodon interactions. Finally, it has been shown that EF-G also accelerates conformational changes that secure the new ribosomal contacts with the tRNA-mRNA complex

after the completion of translocation[68]. Together, these implicate eEF2 as a key factor in reading frame maintenance and the avoidance of frameshifting errors.

Translational recoding

As discussed, noncanonical translation elongation is often detrimental to cells. However, there are some mRNAs where such an event is selectively advantageous[69]. These mRNAs contain *cis*-acting "recoding signals" that can direct the translation apparatus to decode the message in a manner alternative to the standard rules of translation. In particular, programmed ribosomal frameshifting (PRF) signals lead to altered elongation and can be used to modulate gene expression.

PRF signals are *cis*-acting sequences that stimulate frameshifting, typically by inducing a ribosomal pause on a specific sequence that is prone to slippage[70]. The most common forms of PRF induce ribosomal slippage of one nucleotide in the 5' or 3' direction – called -1 and +1 frameshifting, respectively. In the case of -1 PRF, this is accomplished by downstream mRNA structure that pauses the ribosome at a heptameric "slippery sequence" on the mRNA. Slippery sequences typically take the form "X XXY YYZ", where the spaces denote the mRNA codons of the 0 frame[70]. XXX typically refers to any three identical nucleotides, YYY can be either AAA or UUU, and Z ≠ G. Once the ribosome has stopped due to the mRNA structure, this sequence allows the tRNA in the A and P sites to slide one nucleotide in the 5' direction and re-pair with the mRNA with only a mismatch in the wobble position. Specifically, the P site tRNA slips from the "XXY" codon to "XXX" and the A site tRNA moves from "YYZ" to "YYY" in the new reading frame.

-1 PRF is common in RNA viruses where genome space is limited, allowing them to encode multiple, overlapping proteins within one transcript. The archetypical example is the HIV

gag/gag-pol frameshift where the open reading frame encoding the structural protein, Gag, is in the 0-frame and open reading frame encoding the reverse transcriptase, Pol, overlaps the 3' end in the -1 frame[71]. At a frequency of approximately 1 in 20 events (5%), the ribosome shifts into the -1 frame and produces the Gag-Pol fusion protein that is later cleaved into its constituent mature proteins. Here, PRF functions to not only to maximize genome content, but also to ensure a necessary ratio of Gag to Gag-Pol protein[70,72].

While viruses are the most commonly cited example of PRF, there is evidence that suggests it is utilized to regulate cellular gene expression as well. For example, the retrotransposon-derived PEG10 gene, which is highly conserved among mammals and is essential for embryonic development, uses -1 PRF to encode two different isoforms in overlapping reading frames[73]. Additionally, computational analysis has estimated that ~10% of human genes may contain translational recoding signals[74] and it has been shown that PRF can specifically regulate mRNA levels by activating NMD and NGD[75,76]. Therefore, productive and nonproductive PRF are ways in which human gene expression can be modulated at the translational level.

PRF signals that induce +1 frameshifting appear to vary more widely than -1 PRF signals in their constituent parts. While mRNA structures have also been shown to be involved in +1 frameshifting, additional mechanisms to induce ribosome pausing at sequences that promote +1 slips include in-frame termination codons[75] and the use of rare codons[77], where the ribosome must wait for a low-abundance tRNA before translation can continue. Also distinct from the -1 PRF mechanism, +1 PRF typically involves only the slippage of the P site tRNA. For example, the gene encoding ornithine decarboxylase antizyme (OAZ) in eukaryotes (not present in plants) is stimulated by a 3' mRNA structure and, most commonly, the slippery sequence "UCC

UGA"[78]. Here, the pause is induced by the mRNA structure and the in-frame termination codon, while the P site tRNA slips from "UCC" to "CCU".

In addition to *cis*-acting sequences, PRF can also be modulated by trans-acting factors. One of the most well described involves the regulation of the +1 OAZ frameshift by polyamine levels. The +1 frameshift is necessary for production of OAZ and is stimulated by polyamines[79]. Polyamines are synthesized by ornithine decarboxylase (ODC), while OAZ induces degradation of ODC via ubiquitin-independent targeting of the proteosome[80]. Therefore, an increase in polyamine levels stimulates OAZ production, resulting in downregulation of polyamine biosynthesis. Recent evidence has also implicated a human interferon-stimulated gene, Shiftless, in the suppression of -1 PRF of viral origin[81]. It appears to function through recognition and binding of the ribosome during the frameshifting process and stimulating premature termination, which potentially directs the viral mRNA to NMD.

Human disorders of translation

Cells have evolved molecular mechanisms to respond to transient translational infidelity. If defects in translational fidelity reach a certain threshold, a corresponding accumulation of "incorrect" peptide products activate the cell's integrated stress response (ISR) through the unfolded protein response (UPR). UPR is activated when a threshold of unfolded proteins is reached in the ER, signaling the luminal domain of the PKR-like ER kinase (PERK) to autophosphorylate and begin a signaling cascade[82]. In the cytosol, protein folding is monitored by HSF1, a component of the heat shock response (HSR) which acts as a transcription factor to induce expression of chaperones and other HSR genes[83]. The different stress responses of the ISR converge with the phosphorylation of eIF2α, which inactivates translation initiation and

globally downregulates protein synthesis[82]. While these pathways serve to reestablish proteostasis, their influence can be overrun and an inability to handle unfolded proteins can cause apoptosis and cell death (**Figure 5**). Importantly, mutations or conditions that result in continuous activation of the ISR can promote pathological phenotypes.

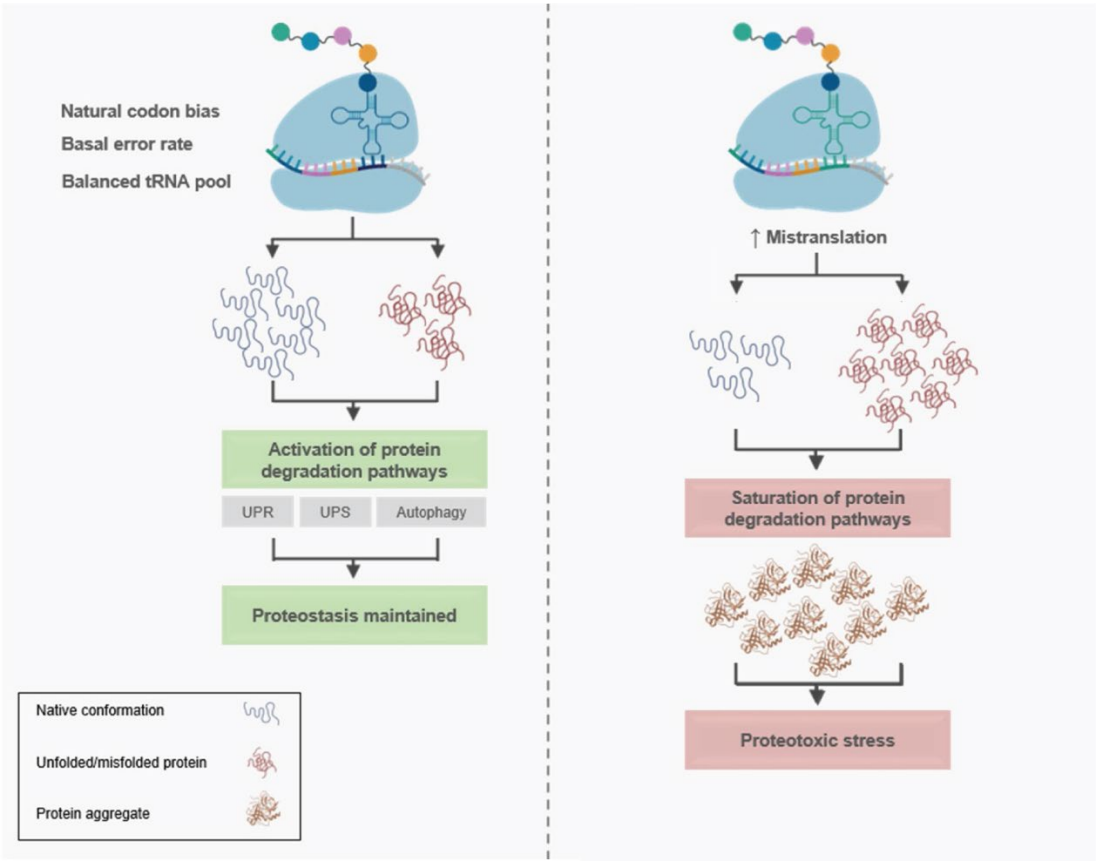

Figure 5: Mistranslation leads to proteotoxic stress

Under normal conditions, cellular stress responses are able to manage aberrant protein products to maintain proteostasis. If there is an increase in mistranslation due to translational fidelity defects, these aberrant products may override the cell's housekeeping abilities, leading to an accumulation of aggregates and potentially cell death. Image adapted from[84].

Ribosomopathies

In humans, impairments to ribosome components or biogenesis factors are called ribosomopathies. These rare genetic disorders were first described in 1999 when Draptchinskaia et al. indicated mutations in a ribosomal protein as the cause for Diamond-Blackfan Anemia

(DBA)[85]. With the advent of improved sequencing technologies, the list of ribosomopathies has continued to expand, now including several other diseases such as 5q syndrome, Treacher Collins syndrome, Dyskeratosis congenita, Cartilage hair hypoplasia, and Schwachman-Diamond syndrome[86]. These diseases lead to a variety of phenotypes, all characterized by developmental defects due to cell hypoproliferation, such as anemia or craniofacial malformations[86,87]. Confoundingly, patients are also more susceptible to various cancers later in life, indicating that there is a transition from a *hypo*proliferative state to a *hyper*proliferative one[87]. This switch from hypo- to hyper-proliferative states, known as "Damashek's Riddle"[88], is regarded as the fundamental paradox of ribosomopathies.

Ribosomopathies have been shown to result from deleterious mutations in genes encoding ribosome biogenesis factors, rRNA modification complexes, and ribosomal proteins (**Table 1A**). Despite this variation in causative alleles, ribosomopathies are mostly clustered around defects in hematopoeisis, or the formation of blood cells. While there are other clinical presentations such as craniofacial and skeletal abnormalities, the majority of currently described ribosomopathies seem to have a specific impact on blood and bone marrow. This is another paradox of ribosomopathies in that the centrality of the ribosome and protein synthesis would suggest that any ribosome defects would present on the organismal level, if such defects result in a viable organism at all. In an attempt to reconcile this, several models to explain the tissue-specific presentations of ribosomopathies are being investigated. One model is that of "specialized ribosomes" where different cell types are dependent on ribosomes with unique RP composition for the translation of particular mRNAs[89]. This is supported by studies that have found certain RPs present at substochiometric concentrations in the global aggregate of cellular ribosomes, suggesting that ribosomes are heterogeneous in composition[90]. Therefore, mutations

in specific RPs may manifest in cell types where they are important while not affecting others at all. On the other hand, the ribosome concentration model posits that global and mRNA-specific translational control is affected by the number of available, active ribosomes. On a specific level, certain mRNAs are initiated less efficiently, so the reduced availability of ribosomes could have deleterious consequences for their expression[91,92]. Global changes can potentially have tissue-specific effects as well, with certain cell types being more susceptible to perturbances in translation, particularly those where rapid and specific translational control is necessary[92].

Table 1: List of ribosomopathies and translationopathies

	Disease	Gene	Protein	Clinical features	Putative effects on translation	Ref
Ribosomopathies (A)	Diamond Blackfan Anemia	Various *RP* genes	Various RPs	Anemia, congenital abnormalities, increased risk of leukemia	18S rRNA processing and 40S formation defects	[85,93]
	5q$^-$ syndrome	*RPS14*	S14 (uS11)	Anemia, increased risk of leukemia	18S rRNA and 40S formation defects	[94]
	Treacher Collins Syndrome	*TCOF1*	Treacle	Craniofacial abnormalities	Impaired rDNA transcription	[95]
	X-linked Dyskeratosis congenita	*DKC1*	Dyskerin	Skin and nail abnormalities, bone marrow failure, increased risk of leukemia and pulmonary fibrosis	Impaired RNA pseudo-uridylation and ribosome biogenesis	[96,97]
	Cartilage hair hypoplasia	*RMRP*	RNase MRP	Skeletal dysplasia, immunodeficiency, predisposition to certain cancers	5.8S and tRNA maturation defects	[98]
	Schwachman-Diamond syndrome	*SBDS*	SDBS	Pancreatic insufficiency, bone marrow dysfunction,	Ribosome biogenesis and RNA processing defects	[99]

				skeletal abnormalities		
	--	*RPL10*	L10 (uL16)	Intellectual disability, microcephaly	Unknown	[100]
	MacInnes syndrome	*RPS23*	S23 (uS12)	Microcephaly, hearing loss, congenital abnormalities	Translational fidelity loss	[101]
Translationopathies (B)	Charcot-Marie-Tooth disease*	Various *ARS* genes	Various tRNA synthetases	Epilepsy, progressive microcephaly, hypomyelination	Increased mischarging of tRNA and nonsense incorporation	[89,102]
	Spinocerebellar ataxia 26	*EEF2*	eEF2	Cerebellar atrophy, loss of muscle coordination	Reading frame maintenance defects	[103]
	--	*DPH1*	Diphthamide biosynthesis 1	Intellectual disability, developmental delay, brain malformations	Impaired eEF2 diphthamide modification leading to reading frame maintenance defects	[104,105]
	Pontocerebellar hypoplasia 2, 4, and 5	Various *TSEN* genes	tRNA-splicing endonuclease complex	Early-onset neurodegeneration, seizures, intellectual disability	Partial loss of pre-tRNA cleavage resulting in impaired tRNA biosynthesis	[106,107]
	--	*eEF1A2*	eEF1A	Epilepsy, intellectual disability, craniofacial abnormalities	Translational fidelity loss	[108–110]
	--	*PUS3*	Pus3	Intellectual disability	Translational fidelity loss resulting from ablation of pseudouridine modifications of tRNA at position 39	[111]
	Galloway-Mowat	*OSGEP (KAE1), TP53RK,*	KEOPS-EKC complex	Neurological abnormalities, early-onset	Impaired t^6A modification of tRNA leading to	[112–114]

syndrome 2, 3, 4, and 5	*TPRKB, LAGE3*	progressive kidney disease	translational fidelity defects

*Specifically, the subtypes CMT2D (*GARS*), CMT2N (*AARS*), CMT2U (*MARS*), CMT2W (*HARS1*), CMTDIC (*YARS*), CMTRIB (*KARS*)[89]

Diamond Blackfan Anemia

DBA is a genetic disorder characterized by anemia (low red blood cell count) without affecting other blood components such as platelets and white blood cells. DBA also presents with congenital abnormalities in 40-60% of patients, which can vary from short stature to cardiac defects[86]. First linked to mutations in *RPS19*, DBA has since been shown to also result from mutations in 12 other RPs, including those from both the large and small subunits. The original *RPS19* variant accounts for ~25% of occurrences[115] and has been shown to negatively impact 18S pre-rRNA processing and 40S subunit production[116]. However, as with ribosomopathies as a whole, it is still not well understood how these variants lead to tissue-specific disorders. New variants can help shed light on this conundrum, such as that of *GATA1*, the first non-ribosomal gene to be found as a cause of DBA[117]. *GATA1* encodes an erythroid transcription factor necessary for red blood cell development and reduced levels of *GATA1* mRNA translation has been shown to lead to DBA. Additionally, researchers demonstrated that RP insufficiency also reduces production of GATA1 due to inefficient initiation in its highly structured 5' region[118], supporting the hypothesis that general RP defects can have mRNA-specific effects. In this way, newly discovered causative variants of DBA and other ribosomopathies can offer valuable information in deciphering the mechanistic complexities of ribosomopathies.

Translationopathies

As translation is a complex process that relies on many interacting molecules besides the ribosome, it is possible that mutations to – or biogenesis defects in – other translation

components could also result in disease. Accordingly, in tandem with the increased availability of patient genome sequencing, a growing list of genes either directly involved in or adjacent to translation have been implicated in genetic disorders. These include tRNA processing and modification proteins, aaRSs, and translation factors (**Table 1B**). Intriguingly, many of the associated disorders are neurological in nature, reproducing the motif of tissue-specificity observed in ribosomopathies. These "translationopathies" also tend to share the salient feature of translational fidelity – or rather the lack thereof.

Spinocerebellar ataxia 26

Spinocerebellar ataxias (SCAs) are a largely heterogenous group of genetic diseases characterized by progressive degeneration of the cerebellum, leading to loss of muscle coordination and a variety of other symptoms[119]. Each of the 31 different subtypes of SCA result from mutations at distinct genetic loci, indicating that Purkinje neurons – which form the cortex of the cerebellum – are particularly susceptible to genetic defects. Indeed, it has been found that neurons are more sensitive to proteotoxic stress than other cell types, presumably due to their large size, branched morphology, and their quality control system's susceptibility to being overloaded by misfolded proteins[69]. In human eEF2, evidence suggests that mutation of proline at position 596 to histidine (P596H) is the causative mutation for the autosomal dominant disorder Spinocerebellar ataxia 26 (SCA26) [103]. This mutation has also been shown to result in translational fidelity loss[103] so it is therefore hypothesized that eEF2-P596H causes cerebellar degeneration by disrupting translational fidelity and causing an increase in protein synthesis errors, which is clinically observed in the degeneration of delicate neurons due to proteotoxic stress.

Research overview

Protein synthesis is a centrally conserved molecular mechanism that consumes the bulk of metabolic resources, particularly in actively growing cells. Defects in translational accuracy can have deleterious effects on organisms, particularly during development and in cell types sensitive to translation perturbations such as bone marrow, neurons, and during fetal development. Here, we have probed the effects of two specific classes of mutations linked to two genetic disorders, on various aspects of translational fidelity and have examined their effects on cellular stress. Our findings suggest that perturbations to translational fidelity are a common factor that link translationopathies and certain ribosomopathies. Furthermore, they help to shed light on the mechanistic aspects of these disorders and contribute to the expanding evidence of translational fidelity importance to human health and disease.

Chapter 2: Ribosomal protein gene RPL9 variants can differentially impair ribosome function and cellular metabolism[120]

Marco Lezzerini[1,†], Marianna Penzo[2,†], Marie-Franc¸oise O'Donohue[3,†], Carolina Marques dos Santos Vieira[4,†], Manon Saby[5,†], Hyung L. Elfrink[1,6], Illja J. Diets[7], Anne-Marie Hesse[8], Yohann Coute´[8], Marc Gastou[9,10,11], Alexandra Nin-Velez[12], Peter G.J. Nikkels[13], Alexandra N. Olson[4], Evelien Zonneveld-Huijssoon[14,15], Marjolijn C.J. Jongmans[14,16], GuangJun Zhang[12], Michel van Weeghe[l6], Riekelt H. Houtkooper[1], Marcin W. Wlodarski[17,18], Roland P. Kuiper[14], Marc B. Bierings[16], Jutte van der Werff ten Bosch[19], Thierry Leblanc[20], Lorenzo Montanaro[2], Jonathan D. Dinman[4], Lydie Da Costa[5,9,10,21], Pierre-Emmanuel Gleizes[3] and Alyson W. MacInnes[1,*]

[1]Amsterdam UMC, University of Amsterdam, Laboratory Genetic Metabolic Diseases, Amsterdam Gastroenterology and Metabolism, Meibergdreef 9, 1105 AZ Amsterdam, The Netherlands,
[2]Laboratorio di Patologia Clinica, Dipartimento di Medicina Specialistica, Diagnostica e Sperimentale and Centro di Ricerca Biomedica Applicata (CRBA), Policlinico Universitario di S. Orsola, Universita di Bologna,Via Massarenti 9, 40138 Bologna, Italy,
[3]LBME, Centre de Biologie Integrative (CBI), Universit´e de Toulouse, CNRS, UPS, 31000 Toulouse, France,
[4]Department of Cell Biology and Molecular Genetics, University of Maryland, College Park, MD, USA,
[5]INSERM UMR S1134, F-75015, Paris, France,
[6]Amsterdam UMC, University of Amsterdam, Laboratory Genetic Metabolic Diseases, Core Facility Metabolomics, Amsterdam Gastroenterology and Metabolism, Meibergdreef 9, 1105 AZ Amsterdam, The Netherlands,
[7]Department of Human Genetics, Radboud University Medical Center, Nijmegen, The Netherlands,
[8]University Grenoble Alpes, CEA, INSERM, IRIG, BGE, F-38000 Grenoble, France,
[9]Paris University, Paris, France,
[10]Laboratory of Excellence for Red Cell, LABEX GR-Ex, F-75015, Paris, France,
[11]Institute Gustave Roussy, Inserm unit U1170, F-94800 Villejuif, France,
[12]Department of Comparative Biology and Center for Cancer Research, Purdue University, West Lafayette, IN 47907, USA,
[13]Department of Pathology, University Medical Center Utrecht, 3584 CX Utrecht, The Netherlands,
[14]Department of Genetics, University Medical Center Utrecht, 3508 AB Utrecht, The Netherlands,
[15]Department of Genetics, University of Groningen, University Medical Center Groningen, Groningen, The Netherlands,
[16]Princess Maxima Center for Pediatric Oncology and Utrecht University Children's Hospital, Utrecht, The Netherlands,
[17]Department of Pediatrics and Adolescent Medicine, Division of Pediatric Hematology and Oncology, Medical Center, Faculty of Medicine, University of Freiburg, D-79106 Freiburg, Germany,
[18]St. Jude's Children Research Hospital, Memphis, TN, USA,
[19]Department of Pediatrics, Universitair Ziekenhuis Brussel, Brussels, Belgium,
[20]Pediatric Hematology/Oncology Service, Robert Debre Hospital, F-75019 Paris, France and
[21]Hematology Lab, Robert Debre Hospital, F-75019 Paris, France

Work adapted from Nucleic Acids Research, January 2020, DOI: 10.1093/nar/gkz1042

Abstract

Variants in ribosomal protein (RP) genes drive Diamond-Blackfan anemia (DBA), a bone marrow failure syndrome that can also predispose individuals to cancer. Inherited and sporadic RP gene variants are also linked to a variety of phenotypes, including malignancy, in individuals with no anemia. Here we report an individual diagnosed with DBA carrying a variant in the 5′UTR of *RPL9* (uL6). Additionally, we report two individuals from a family with multiple cancer incidences carrying a *RPL9* missense variant. Analysis of cells from these individuals reveals that despite the variants both driving pre-rRNA processing defects and 80S monosome reduction, the downstream effects are remarkably different. Cells carrying the 5′UTR variant stabilize TP53 and impair the growth and differentiation of erythroid cells. In contrast, ribosomes incorporating the missense variant erroneously read through UAG and UGA stop codons of mRNAs. Metabolic profiles of cells carrying the 5′UTR variant reveal an increased metabolism of amino acids and a switch from glycolysis to gluconeogenesis while those of cells carrying the missense variant reveal a depletion of nucleotide pools. These findings indicate that variants in the same RP gene can drive similar ribosome biogenesis defects yet still have markedly different downstream consequences and clinical impacts.

Introduction

Diamond-Blackfan anemia (DBA) (OMIM# 105650) is an inherited bone marrow failure disorder that typically presents in children less than one year of age. While the central phenotype is pure red cell aplasia and a paucity of erythroblast precursor cells in the bone marrow, a number of physical malformations are also linked to DBA[121]. These include (but are not limited to) craniofacial malformations, growth retardation, abnormalities in the extremities (especially

the thumb), heart defects, and urogenital defects[122,123]. DBA patients also have an elevated cancer risk, particularly hematologic malignancies, osteosarcoma, and colon carcinoma[124,125].

With rare exceptions, DBA is a disease linked to RP gene variants[126]. These RPs include eS7 (*RPS7*), uS8 (*RPS15A*), eS10 (*RPS10*), eS17 (*RPS17*), eS19 (*RPS19*), eS24 (*RPS24*), eS26 (*RPS26*), eS27 (*RPS27*), eS28 (*RPS28*), uS14 (*RPS29*), uL18 (*RPL5*), uL5 (*RPL11*), eL15 (*RPL15*), eL18 (*RPL18*), uL24 (*RPL26*), eL27 (*RPL27*), eL31 (*RPL31*), uL29 (*RPL35*), eL33 (*RPL35A*)[85,115,127–139], and a phenotype resembling DBA has been identified in one individual carrying a variant in uL4 (*RPL4*)[140]. DBA mutations are heterozygous and result in haploinsufficiency of the corresponding RP, which affects processing of the pre-ribosomal RNA (pre-rRNA) in a RP-specific manner. *RPL9* gene allelic variation has so far been reported in one DBA-affected individual, however this c.375G>C; p.Arg125Ser variation was declared to be a variant of unknown significance (VUS) since cells from this patient did not show a pre-rRNA processing defect similar to that observed upon knockdown of RPL9 with siRNAs[115]. Although the pathophysiology linking RP variants to the DBA bone marrow failure phenotype is not entirely understood, the stabilization of the TP53 tumor suppressor protein is thought to occur due to ribosomal stress and in turn plays a role in impairing the proliferation of $CD34^+$ erythroblast precursor cells[141–143]. In fact, a recent study reported germinal *TP53* gene activating variants in two individuals with a DBA-like phenotype that includes erythroblastopenia[144].

An increasing number of RP genes carrying inherited or sporadic variants are being uncovered that do not drive the bone marrow failure that is the hallmark of DBA. Missense variants in *RPS23* (OMIM #617412) and *RPL10* (OMIM #300847 and #300998) are found in individuals with dysmorphism, autism, and intellectual disability who have no evidence of a

hematological phenotype[101,145–147]. Somatic variants in RP genes have also been found in several cancer exomes. These include acute lymphoblastic T-cell leukemia (T-ALL) (*RPL10* and *RPL5*); glioma, melanoma, and breast cancer (*RPL5*); colorectal and endometrial cancer (*RPL22*); and chronic lymphocytic leukemia (*RPS15*)[148–151]. Inherited variants in *RPS20* have also been reported linked to hereditary nonpolyposis colon carcinoma (OMIM #120435)[152]. Although none of these variants have been shown to drive stabilization of TP53, the *RPS23* p.Arg67Lys variant linked to dysmorphism and the *RPL10* p.Arg98Ser variant linked to T-ALL are reported to alter the translational fidelity of ribosomes by increasing frameshifting and the readthrough of stop codons[101,153]. Interestingly, despite not driving an anemia phenotype and having no observed effect on TP53, the missense variants in *RPS23* p.Arg67Lys and *RPL10* p.Arg98Ser have been reported to impair the processing of pre-rRNA and affect the formation of polysomes[101,154]. Thus, it appears that variants in RPs that impair ribosome biogenesis do not universally drive anemia and that the clinical phenotypes linked to the variants are dependent on a more complex set of events.

Here, we report that different variants in *RPL9*, a gene that has not been definitively described in DBA or other human diseases, drive similar defects in the processing of pre-rRNA during ribosome biogenesis yet reveal markedly different downstream effects on the TP53 pathway, erythrocyte development, metabolism, and the ability of ribosomes to recognize mRNA stop codons. This study endeavors to unravel the similarities and differences between variants found in the same RP gene and how they might ultimately contribute to the resulting clinical phenotypes.

Materials and methods

For full methods, see published manuscript

Patients

One individual was identified within the European DBA (EuroDBA) consortium registries. The diagnosis of DBA in this individual was established based on typical features including aregenerative anemia with erythroid hypoplasia[121]. Two other individuals (mother and son) were identified in a study on genetic predisposition for childhood cancer. Written informed consent was obtained from patients and/or parents prior to inclusion in this study, which was performed in accordance with the ethical standards of the Declaration of Helsinki. All procedures herein were performed according to the standards of the institutional and national ethical boards.

Cell culture and treatment with siRNA duplexes

Lymphoblastoid cell lines (LCLs) were derived from EBV-immortalization of peripheral mononuclear cells isolated from whole blood using Ficoll (GE Life Sciences) and grown in RPMI (Gibco) containing 10% fetal calf serum (FCS), 1% L-glutamine, and 1% penicillin/streptomycin as previously described[155]. HeLa cells were cultured in DMEM (Gibco) supplemented with 10% fetal calf serum and 1 mM sodium pyruvate (Sigma). Two 19-mer siRNAs (Eurogentec), whose efficiency was verified by qPCR, were used to knock down expression of human uL6 mRNAs in HeLa cells: si-uL6-1 (5′-CCCAGAAAGAUGAAUUAAUdTdT-3′) and si-uL6-2 (5′-GGGACUUCAAUCACAUCAAdTdT-3′). Each siRNA solution was added at a final concentration of 500 nM to 10^7 cells diluted in sodium phosphate buffer, pH 7.25, containing 250 mM sucrose and 1 mM $MgCl_2$. Electro-transformation was performed at 240 V with a Gene Pulser (Bio-Rad)[156]. Control HeLa cells were electro-transformed with a scramble siRNA

(siRNA-negative control duplex; Eurogentec). After 10 min incubation at ambient temperature, cells were plated and grown at 37°C for 48 h.

Sanger sequencing of LCLs

mRNA from LCLs was isolated with Trizol (ThermoFisher) for generation of cDNA using the QuantiTect Reverse Transcription Kit 400 (Qiagen) per the manufacturers' instructions. Primers used for Sanger sequencing of the 5′ UTR variant are FW:5′-TTCTCAGCAATCAGACTGTCG-3′ and REV:5′-AGGCTGGTATTCTGGACAGC-3′. Primers used for sequencing the p.Leu20Pro variant are FW:5′-CGGGAAAGGACAGGTCGAAA-3′ and REV:5′-GACAAGGTTCCGAGAGTGGG-3′.

Total RNA extraction and analysis of pre-rRNA processing by northern blot

Total RNAs were extracted with Trizol from cell pellets containing 20×10^6 cells. The aqueous phase was further extracted with phenol-chloroform-isoamylic alcohol (25:24:1; Sigma), then with chloroform. Total RNAs were recovered after precipitation with 2-propanol. For Northern blot analyses, RNAs were dissolved in formamide, denatured for 10 min at 70°C and separated on a 1.2% agarose gel containing 1.2% formaldehyde and 1× Tri/Tri buffer (30 mM triethanolamine, 30 mM tricine, pH 7.9) (3 µg RNAs/lane). RNAs were transferred to a Hybond N^+ nylon membrane (GE Healthcare) by passive transfer. Pre-hybridization was performed for 1 h at 45°C in 6× SSC, 5× Denhardt's solution, 0.5% SDS, 0.9 g/ml tRNA. The 5′-radiolabeled oligonucleotide probe was incubated overnight. The sequences of the probes were: 5′ITS1 (5′-CCTCGCCCTCCGGGCTCCGTTAATGATC-3′), ITS1-5.8S (5′-CTAAGAGTCGTACGAGGTCG-3′), ITS2 (ITS2b: 5′-CTGCGAGGGAACCCCCAGCCGCGCA-3′ and ITS2d/e: 5′-

GCGCGACGGCGGACGACACCGCGGCGTC-3′), 18S (5′-TTTACTTCCTCTAGATAGTCAAGTTCGACC-3′), 28S (5′-CCCGTTCCCTTGGCTGTGGTTTCGCTAGATA-3′). Membranes were washed twice for 10 min in 2× SSC, 0.1% SDS and once in 1× SSC, 0.1% SDS, and then exposed. Signals were acquired with a Typhoon Trio PhosphoImager (GE Healthcare) and quantified using the MultiGauge software.

Polysome profiling analysis

600 µg to 1 mg of total proteins from freshly lysed LCLs was loaded onto 10–50% sucrose gradients as previously described[157]. The tubes were centrifuged at 4°C and at 36 000 rpm for 2 h in a SW41 rotor (Optima L100XP ultracentrifuge; Beckman Coulter). The gradient fractions were measured at OD_{254nm} using a syringe pump and UV detector (Brandel) and collected with a Foxy Jr gradient collector (Teledyne Isco).

Translational fidelity reporters

For the cell-based assays a new generation of dual luciferase reporters was generated by Loughran *et al.* to correct interference of test sequence with stability and activity of *Renilla* and firefly luciferases[158]. Plasmid pSGDluc, which contains tandem StopGo sequences (2A) on either side of the test sequence[158], was kindly provided by Dr John Atkins, at University College Cork. In order to disrupt the *BamHI/SalI* sites present downstream of the firefly luciferase coding sequence, complimentary oligonucleotides (BamSalKilT and BamSalKilB, sequences available upon request) were ligated with linearized vector. The resulting plasmid was doubly digested with *XhoI* and *ApaI*, and the vector portion was used in Gibson assembly. A gBlock (sequences available upon request) was used to insert the HIV -1 PRF signal[71,159] between

new *SalI* and *BamHI* sites. After sequence verification, the resulting plasmid (pJD2256) was linearized with *BamHI* and *SalI*, and another set of complementary oligonucleotides (Alphahelixspacer-T2 and Alphahelixspacer-B2, sequences available upon request) was used to insert an alpha helix spacer which creates an open reading frame encoding the peptide sequence: EAAAKEAAAKA. The resulting plasmid, pJD2257, was used as the zero frame dual luciferase reporter. pJD2337 (PEG10) was used to monitor −1 PRF, and pJD2349 (OAZ1) was used to monitor +1 PRF. pJD2443 (UAA), pJD2444 (UGA) and pJD2445 (UAG) were used to monitor stop codon readthrough. To make the constructs used to monitor PEG10[160,161] and OAZ1[162] mediated −1 and +1 PRF, gBlocks were inserted in linearized pJD2257 by Gibson Assembly (sequences available upon request). To make the constructs used to monitor stop codon readthrough, sets of complimentary oligonucleotides (sequences available upon request) were ligated with linearized pJD2257.

Translational fidelity cell-based assays

Deidentified LCLs were transfected by electroporation using an Amaxa™ Nucleofector II apparatus and Cell Line Nucleofector® Kit V (Lonza), per the manufacturer's instructions. For each transfection, 1.5×10^6 cells were mixed with 1.5 μg of plasmid DNA. All assays were performed in triplicate four independent times. Cell lysates were prepared using passive lysis buffer and luciferase activities were determined using the Dual-Luciferase® Reporter Assay System and a GloMax-Multi+ Detection System (Promega), per the manufacturer's instructions 24 hours post-transfection. Data were analyzed by dividing the ratio of firefly luciferase to *Renilla* luciferase for each of the experimental plasmids by the same ratio for the readthrough plasmid control in the same experiment. Data were plotted on GraphPad Prism as percent translational recoding, with each symbol representing one biological sample assayed in triplicate.

Error bars represent standard deviation. Normal distribution of the data was determined by the Shapiro–Wilk normality test. Statistical significance was obtained by one-way ANOVA, followed by Holm–Sidak's multiple comparisons test. Adjusted *P*-values were reported on graphs as $*P < 0.05$ and $**P < 0.01$.

Translational fidelity cell-free assays

Cell-free assessment of ribosome fidelity was performed essentially as previously described[163,164]. Briefly, cytoplasmic cellular lysates were prepared from subconfluent LCLs. From these lysates, ribosomes were purified in stringent conditions on a discontinuous sucrose gradient by a 15–16 h centrifugation at 160 000g. To test STOP codon readthrough, assays were performed for 60 min at 30°C in reaction mixtures containing 30 mM HEPES/KOH, pH 7.5, 80 mM KCl, 1.8 mM magnesium acetate, 50 μM of each amino acid, 1 mM ATP, 0.25 mM GTP, 5 mM creatine phosphate, 0.18 mg/ml creatine phosphokinase, 0.5 mM DTT, 0.4 mM spermidine, S-140 (40% of reaction volume), ribosomal salt wash (4% of reaction volume), 300 ng of capped reporter mRNA [wild type (WT) or STOP mutant firefly luciferase (FLuc) mRNAs were mixed with an mRNA coding for Renilla luciferase (RLuc), as an internal reference, in a 49:1 ratio], and 0.125 pmol ribosomes. After incubation time, the reactions were stopped on ice and RLuc and FLuc activities were measured using a Dual-Luciferase Reporter assay (Promega Corp.), following manufacturer's specifications. To calculate the relative STOP codon readthrough (expressed in %), FLuc/RLuc ratios were calculated for each sample, after background subtraction. Then, for each ribosome type, the STOP mutant FLuc/Rluc ratio was expressed as percentage of WT FLuc/RLuc ratio. Subsequently, the ratios obtained for mutant samples were normalized on the averaged ratios obtained for WT samples.

Mass spectrometry (MS)-based proteomic analyses

Proteins from cell-free ribosomal preparations were solubilized in Laemmli buffer before being stacked in the top of a 4–12% NuPAGE gel (Life Technologies), stained with R-250 Coomassie blue (Bio-Rad) and in-gel digested using modified trypsin (sequencing grade, Promega) as previously described[165]. The dried extracted peptides were resuspended in 5% acetonitrile and 0.1% trifluoroacetic acid and analyzed by online nanoliquid chromatography coupled to tandem mass spectrometry (LC–MS/MS) (Ultimate 3000 RSLCnano and the Q-Exactive HF, Thermo Fisher Scientific). Peptides were sampled on a 300 µm 5mm PepMap C18 precolumn (Thermo Fisher Scientific) and separated on a 75 µm 250 mm C18 column (Reprosil-Pur 120 C18-AQ, 1.9 µm, Dr. Maisch HPLC GmbH). The nano-LC method consisted of a 120 min multi-linear gradient at a flow rate of 300 nl/min, ranging from 5 to 33% acetonitrile in 0.1% formic acid. The spray voltage was set at 2 kV and the heated capillary was adjusted to 270°C. Survey full-scan MS spectra (m/z = 400–1600) were acquired with a resolution of 60 000 after the accumulation of 10^6 ions (maximum filling time 200 ms). The 20 most intense ions were fragmented by higher-energy collisional dissociation after the accumulation of 10^5 ions (maximum filling time: 50 ms). MS and MS/MS data were acquired using the software Xcalibur (Thermo Scientific).

Data were processed automatically using Mascot Distiller software (version 2.7.1.0, Matrix Science). Peptides and proteins were identified using Mascot (version 2.6) through concomitant searches against Uniprot (Homo sapiens taxonomy, June 2019 version), the mutated RPL9 protein sequence, classical contaminants database (homemade) and their corresponding reversed databases. Trypsin/P was chosen as the enzyme and two missed cleavages were allowed. Precursor and fragment mass error tolerance were set, respectively, to 20 ppm and 25

mmu. Peptide modifications allowed during the search were: carbamidomethylation (fixed), acetyl (protein N-terminal, variable) and oxidation (variable). The Proline software (http://proline.profiproteomics.fr) was used to filter the merged results: conservation of rank 1 peptide-spectrum match (PSM) with a minimal length of 7 and a minimal score of 25. PSM score filtering is then optimized to reach a False Discovery Rate (FDR) of PSM identification below 1% by employing the target decoy approach. A minimum of one specific peptide per identified protein group was set. Proline was then used to perform MS1-based label free quantification of the peptides and protein groups from the different samples. The mass spectrometry proteomics data have been deposited to the ProteomeXchange Consortium via the PRIDE partner repository with the dataset identifier PXD015218[166].

uL6 structure modeling

Modeling of wild type uL6 structure compared to uL6 p.Leu20Pro was performed in Pymol using the mutagenesis function. Source file for this was RCSB PDB entry 3J7P, the structure of the 80S mammalian ribosome bound to eEF2[167].

Results

Gene variants in RPL9 link to DBA and multiple cancer incidences

Whole exome sequencing (WES) of patient-parent trios identified an individual within the EuroDBA consortium registries with the heterozygous variant c.-2+1G>C (P1) in the 5′UTR of the *RPL9* gene (NM_000661.4) (**Table 2 and Figure 6**). The c.-2+1G>C variant appears to be *de novo* as both parents tested wild-type for *RPL9*. Sanger sequencing of cDNA from EBV-immortalized lymphoblast cell lines (LCLs) derived from these individuals confirmed the

presence of double peaks, indicating that the variant allele is expressed (**Figure 6B**). The c.-2G+1>C variant is predicted to be a splice site variation affecting the donor splice site of exon 1 (**Figure 6C**) and has previously not been reported in SNP databases. This individual, in addition to anemia, presented with an abnormal thumb and colitis, the pathology of which was marked by apoptotic bodies, $CD3^+$ lymphocyte infiltration, and TP53 stabilization (**Table 2**).

Table 2: Clinical features of individuals carrying variants in *RPL9*

Patient;sex	RP gene variant	Clinical presentation and therapies	Gestational age; malformations; other	Age and status at last follow-up	Family History
1;F	*RPL9* c.-2+1G>C;p.?	DBA onset: 6 months old; Hb 8.7 g/dL Lab: MCV/eADA normal HbF↑(1.7%) Evolution: 2 failed steroid courses. Transfusion-dependent for 1 year, thereafter fewer transfusions required.	37 weeks, microcephaly, colitis, thumb anomaly (1 side afunctional, other side finger- like), failure to thrive. Autoimmune colitis at age 6 months, received steroids and azathioprine.	4 years, irregular transfusions.	Parents wild type. Two miscarriages, one healthy newborn brother.
2;F	*RPL9* c.59T>C; p.Leu20Pro	Squamous cell carcinoma of the vulva diagnosed at age 43. Tumor was surgically resected.	Short stature (length 155cm, -2SD). Tested negative for HPV.		Mother of P3
3;M	*RPL9* c.59T>C; p.Leu20Pro	Conventional type osteosarcoma diagnosed at age 11. Chemotherapy according to the EURAMOS-1 protocol (good responder arm: 4x MAP, 2x MAPEI). AML subtype M5 diagnosed at age 13. Treated with induction- and consolidation chemotherapy according to the NOPHO-DHB AML 2012 protocol, and a	Micropenis and short stature (length 165cm, −2.25SD).		Son of P2

		subsequent allogeneic stem cell transplantation from a matched-unrelated donor (MUD).			

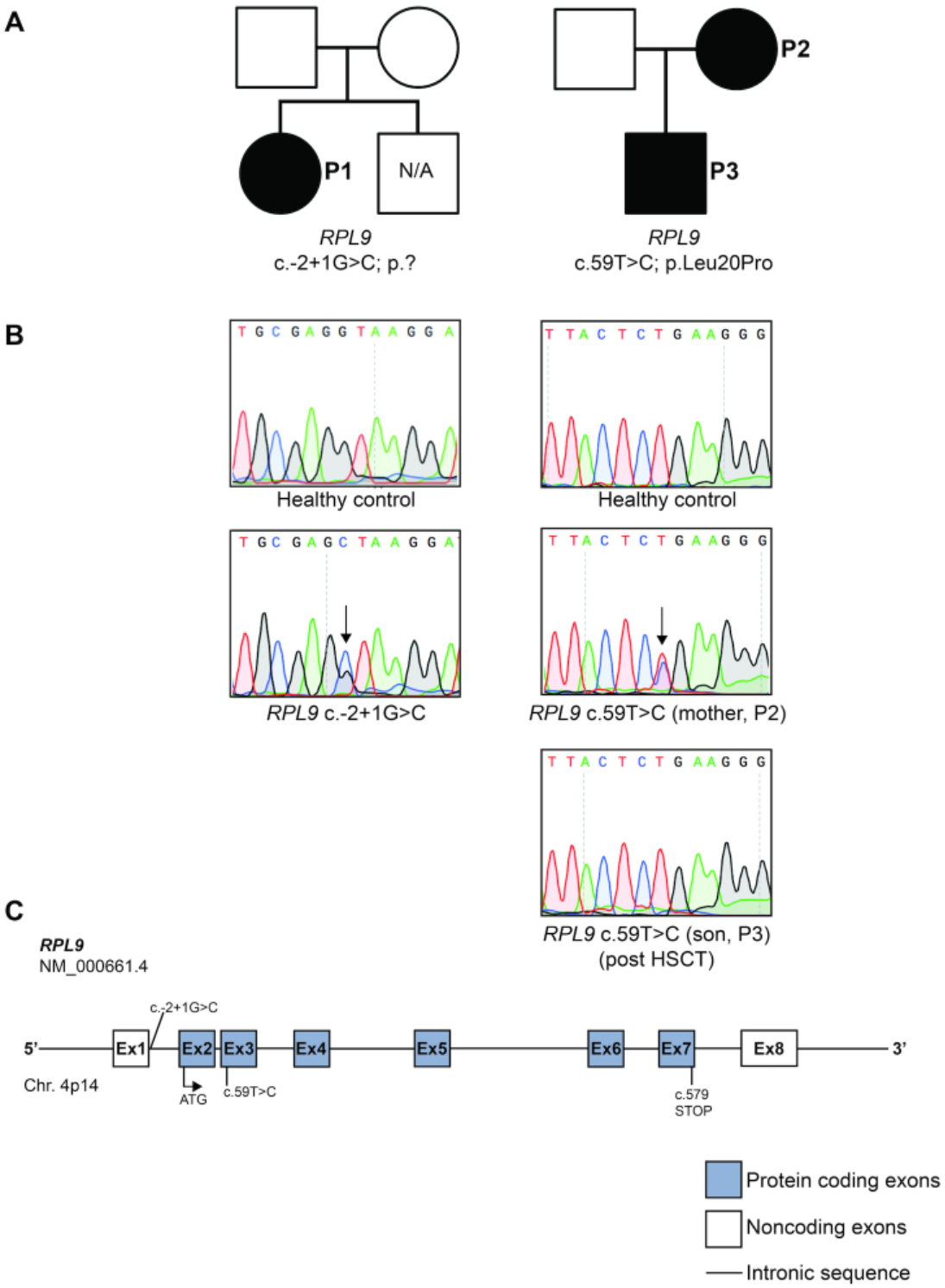

Figure 6: Heterozygous variants in *RPL9* are linked to human disease

A) Two pedigrees of individuals affected by DBA (left) or multiple cancer incidences (right). Affected variant carriers are indicated with filled squares (male) or circles (female) and are identified as Patients 1–3 (P1–4). Unaffected individuals are indicated by unfilled symbols. N/A indicates unaffected family members who were not investigated for the presence of variants. B)

Sanger sequencing results of LCLs derived from heathy controls or the affected individuals in (A). The double peaks illustrating variant allele expression are indicated with arrows. C) Schematic representation of the human *RPL9* gene depicting localization of the variants identified in the families in (A). This work was performed by our collaborators.

Another family carrying a *RPL9* variant was identified by WES within a study on childhood cancer predisposition [methods described in[168]]. This family consisted of a boy (P3) diagnosed with childhood cancer twice, and his mother (P2). P3 presented with conventional type osteosarcoma (**Table 2**). Physical examination revealed a micropenis, short stature (-2.25SD), and no dysmorphic features. He was treated with chemotherapy according to the EURAMOS-1 protocol (good responder arm: 4× MAP, 2× MAPEI). Less than two years later at age 13, he developed acute myeloid leukemia (AML), subtype M5. This AML may have been secondary to the chemotherapy received for the osteosarcoma. However, this possibility was considered not likely given the short period of time between the chemotherapy and the AML, the fact that the karyotype was normal, the patient did not receive etoposide, and because the AML was very treatable (remission occurred very quickly, which is unusual with a typically aggressive secondary AML). The AML was treated with induction and consolidation chemotherapy according to the NOPHO-DHB AML 2012 protocol, and a subsequent HCT from a matched-unrelated donor (MUD). Family history showed that his mother (P2) was diagnosed with a squamous cell carcinoma of the vulva at age 43 and that she had tested negative for the human papilloma virus (HPV). She had no congenital anomalies or dysmorphic features, but had short stature as well (length 155 cm, −2SD) which is a feature that is commonly reported in DBA-affected individuals[169].

WES was performed on germline DNA of both parents of P3, and tumor-derived DNA from both the osteosarcoma and the AML. No germline material of P3 could be obtained, since he had been HCT-treated. A missense variant in *RPL9* c.59T>C; p.Leu20Pro was identified in

both types of tumors of P3, which was maternally inherited (from P2) and occurs in exon 3 (**Figure 6C**). Given that this variant appeared in both tumors and in one parent of P3, we consider it a germline mutation. This Leu20 residue precedes a universally conserved residue in uL6 (Lys21), and is itself highly conserved in mammals, birds, frogs, and fish (**Figure 7**). Importantly, this residue preceding Lys21 is invariably hydrophobic, as it is found as isoleucine or valine in flies, worms, and yeast (**Figure 7**). No loss of heterozygosity or second hit mutations in *RPL9* in either of the tumors of P3 was present. Moreover, the exome sequencing of the two tumors revealed variants that were not present in either parents and as such considered to be somatic, however none of these variants to date have any reported links to cancer. Sanger sequencing of LCLs derived from the mother (P2) revealed a double peak which was not present in the son (P3) given the LCLs were derived post-HCT (**Figure 6B**). This variant has been previously reported (rs141176319) at a very low frequency of 0.00005767. While it may be that some individuals carrying the variant are unaffected due to decreased penetrance of the variant, it is also possible that these individuals may be predisposed to developing cancer later in life. Another possibility is that p.Leu20Pro is a VUS, although the following functional data suggest that this variant does have a detrimental effect on ribosome biogenesis resembling pathogenic DBA-linked RP gene variants.

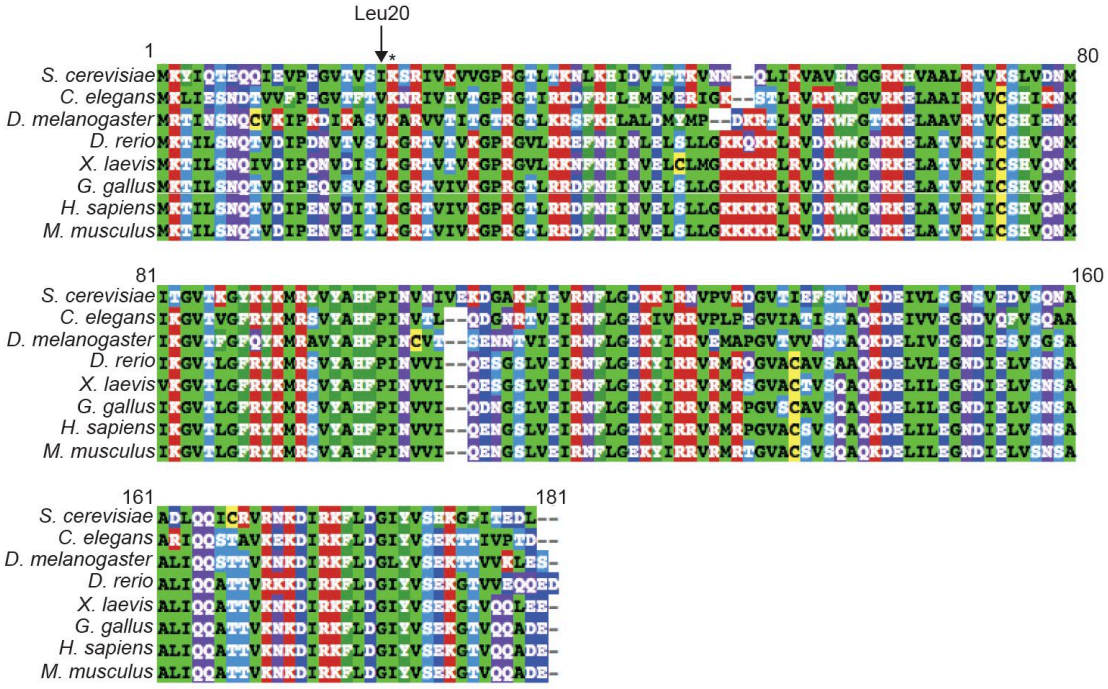

Figure 7: Multiple sequence alignment (MSA) of uL6 proteins.

The human Leu20 residue in uL6 (RPL9) precedes a universally conserved Lys21 residue (indicated with *) and is itself conserved in mammals, birds, frogs, and fish. The hydrophobicity of residue 20 is also conserved in eukaryotes, as yeast, worms, and flies reveal either Ile20 or Val20 in this position. Color coding is based on the physicochemical properties of the amino acids,with hydrophobic amino acids shown in green (black font), large hydrophobic in green (white font), negatively charged in dark blue, positively charged in red, cysteines in yellow, polar in purple, and small alcohol in light blue.

RPL9 variants impair the processing of pre-rRNAs

The normal processing and maturation of pre-rRNAs in humans, illustrated in **Figure 8**, is impaired at different steps by DBA-linked RP gene variants[93,115,129,131–133]. To investigate the functional consequences of the newly identified RP gene mutations reported here, EBV-immortalized LCLs were generated from peripheral blood of the individuals in this study for ribosome biogenesis analysis. For comparison, two different siRNAs were used to knock down uL6 in HeLa cells (**Figure 9**). As seen on the northern blot of **Figure 9A**, depletion of uL6 leads to a clear accumulation of long early precursors [i.e. 45S, 43S, and 41S, as seen with the (ITS1)-

5.8S probe]. Although 32S pre-rRNAs accumulate only slightly, 12S pre-rRNAs are clearly underrepresented (**Figure 9A**). This is evidenced by the 12S/32S ratio which is lower upon depletion of uL6 (**Figure 9B**) and suggests impairment in cleavage at site 4 in the maturation of 28S rRNA (**Figure 8**). A similar defect has been reported in yeast *S. cerevisiae* with an impaired cleavage at site C2 (similar to site 4 in humans) upon uL6 depletion[170]. Our data show that the small subunit production is also impacted, with a clear accumulation of 30S and 18S-E pre-rRNAs (5′ITS1 probe, **Figure 9A**). Indeed, defective processing of pre-rRNAs of the large ribosomal subunit often affects 18S rRNA formation too. This is usually due to a delayed/impaired processing at site 2, which then favors direct cleavage at site E (thus leading to an accumulation of 36S and 36S-C pre-rRNAs, as well as 18S-E pre-rRNA; **Figure 8**). This is shown experimentally by a decrease of the 21S/30S ratio and an increase of the 18S-E/21S ratio for cells treated with uL6 siRNAs (**Figure 9B**) and suggests that cleavage of both the 5′ external transcribed spacer (5′ETS) and internal transcribed spacer (ITS1) flanking the 18S rRNA is delayed.

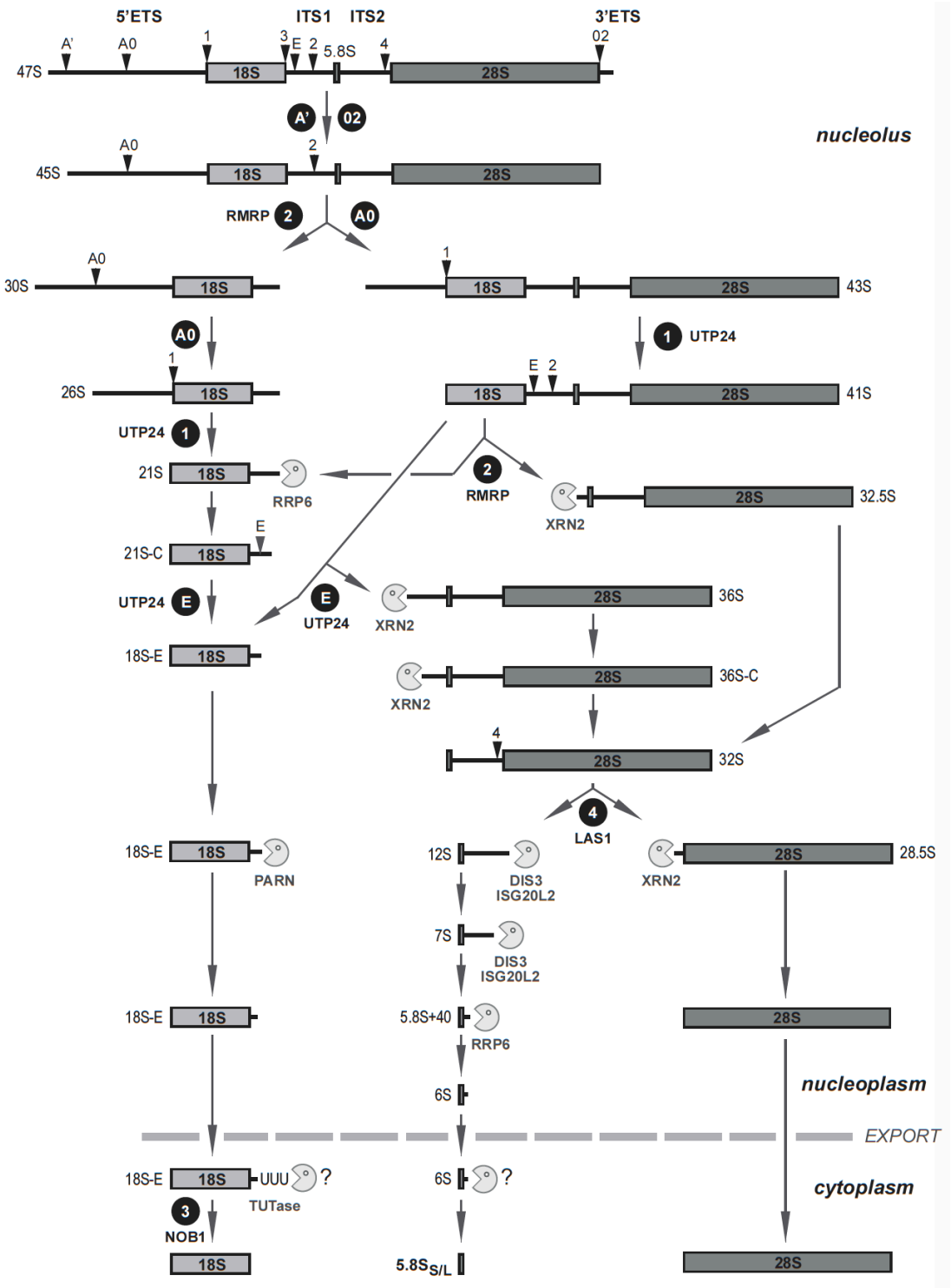

Figure 8: A schematic of pre-rRNA processing in human cells

Major endonucleolytic cleavage steps are labeled with black circles, the relevant enzymes are also noted.

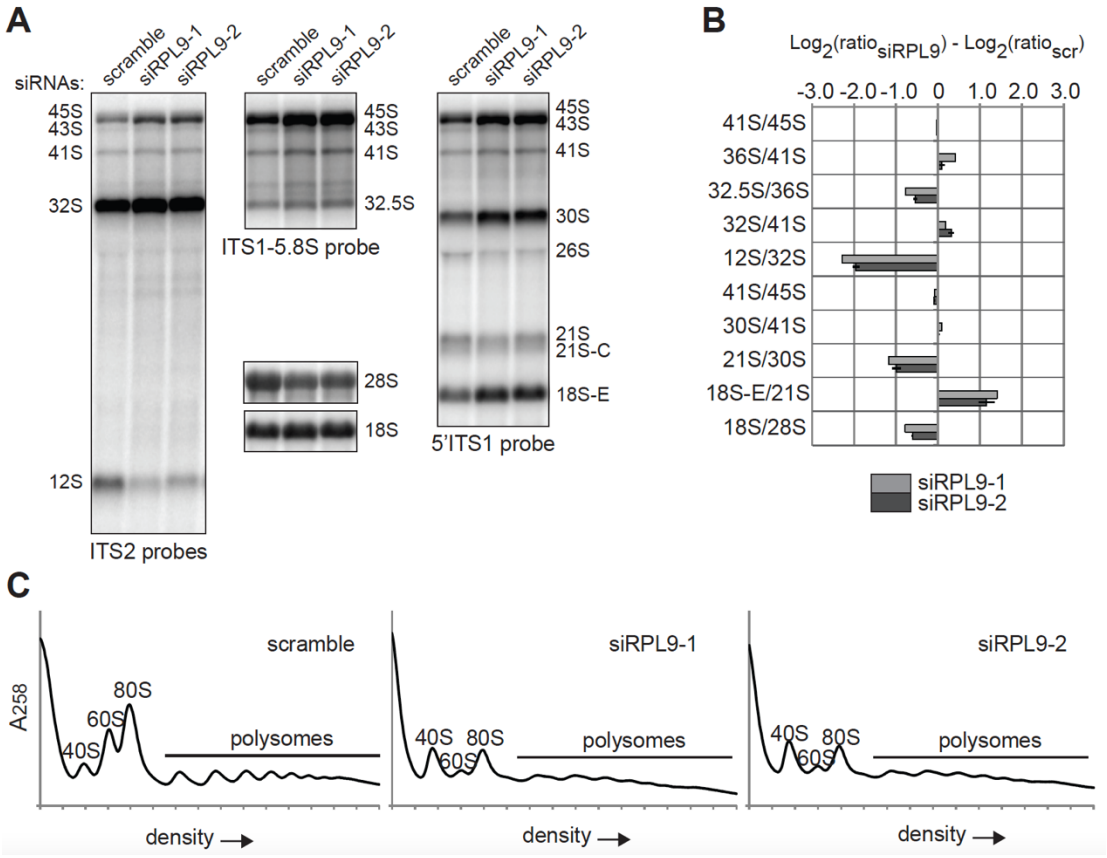

Figure 9: Reductions of RPL9 levels by siRNAs in HeLa cells reveal pre-rRNA processing defects and impair 60S ribosomal subunit formation

A) Northern blot analysis of HeLa cells transfected with scrambled control siRNAs or siRNAs against RPL9 mRNA. Probes used are against ITS2, ITS1-5.8S, and 18S-ITS1 (5'ITS1). B) Quantitative RAMP analysis of (A) (three independent experiments). C) Polysome profile analysis of HeLa cells transfected with scrambled control siRNAs or siRNAs against RPL9. The small (40S) and large (60S) ribosomal subunits are labeled as well as the 80S monosome and the polysomes. Note the strong reduction of the 60S peaks in the siRPL9 samples. This work was performed by our collaborators.

Figure 10 summarizes the northern blot results obtained with LCLs derived from Patients 1 and 2 carrying the variants *RPL9* c.-2+1G>C and uL6 p.Leu20Pro, respectively, and the post-HCT LCLs from P3 (where the uL6 p.Leu20Pro variant is no longer present, see **Figure 6B**). The pre-rRNA profiles were compared to 2 healthy control LCLs. The phenotypes in cells from Patients 1 and 2 recapitulate key features of the profile observed with *RPL9* siRNAs, namely the decrease of the 12S/32S and 21S/30S ratios (**Figure 10A, 10B**). An increase in the 30S/41S ratio

(reflecting a decrease in 41S pre-rRNA) was observed only in the uL6 p.Leu20Pro LCLs of P2 and not the others, unveiling some difference in this variant compared to P1 (**Figure 10B**). The 18S-E/21S ratios were also slightly increased in LCLs from patients, although not as much as in the *RPL9*-depleted HeLa cells. As expected, pre-rRNA from post-HCT LCLs from P3 showed little difference from control cells.

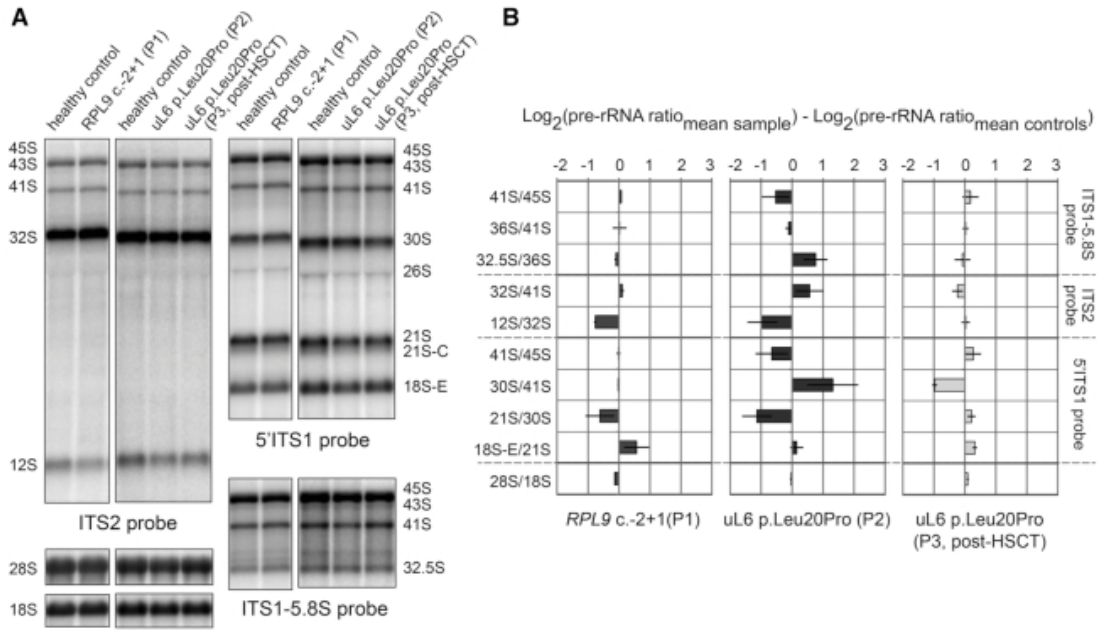

Figure 10: Variants in *RPL9* recapitulate specific pre-rRNA processing defects found in RP depleted cells and show key differences

A) Northern blot analysis of LCLs derived from individuals carrying *RPL9* variants. Radio-labeled probes against ITS2 (left panels), ITS1–5.8S (upper right panels), 5′ITS1 (middle panels), or 18S and 28S (lower right panels) rRNA sequences were used to blot 3 µg total RNA isolated from cells. B) Quantification of three independent experiments analyzing rRNA precursors in LCLs derived from individuals carrying *RPL9* variants using RAMP. This work was performed by our collaborators.

RPL9 variants impair ribosomal subunit formation

In order to determine how the variants in *RPL9* affect 40S and 60S ribosomal subunit formation, lysates of the HeLa cells transfected with the siRNAs against *RPL9* were first fractionated by ultracentrifugation on sucrose gradients and polysome profiles were analyzed by optical density (**Figure 9C**). These results show that the reduction of *RPL9* leads to a substantial

reduction of the 60S large ribosomal subunits, along with a reduction of 80S monosomes, polysomes, and 40S ribosomal subunits peaks that accumulate likely due to the loss of available 60S subunits for joining (**Figure 9C**). Lysates of LCLs from healthy controls or individuals carrying *RPL9* variants were next fractionated on sucrose density gradients and peak sizes measured (**Figure 11**). A substantial reduction of the 60S large ribosomal subunit, coupled to a reduction of the 80S monosomes, was observed in the polysome profiles of LCLs carrying the *RPL9* c.-2+1 variant (from P1) compared to control cells (**Figure 11A, 11B**), consistent with what is observed in **9C** when uL6 is knocked down in HeLa cells. A similar profile was observed with LCLs carrying the uL6 p.Leu20Pro variant (from P2), but the reduction of the 60S subunit was not as pronounced (**Figure 11C**). These results indicate that production of the 60S subunit is impaired in P1 and P2 cells, consistent with the pre-rRNA processing defects observed by northern blot in **Figure 10**.

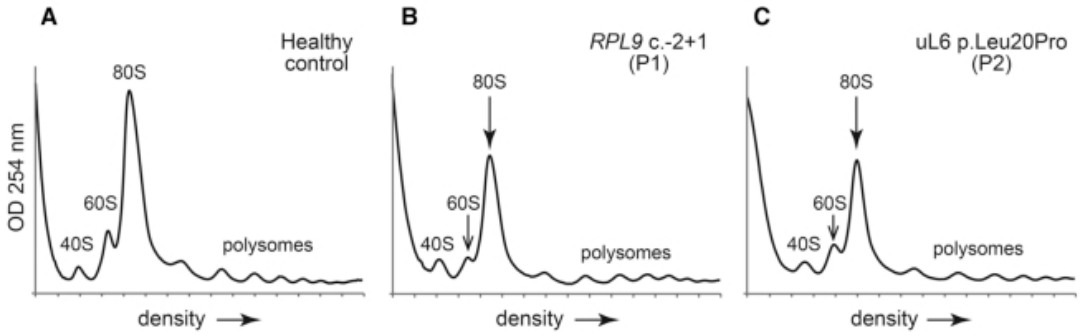

Figure 11: Variants in *RPL9* confer different polysome profile peak ratios

(A–C) Representative polysome profiles of LCLs derived from a healthy control (A), a DBA-affected individual (P1) carrying the *RPL9* c.-2+1 variant (B), and an individual (P2) carrying the uL6 p.Leu20Pro variant (C). The free 40S and 60S subunits, 80S monosomes, and polysomes are labeled. The reduced 60S peaks in the profiles are indicated with open arrows, the reduced 80S monosomes indicated by filled arrows. This work was performed by our collaborators.

Zebrafish models of RPL9 loss-of-function recapitulate the anemia but not the cancer phenotype

Many (if not most) homozygous mutant zebrafish models of RP gene knockout by viral insertion[171] reveal a depletion of hemoglobin-expressing cells when embryos are stained with o-dianisidine[172,173]. Interestingly, several of these zebrafish lines (17/28) as heterozygous adults are also prone to developing peripheral nerve sheath tumors (MPNSTs)[174]. We characterized the hematopoietic phenotype of a zebrafish line carrying a viral insertion in the *rpl9* gene that was previously generated[171]. **Figure 12A** shows that at 4 days post-fertilization (dpf) embryos homozygous for the viral insertion in *rpl9* (*rpl9*$^{-/-}$) fail to inflate their swim bladders and subsequently die by 6–7 dpf. Staining of wild type and mutant zebrafish embryos at 2 dpf with *o*-dianisidine (followed by genotyping of single embryos) reveals different severities of the loss of hemoglobin-expressing cells, illustrated in **Figure 12B**. In clutches of embryos generated from mating two heterozygous *rpl9* mutant fish we found that both hetero- and homozygous embryos fail to generate hemoglobin-expressing cells to the same degree as wild type fish, in effect phenocopying the DBA anemia phenotype (**Figure 12C**). However, the *rpl9* heterozygous line is reported to be a non-tumor prone line, suggesting that at least in zebrafish models the mere reduction of *rpl9* mRNA is insufficient to drive cancer[175].

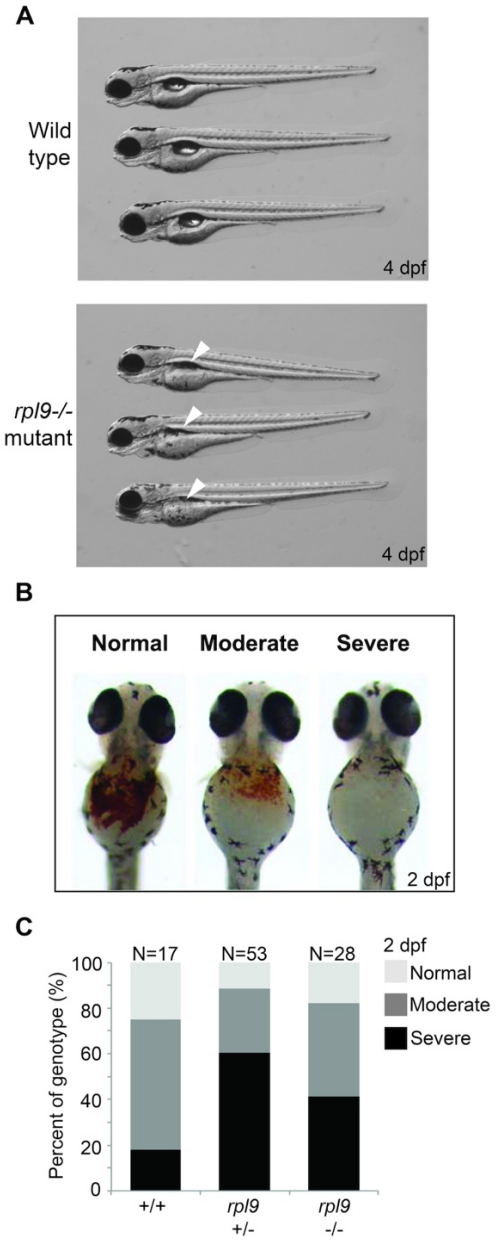

Figure 12: Zebrafish models of *rpl9* loss recapitulate the anemia phenotype of DBA

A) Morphology at 4 dpf of wild type embryos or hi1422 mutants that reduce levels of uL6 protein coded for by *rpl9*. White arrowheads indicate the failure of swim bladder inflation. B) Illustration of scoring embryos at 2 dpf stained with o-dianisidine as having a normal, moderate, or severe phenotype of hemoglobin-expressing cells. C) Scoring and genotypes of o-dianisidine stained embryos from clutches of hi1422 matings stained at 2 dpf. This work was performed by our collaborators.

Erythroid cell culture assays reveal primary CD34+ cells carrying RPL9 5'UTR variants fail to proliferate

Erythroid cell culture assays show that hematopoietic progenitor cells can reveal reduced proliferation rates, delayed differentiation, and increased TP53-induced apoptosis in a manner that is largely dependent on which RP gene is mutated or knocked down[143]. To investigate the effects of the different *RPL9* variants, $CD34^+$ primitive erythroid progenitor (BFU-e) cells from Patients 1 and 2 were isolated from peripheral blood and plated in erythroid cell culture medium, then allowed to grow for 12–15 days alongside $CD34^+$ BFU-e cells isolated from a healthy individual. **Figure 13A** shows that $CD34^+$ cells derived from P1, the DBA-affected individual carrying the *RPL9* c.-2+1G>C variant in the 5′UTR, do not proliferate in red cell culture medium compared to cells from a healthy control. **Figure 13B** reveals that the expression of uL6 on Day 7 is lower in cells carrying the 5′UTR variants. In contrast, **Figure 13C** reveals that $CD34^+$ cells derived from P2 carrying the p.Leu20Pro missense variant in uL6 (*RPL9*) proliferate normally compared to cells from a healthy control. Moreover, in contrast to cells carrying the 5′UTR variant in **Figure 13B**, western blots in **Figure 13D** show that cells carrying the p.Leu20Pro variant do not reveal any reduction of uL6 protein. This result is consistent with the polysome profiles in **Figure 11** revealing a greater reduction of 60S ribosomal subunits in the cells carrying the 5′UTR variant compared to the p.Leu20Pro variant.

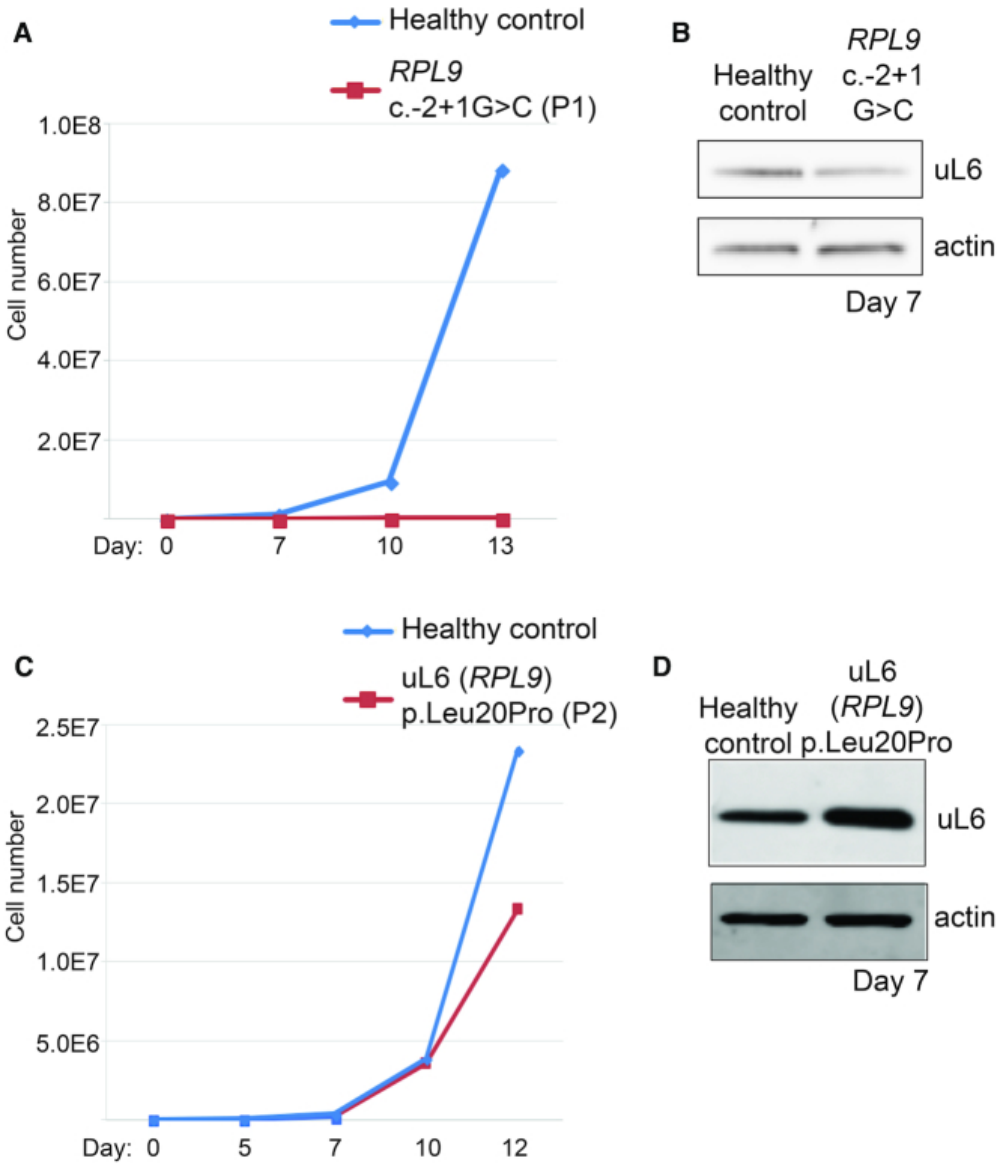

Figure 13: Erythroid cell culture assays of primary CD34+ cells reveal proliferation defects only in cells with 5'UTR variants

A) Growth curves of $CD34^{+}$ cells isolated from peripheral blood of the DBA-affected individual carrying the *RPL9* c.-2+1 variant (P1, red) compared to erythroid cells from a healthy control (blue). B) Western blotting of lysates from cells in (A) collected at Day 7 and probed with antibodies against uL6 protein. C) Growth curves of $CD34^{+}$ cells isolated from the individual carrying the uL6 (*RPL9*) p.Leu20Pro variant (P2, red) compared to cells from a healthy control (blue). D) Western blotting of lysates from cells in (C) collected at Day 7 and probed with antibodies against uL6 protein. This work was performed by our collaborators.

The 5'UTR variant of RPL9 is linked to TP53 stabilization in LCLs

One of the potential mechanisms behind the inability of $CD34^+$ cells to properly proliferate in DBA-affected individuals is that the RP variant drives ribosomal stress which in turn activates the TP53 pathway resulting in TP53 stabilization and initiation of apoptosis[176]. This TP53 stabilization is shown in the differentiating erythroid cells carrying the 5′UTR variant. To confirm this result, **Figure 14** shows western blotting of LCLs derived from a healthy control, the DBA-affected individual carrying the 5′UTR variant in *RPL9* (P1, c.-2+1G>C), two other DBA-affected individuals (carrying truncating variants in *RPL15*[139]), and from P2 carrying the uL6 (*RPL9*) p.Leu20Pro missense variant. LCLs were treated with DMSO (as a vehicle control) or the topoisomerase inhibitor camptothecin (CPT) as a positive control for 6 h before lysis. The blots were then probed with antibodies against TP53. **Figure 14A and 14B** show that LCLs derived from a healthy control reveal minimal expression of TP53 under basal (DMSO-treated) conditions, and the expected stabilization of TP53 upon a 6-hour treatment with CPT. In contrast, **Figure 14A** shows that LCLs derived from all the DBA-affected individuals including P1 with the *RPL9* c.-2+1 variant reveal substantially more stabilization of TP53 at basal levels, suggesting activation of the TP53 pathway even in the absence of exogenous stress. The addition of CPT to these cells results in further stabilization of TP53. In contrast to the LCLs derived from DBA-affected individuals, **Figure 14B** shows that cells carrying the uL6 (*RPL9*) p.Leu20Pro missense variant do not reveal any basal level stabilization of TP53. These results are in line with the results in **Figure 13**, suggesting that cells carrying the p.Leu20Pro missense variant proliferate normally and are not subject to apoptosis as observed in the cells from the DBA-affected individual.

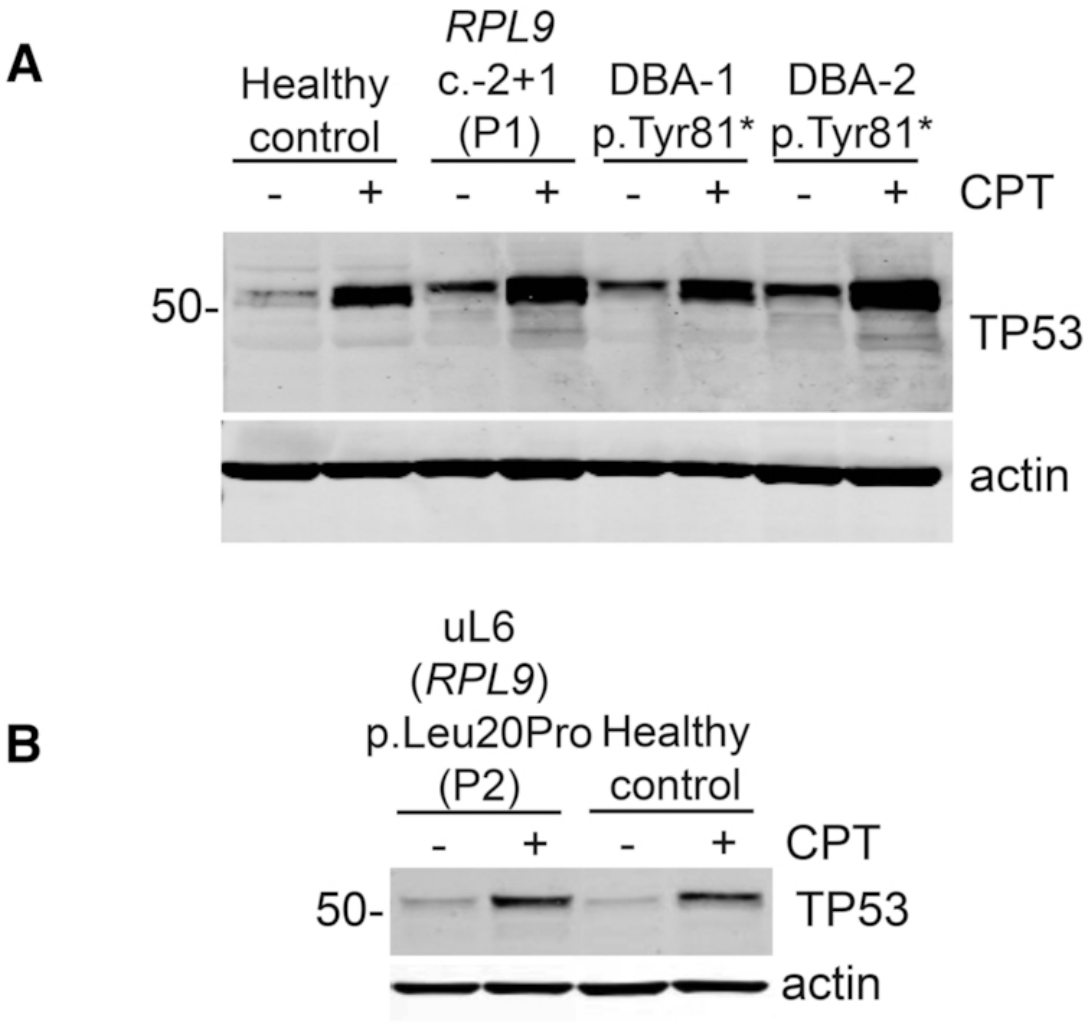

Figure 14: TP53 protein is stabilized in cells carrying the *RPL9* 5'UTR variant

A) Western blots of LCL lysates either treated for 6 h with a DMSO vehicle control (−) or 100 nM camptothecin (CPT, +) probed with antibodies against TP53. LCLs are derived from a healthy control, the DBA-affected individual carrying the *RPL9* c.-2+1 variant (P2), or two unrelated DBA-affected individuals carrying truncations in *RPL15*[139]. B) Similar western blots as in (A) using LCLs derived from the individual carrying the uL6 (*RPL9*) p.Leu20Pro variant (P3). This work was performed by our collaborators.

The uL6 p.Leu20Pro variant is linked to impaired translational fidelity

It has been previously reported that the somatic *RPL10* gene variant (uL16 p.Arg98Ser) linked to T-ALL in humans drives defects in translational fidelity by increasing frequencies of programmed −1 ribosomal frameshifting (-1 PRF) in yeast models[153]. In order to determine if the

uL6 (*RPL9*) p.Leu20Pro variant that is linked to cancer also reveals translational fidelity defects, we measured frameshifting and stop codon readthrough in two different assays with dual luciferase reporter vectors. First, we transfected deidentified LCLs [from a healthy control, P1 carrying the c.-2+1G>C variant or P2 carrying the uL6 (*RPL9*) p.Leu20Pro variant] by nucleofection with reporters designed to measure −1 or +1 PRF or readthrough of stop codons UAA, that have been previously described[101]. **Figure 15** shows that none of the LCLs tested in this assay reveal defects in −1 or +1 PRF or in readthrough of the UAA stop codon.

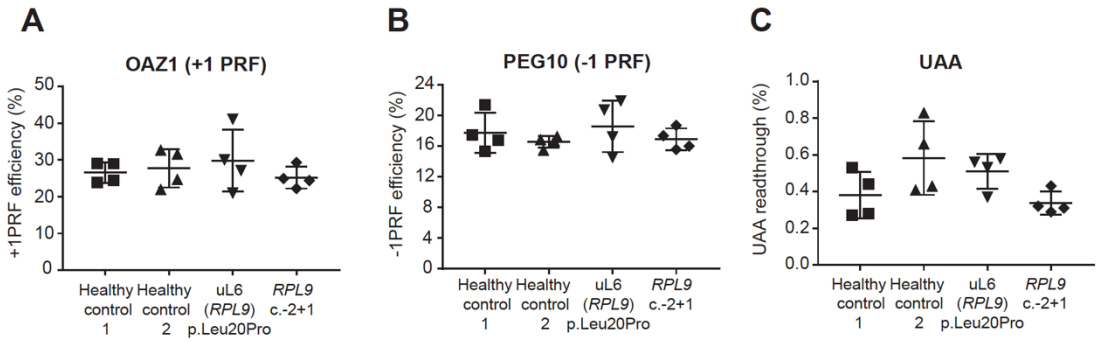

Figure 15: Cell-based assays measuring translational fidelity

A) +1 Programmed Ribosomal Frameshifting (PRF) levels in LCLs derived from individuals carrying variants in RPL9 compared to LCLs derived from two unrelated healthy controls. B) -1 PRF levels in LCLs analyzed in (A). C) UAA stop codon read through levels in LCLs analyzed in (A). This work was performed by the dissertation author.

However, **Figure 16A** shows that LCLs carrying the uL6 (*RPL9*) p.Leu20Pro variant do reveal significant increases ($P < 0.05$ and 0.01) in the readthrough of UAG and UGA stop codons, with the most significant increase being a 2-fold increase of UGA readthrough compared to healthy control LCLs and those carrying the 5′UTR variant. This observation was supported by a separate cell-free assay in **Figure 16B** designed to measure the translational fidelity of purified ribosomes isolated from the LCLs that has also been previously described[163]. This assay showed that only ribosomes isolated from LCLs carrying the uL6 (*RPL9*) p.Leu20Pro variant

(but not the *RPL9* c.-2+1G>C variant) revealed a significant increase in the readthrough of the UAG stop codon over ribosomes purified from healthy control LCLs (**Figure 16B**).

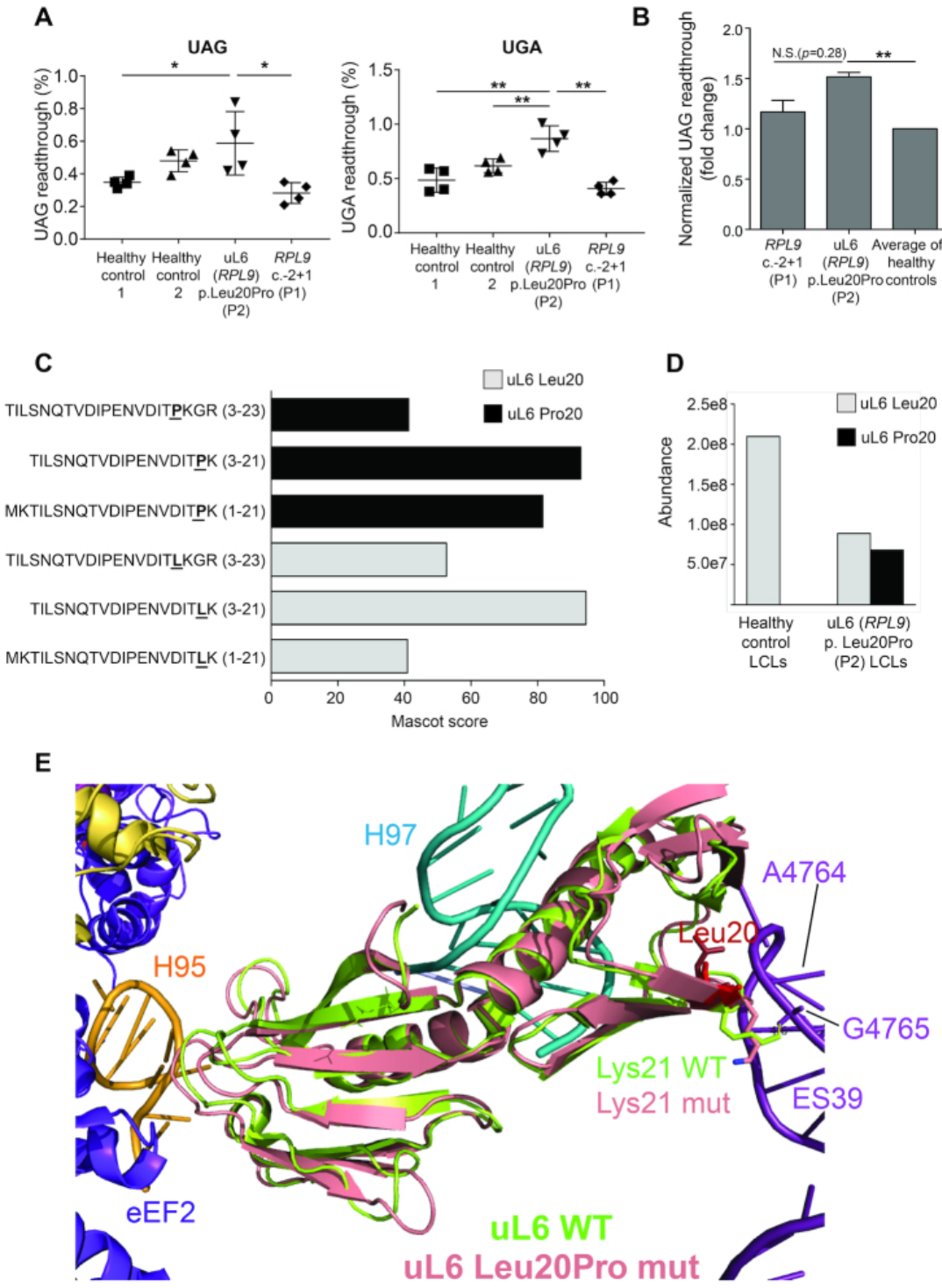

Figure 16: Cells carrying the uL6 p.Leu20Pro variant reveal translational fidelity defects

A) Cell-based assay to measure UAG and UGA stop codon readthough using bicistronic luciferase reporters transfected in LCLs derived from individuals carrying the *RPL9* c.-2+1G>C variant (P2), the uL6 p.Leu20Pro variant (P3), or unrelated healthy controls. *$P < 0.05$, **$P < 0.01$. B) Cell-free assay measuring the level of UAG stop codon readthrough in ribosomes purified from LCLs carrying the *RPL9* c.-2+1G>C (P2) or uL6 p.Leu20Pro (P3) variant compared to LCLs from three unrelated healthy controls. Experiments were performed three times in duplicate with two different preparations of ribosomes per cell type; error bars represent standard error. To determine statistical significance, a paired Student's t-test was applied. **$P < 0.01$. C) MS-based proteomic characterization of ribosomes purified from LCLs of P2 carrying the uL6 p.Leu20Pro variant ($N = 3$). Sequences and scores of peptides identified by Mascot search engine and covering the position 20 of uL6 are presented. On the *y*-axis the amino acid in position 20 of uL6 is in bold font and underlined. D) Quantification of the abundance of uL6 peptides carrying Pro20 or Leu20 measured in purified ribosomes from LCLs generated from a healthy control or P2. E) Predicted structure of uL6 p.Leu20Pro variant protein (in pink) superimposed on the known structure of wild type uL6 (in lime green). Helix 95 of the SRL is shown in gold, amino acid 20 (aa20) is shown in red, rRNA helix 97 is shown in cyan, rRNA extension segment 39 (ES39) is shown in light purple, eEF2 is shown in dark purple, and the positions of the Lys21 (wild type in lime green, variant in pink) are indicated with arrows. Translational fidelity assays performed by the dissertation author and MS characterization was performed by our collaborators.

In order to validate that the ribosomes from the LCLs eliciting the translation fidelity defect do in fact carry the uL6 p.Leu20Pro variant protein, we performed a MS-based proteomic analysis on triplicate purifications of mature ribosomes from P2 LCLs. This allowed the reliable identification of six different peptides mapping to the N-terminal of uL6. Three of these peptides carry a leucine residue at amino acid position 20 and correspond to the wild type sequence of *RPL9*, whereas the three others carry a proline residue at this position and correspond to the *RPL9* variant sequence (**Figure 16C**), indicating that both versions are present in mature ribosomes of P2. Since the identified Leu20 and Pro20 containing peptides are very close in sequence, we used label-free quantification to estimate and compare the abundances of the two uL6 peptide versions in ribosomes purified from P2 LCLs. As shown in **Figure 16D**, it revealed that these ribosomes from P2 LCLs contain about the same quantity of uL6 p.Leu20 and of uL6 p.Pro20 peptides compared to ribosomes purified from healthy control LCLs that exclusively contain uL6 p.Leu20 peptides. These data suggest that the uL6 proteins generated from the wild

type and mutated alleles of *RPL9* contribute about equally to the structure of mature ribosomes in LCLs carrying the uL6 p.Leu20Pro variant.

In order to visualize how the incorporated uL6 p.Leu20Pro protein might alter the ribosome we used Pymol software to model the uL6 structure and its surroundings with either the WT or variant **Figure 16E**, where the protein is found situated in the ribosome between rRNA helix H97 (in cyan) and expansion segment 39 (ES39, in light purple). The WT version containing Leu20 is shown (in lime green), superimposed with the predicted structure of the variant uL6 p.Leu20Pro protein (in pink). The position of amino acid 20 is shown in red. This model predicts that a p.Leu20Pro variant changes the orientation of the end of a beta sheet, which in turn alters the angle of Lys21. Normally, Lys21 interacts with the phosphate group between A4764 and G4765 located in ES39 of the 28S rRNA (measured distance is 4.6 Angstroms, suggesting that this is a salt bridge)[167]. A Pro20 is predicted to alter the orientation of Lys21, disrupting this interaction. This in turn is predicted to weaken the interaction between uL6 and the 28S rRNA. The model also predicts that the p.Leu20Pro variant has some large-scale effects on uL6 folding. These are predicted to affect the other side of the protein, particularly the loop domain that interacts with Helix 95 (H95) of the Sarcin/ricin loop (SRL, shown in gold). Importantly, the SRL plays a key role in activation of the GTPase activity of both the elongation factors (eEF1A and eEF2) as well as the release factor eRF1 (eEF2 is shown in dark purple). Specifically, the model predicts that this loop is displaced toward the SRL, creating the potential for a steric clash. We suggest that this may displace the SRL, interfering with its ability to optimally interact with the elongation and release factors. Consistent with the translational fidelity assays, it also suggests that this potentially altered interaction affects ribosome function, i.e. the ability to faithfully decode mRNAs.

RPL9 variants drive different metabolic profiles in LCLs

In order to determine how the different *RPL9* variants affect cellular metabolism, we used a MS-metabolomics approach to measure the levels of over 120 polar metabolites in LCLs derived from affected individuals and compared them to cells from three unrelated healthy controls. **Figure 17A** shows a heat map of metabolites in LCLs carrying the 5′UTR variant compared to the healthy controls sorted according to their Variable Importance in Projection (VIP) score, with only metabolites with a VIP score >1 shown. The enrichment analysis performed with Metabolanalyst 3.0[177] showing the top 12 terms is shown for this profile in **Figure 17B**. These results suggest that glycolysis in the cells with the 5′UTR variant in *RPL9* is impaired and that the cells have switched to gluconeogenesis, the pathway that results in the formation of glucose from non-carbohydrate carbon sources such as gluconogenic amino acids. The catabolism of amino acids produces ammonia[178]. As such, these cells also reveal significant enrichment of the terms ‘ammonia recycling’ and the ‘urea cycle’, presumably reflecting an excretion of the ammonia (which is highly toxic) resulting from the upregulated catabolism of amino acids during gluconeogenesis.

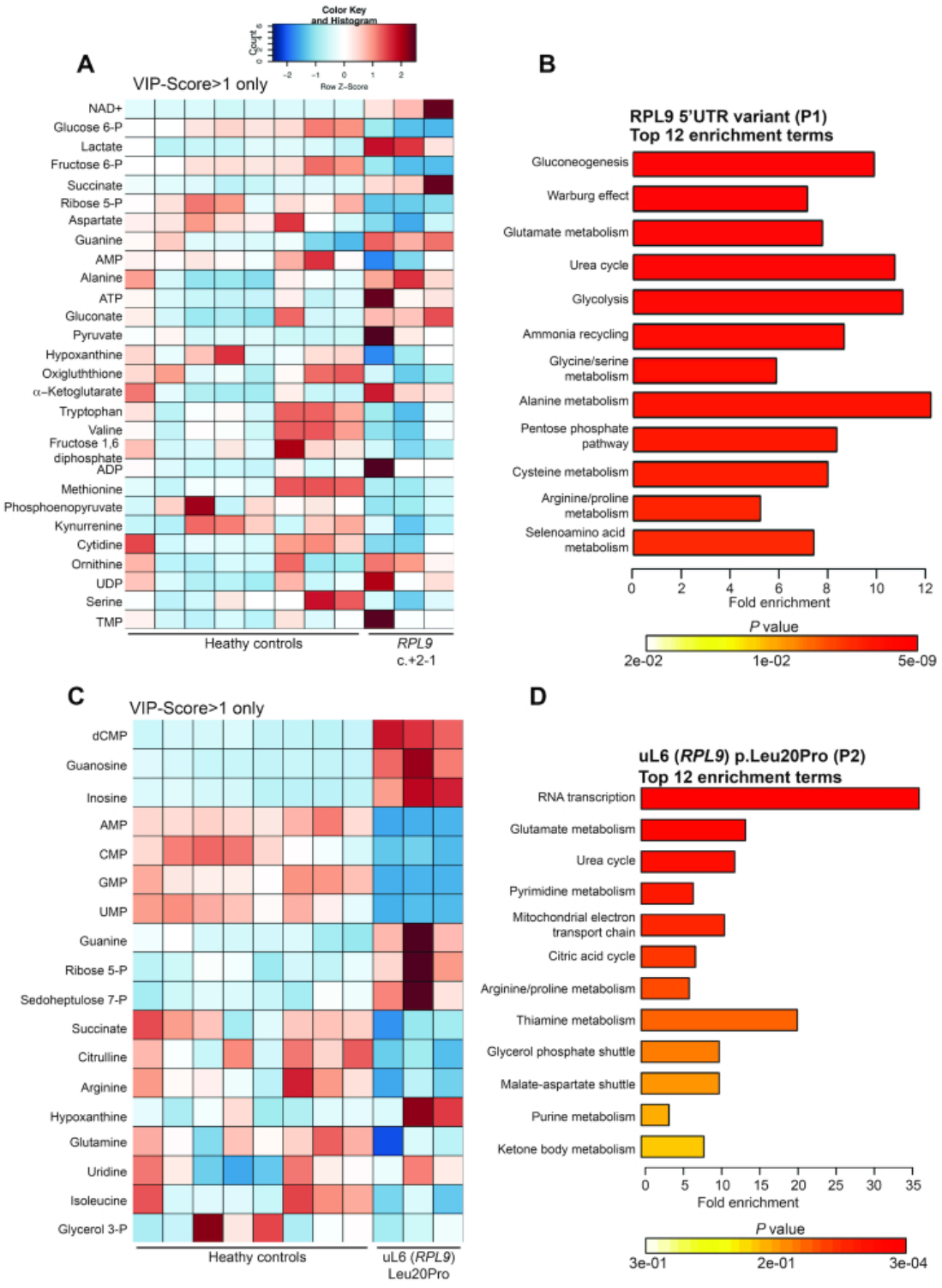

Figure 17: Metabolic profiles and enrichment analysis of LCLs carrying *RPL9* variants

A) Metabolic profile heat map showing *Z*-scores of LCLs derived from three unrelated healthy controls compared to cells from DBA-affected individual (P1) carrying variants in the 5′UTR of *RPL9*. B) Enrichment analysis (using Metabolanalyst 3.0 online software) of significantly

changed metabolites from (A). C) Metabolic profile heat map showing *Z*-scores of LCLs derived from three unrelated healthy controls compared to cells from an individual carrying the uL6 (*RPL9*) p.Leu20Pro variant (P2). D) Enrichment analysis of significantly changed metabolites from (B). For (A) and (C) only metabolites with comparative VIP-Scores >1 (out of 63 metabolites measured) are listed. This work was performed by our collaborators.

A remarkably different metabolic profile and set of enrichment terms are revealed when the same healthy control LCLs are compared to cells carrying the missense uL6 (*RPL9*) p.Leu20Pro variant. **Figure 17C** shows the most significantly downregulated metabolites are nucleotides AMP, CMP, GMP and UMP while the most significantly upregulated metabolites are dCMP, guanosine, and inosine. In contrast to the LCLs carrying the 5′UTR variant, only the amino acid arginine is found significantly downregulated in LCLs carrying the missense variant. **Figure 17D** shows that the top enrichment term in the profiles from LCLs carrying the missense variant is 'RNA transcription' with a 35-fold enrichment (due to the significant reduction of nucleotides) and there is no indication of impaired glycolysis as in the cells with 5′UTR variant. These results suggest that there are some substantial and fundamental differences in the metabolic consequences of the two variants.

Discussion

This study reports that different variants of *RPL9*, a gene that has not been definitively associated with human disease before, are linked to DBA or multiple cancer incidences. Exome sequencing of trios revealed an individual with DBA (P1) carrying a variant of *RPL9* in the 5′UTR. Exome sequencing of tumor and germ line DNA from a family with multiple cancer incidences (P2 and P3) brought to light a missense p.Leu20Pro variant in uL6 (*RPL9*) that is predicted to be damaging. All the variants tested showed defects in the processing of pre-rRNA

and reductions of 80S monosomes that mimic the knockdown of *RPL9* in HeLa cells (**Figures 9, 10, 11**), which strongly suggests that the variants are pathogenic.

Remarkably, the downstream effects of these seemingly similar pre-rRNA defects appear to be largely dependent on the type of variant. The stabilization of TP53 is only observed in cells carrying the *RPL9* 5′UTR variant (**Figure 14**). In turn, only erythroid cells cultured from primary $CD34^+$ cells carrying the 5′UTR variant have defects in proliferation and differentiation and undergo apoptosis (**Figure 13**). In contrast, the p.Leu20Pro missense variant has little effect on $CD34^+$ cells in the erythroid cell culture assay (**Figure 13**). This is well in line with the fact that the individuals carrying the missense variant do not have any bone marrow failure or anemia phenotype.

The polysome profile results in **Figure 11** indicate that the cells carrying the 5′UTR variant of *RPL9* suffer a very substantial reduction of the number of 60S ribosomal subunits. Given that this variant does not modify the uL6 protein itself, it is likely that it impairs translation of *RPL9* mRNA, which results in haploinsufficiency of this ribosomal protein gene as classically described in DBA. Consistently, TP53 is activated, presumably in response to the ribosomal stress resulting from uL6 limiting amount. The p.Leu20Pro variant in turn shows much less impairment of 60S subunit production on the gradients. While pre-rRNA processing is affected in this patient, this variant does incorporate in the mature ribosome and impairs its translational fidelity by increasing the readthrough of UAG and UGA stop codons in a way that is not observed with the 5′UTR variant (**Figure 16**). As such, the uL6 p.Leu20Pro variant may be described as a gain-of-function, since it is changing how certain mRNA stop codons are interpreted. The structural analysis in **Figure 16E** suggests that the incorporation of the uL6 p.Leu20Pro variant may affect ribosomal domains such as the peptidyltransferase center and/or

the Sarcin/Ricin loop (SRL) that are critical for maintaining translational fidelity of the ribosome[179]. However, bona fide structural analysis of 60S ribosomal subunits incorporating the uL6 p.Leu20Pro variant will be required to make any conclusive statements in this regard. Some of the most striking differences of the downstream effects of these *RPL9* variants may be found in the metabolic profiles. The profiles and enrichment analysis of LCLs derived from the DBA-affected individual (**Figures 17A, 17B**) suggest that the 5′UTR variant impairs glycolysis and causes the cells to switch to gluconeogenesis as a means of generating glucose from non-carbohydrate sources, such as glucogenic amino acids. This catabolism of amino acids likely results in an increase of highly toxic ammonia which the cells then excrete by upregulating the urea cycle (another highly enriched term in the analysis of **Figure 17B**). In contrast, cells carrying the missense variant reveal a dramatic reduction of nucleotides that is not observed in the cells with the 5′UTR variant (**Figure 17C**). This is coupled to changes in glutamate metabolism that suggest an accelerated synthesis of RNA, a term that dominates the enrichment analysis in **Figure 17D**. A likely explanation for this profile and accompanying enrichment analysis is that the cells carrying the missense variant are signaling to increase the manufacturing of new ribosomes, which by definition would require a strong upregulation of rRNA synthesis and a depletion of nucleotide pools. Such a metabolic change is not observed with the 5′UTR variant, which may be partly explained by previous observations showing that cells carrying DBA-related RP gene mutations slow down the overall rate of protein synthesis compared to cells carrying RP gene mutations that predominantly affect translational fidelity[101]. The switch to gluconeogenesis observed in the cells carrying the 5′UTR variant also suggests that amino acids in these cells are being preferentially used to supply the cell with energy and not for protein synthesis. The stabilization of TP53 in these cells that we observe may be an important factor

governing this metabolic switch, as it is known that TP53 is able to suppress glucose transport into cells in addition to inducing gluconeogenesis[180].

We propose a genotype:phenotype model for *RPL9* whereby variants that drive the reduction of uL6 are sufficient to drive DBA but not cancer, in contrast to variants that impair translational fidelity. This is supported by the fact that heterozygous *rpl9* zebrafish are not reported to develop tumors[175], although our results in **Figure 12** suggest that both the hetero- and homozygous mutant embryos recapitulate the DBA anemia phenotype. We recognize that in the absence of a mouse model it is difficult for us to state definitively that the cancers found in individuals P2 and P3 are directly linked to the *RPL9* p.Leu20Pro variant. The evidence suggesting the connection is as follows: (i) There are no other obvious driver mutations found in the exomes of either tumor subject to sequence analysis. (ii) The p.Arg98Ser variant in *RPL10*/uL16, linked to human T-ALL, drives translational fidelity defects including stop codon readthrough in yeast[153]. (iii) An increasing body of evidence is linking RP gene variants to different forms of human cancer. This includes DBA-linked and other inherited RP variants that increase the predisposition to cancer as well as variants that arise spontaneously[124,148,152]. (iv) The osteosarcoma and AML described here are cancers frequently observed in DBA patients. So, although we must remain cautious when describing the potential impact of the uL6 p.Leu20Pro variant, it does seem possible that the translational fidelity defects are contributing to instability in cells that ushers them closer to the tipping point of malignancy. Supporting this mechanism is the finding that yeast cells with a defective non-stop decay pathway (and synthesizing aberrant proteins coded from 3′UTRs) reveal an increased sensitivity to oxidative stress, which has well-known links to cancer[181,182]. This will be a very interesting area of future study as more variants

in human genes coding for components that regulate mRNA translation are identified and characterized.

In sum, this study reports different variants of *RPL9*, a gene that has not been previously associated with human disease, drive similar defects in pre-rRNA processing yet have remarkably different impacts downstream of this initial ribosome biogenesis defect. The results suggest a model whereby cells carrying a DBA-linked RP variant generate fewer 60S ribosomal subunits overall, reduce glycolysis, switch to gluconeogenesis, and catabolize amino acids as a carbon source. This is accompanied by reduced cell proliferation, increased TP53 stabilization, and apoptosis. In contrast, the incorporation of the uL6 p.Leu20Pro variant into 60S ribosomal subunits does not severely affect the production rate of 60S subunit, but compromises the fidelity of the ribosome by increasing the readthrough of stop codons. Taken together, these results underscore the widening landscape of cellular and clinical phenotypes that are associated with human RP gene variants. They also suggest that despite similar pre-rRNA processing defects in cells carrying different variants of the same RP gene, the downstream effects can diverge dramatically and in ways that may help to clarify the biology underlying these complex genotype:phenotype relationships.

Acknowledgements

Our most special thanks go to the patients and their families. Very special thanks also to the DBA UK Charity for their generous support.

Funding

Specific E-Rare grants funding EuroDBA researchers [ZonMW #40-44000-98-1008 in the Netherlands to A.W.M.; #BMBF 01GM1609 in Germany to M.W., #ANR-15-RAR3-0007-04 to P.E.G. and M.O.D., #ANR-15-RARE-0007-03 to L.D.C. in France]; P.E.G., M.F.O.D. and L.D.C. are also funded by ANR-15-CE12-0001 (DBA-Multigenes); L.D.C. is additionally supported by the Laboratory of Excellence for Red Cells [(LABEX GR-Ex)-ANR Avenir-11-LABX-0005-02]; French National PHRC OFABD (DBA registry); J.D.D. and C.M.dS.V. are supported by a grant from the United States National Institutes of Health/National Heart Lung and Blood Institute [R01HL119439-01A1]; G.Z. and A.N.O. are supported by Jim and Diann Robbers Cancer Research Grant for New Investigators; I.J.D. is funded by the KiKa Foundation [127]; M.C.J.J. and I.D. are supported by Stichting Loeka (http://www.stichtingloeka.nl/); M.P. and L.M. are supported by Pallotti Legacy for Cancer Research. Funding for open access charge: ZonMW; DBA UK. Proteomic experiments were partly supported by ProFI [ANR-10-INBS-08-01 grant].

Chapter 3: De Novo variants in EEF2 cause a neurodevelopmental disorder with benign external hydrocephalus[183]

Maria J. Nabais Sá[1,2,‡,†], Alexandra N. Olson[3,‡], Grace Yoon[4], Graeme A.M. Nimmo[5], Christopher M. Gomez[6], Michèl A. Willemsen[7], Francisca Millan[8], Alexandra Schneider[3], Rolph Pfundt[1], Arjan P.M. de Brouwer[1], Jonathan D. Dinman[3,*,‡] and Bert B.A. de Vries[1,*,¶]

[1]Department of Human Genetics, Radboud University Medical Center and Donders Institute for Brain, Cognition and Behavior, 6525 GA Nijmegen, The Netherlands,
[2]Unit for Multidisciplinary Research in Biomedicine, Instituto de Ciências Biomédicas Abel Salazar/Universidade do Porto, 4050-313 Porto, Portugal,
[3]Department of Cell Biology and Molecular Genetics, University of Maryland, College Park, MD 20742, USA,
[4]Division of Clinical and Metabolic Genetics and Division of Neurology, The Hospital for Sick Children, University of Toronto, Toronto, ON M5G 1X8, Canada,
[5]Fred A Litwin Family Centre for Genetic Medicine, University Health Network/Mount Sinai Hospital, Toronto, ON M5T 3L9, Canada,
[6]Department of Neurology, The University of Chicago, Chicago, IL 60637, USA,
[7]Department of Pediatric Neurology, Radboud University Medical Center and Donders Institute for Brain, Cognition and Behavior, Amalia Children's Hospital, 6525 GA Nijmegen, The Netherlands and
[8]GeneDx, Gaithersburg, MD 20877, USA

[‡]Authors contributed equally

Work adapted from Human Molecular Genetics, December 2020, DOI: 10.1093/hmg/ddaa270

Abstract

Eukaryotic translation elongation factor 2 (eEF2) is a key regulatory factor in gene expression that catalyzes the elongation stage of translation. A functionally impaired eEF2, due to a heterozygous missense variant in the *EEF2* gene, was previously reported in one family with spinocerebellar ataxia-26 (SCA26), an autosomal dominant adult-onset pure cerebellar ataxia. Clinical exome sequencing identified *de novo EEF2* variants in three unrelated children presenting with a neurodevelopmental disorder (NDD). Individuals shared a mild phenotype comprising motor delay and relative macrocephaly associated with ventriculomegaly.

Populational data and bioinformatic analysis underscored the pathogenicity of all *de novo* missense variants. The eEF2 yeast model strains demonstrated that patient-derived variants affect cellular growth, sensitivity to translation inhibitors and translational fidelity. Consequently, we propose that pathogenic variants in the *EEF2* gene, so far exclusively associated with late-onset SCA26, can cause a broader spectrum of neurologic disorders, including childhood-onset NDDs and benign external hydrocephalus.

Introduction

The *EEF2* gene (MIM: 130610) encodes the eukaryotic translation elongation factor 2 (eEF2), a catalyst required for the elongation of polypeptide chains during mRNA translation[21]. It coordinates structural changes in the ribosome—from its pre- to post-translocational state—that result in the displacement of messenger RNA (mRNA) and transfer RNA (tRNA) molecules. Specifically, after peptide bond formation, eEF2 catalyzes the GTP-dependent translocation of a peptidyl-tRNA from the A to the P site and a deacylated-tRNA from the P to the E(xit) site while moving the ribosome one codon in the 3′ direction along the mRNA. In line with its fundamental role in protein synthesis, eEF2 is ubiquitously expressed. The functional conservation of eEF2 mirrors the structural conservation of this gene sequence among eukaryotes, from yeast to human[184,185]. The eEF2 is composed of five domains involved in polypeptide elongation. Domains I and II cluster together to form the GTP-binding pocket. The interactions between domains I, II, III and V with Helices 98 (the Sarcin/Ricin loop or SRL) and 43 (the GTPase associated center or GAC) of the large ribosomal subunit rRNA coordinate and stimulate the GTPase activity of eEF2 and translocation. The interaction of domain IV Helix 69 is thought to

help coordinate the movement of eEF2 with the peptidyl and deacylated tRNAs in the ribosome[186].

To date, the heterozygous p.(Pro596His) substitution was the only known variant of the *EEF2* gene associated with human disease, specifically the autosomal dominant late-onset spinocerebellar ataxia 26 (SCA26 [MIM: 609306])[103]. This variant was carried by 24 affected individuals and two asymptomatic individuals (age range: 26–60 years) of a six-generation Norwegian family with pure cerebellar ataxia[103]. Atrophy of the cerebellum was demonstrated in 11 affected individuals[103]. Functional studies in yeast demonstrated that the SCA26 p.(Pro596His) variant (P580H in the *EFT2* gene in yeast) resulted in specific translational fidelity defects and a greater susceptibility to proteostatic stress[103]. As the *EFT2* P580H substitution did not cause gross destabilization or mislocalization of the protein, it was concluded that it retained a degree of biological function that is compatible with life[103]. We identified *de novo EEF2* missense variants in three children with neurodevelopmental delays and various structural brain abnormalities, including benign external hydrocephalus. Additionally, we provide *in vitro* and *in vivo* evidence that these variants alter cell growth and translational fidelity, resulting in a broader spectrum of *EEF2*-related neurodevelopmental disorders (NDD).

Materials and methods

Patients

Two unrelated Dutch individuals were enrolled at the outpatient clinic of the Department of Human Genetics, Radboudumc (Nijmegen, The Netherlands). One additional individual was identified with the collaboration of GeneDx through GeneMatcher[187]. Likely pathogenic variants were detected by performing clinical exome sequencing of DNA extracted from peripheral blood

samples of the affected individuals and parents (trio analysis). This study was approved by the institutional review board Commissie Mensgebonden Onderzoek Regio Arnhem-Nijmegen (CMO-nr 2018-4736) and informed consent for enrollment was obtained from all legal representatives.

Exome sequencing

Individual 1

Using genomic DNA from the proband and parents, the exonic regions and flanking splice junctions of the genome were captured using the IDT xGen Exome Research Panel v1.0. Massively parallel (NextGen) sequencing was done on an Illumina system with 100 bp or greater paired-end reads. Reads were aligned to human genome build GRCh37/UCSC hg19, and analyzed for sequence variants using a custom-developed analysis tool. Additional sequencing technology and variant interpretation protocol has been previously described[188]. The general assertion criteria for variant classification are publicly available on the GeneDx ClinVar submission page (http://www-ncbi-nlm-nih-gov.proxy-um.researchport.umd.edu/clinvar/submitters/26957/).

Individuals 2 and 3

Exome sequencing was performed as previously described[189].

The variants identified in this study were submitted to the Leiden Open Variation Database (https://databases.lovd.nl/shared/genes/EEF2).

Yeast strains

EFT2-6xHis variants were generated by site-directed mutagenesis of pJD2490 (YCp*EFT2-LEU2*) using the Aligent QuikChange Lightning Kit (Aligent Technologies, catalog #210519) per the manufacturer's instructions. Mutagenic oligos were synthesized by Genewiz

(See Appendix 4). *EFT2* strains were generated by alkali cation transformation of *EFT2*-6xHis encoding plasmids into yJD995 (MATa *ade2 ura3 his3 leu2 trp1 eft::HIS3 eft2::TRP1* +YCp*EFT1*-*URA3*) using negative 5-FOA selection to shuffle out the endogenous *EFT1* plasmid (See Appendix 1 and 2). Once viable colonies were obtained, cells were grown in YPAD and the plasmids were isolated using the GeneJET Plasmid Miniprep Kit (Thermo Scientific, Catalog # K0503) and transformed into Stellar competent cells (Clontech, catalog # 636766) to generate plasmid for sequencing. Bacterial colonies were miniprepped using the GeneJET kit and the plasmids were sequence-verified by Genewiz using Sanger sequencing.

Translational fidelity assays

EFT2 variant yeast strains were transformed with dual-luciferase reporter constructs as above. Transformants were selected auxotrophically for the *URA3* gene encoded on the reporter plasmid. For each assay, reporter-transformed yeast cultures were inoculated in synthetic-complete medium lacking uracil and allowed to grow to late logarithmic phase. Strains were then diluted to an optical density at 600 nm (OD_{600}) of 0.4 in fresh medium and allowed to grow for 2 h. Yeast strains were lysed in Passive Lysis Buffer (Promega) and the lysate was split into three wells of a white 96-well plate. Dual-luciferase assays were conducted with a Promega GloMax Multi+ Detection System using the Dual-Luciferase Reporter Assay System (Promega, Catalog # E1960) as described by the manufacturer. For each strain, the Firefly and *Renilla* luminescences were found by averaging the luminescence for the three triplicate wells. Ratios of programmed ribosomal frameshifting (PRF) for each strain were calculated by dividing the ratios of Firefly to *Renilla* luminescence of the test reporter by the read-through luminescence ratio for that strain. Assay replicates were normalized by dividing recoding

percentages by that of the WT strain to give fold-change (FC) values. Experiments were repeated with 10 biological replicates for each reporter construct and data were analyzed by ordinary one-way ANOVA using GraphPad Prism. *P*-values were calculated from Tukey's multiple comparisons tests between the WT and each variant. $^{*}P<0.05$, $^{**}P<0.01$, $^{***}P<0.001$. Graphs show the median, interquartile range and range of data for each genotype.

Assays of cellular growth

Yeast strains were grown to logarithmic phase in YPAD medium at 30°C then diluted to an OD_{600} of 0.05 in 100 µL of YPAD medium or YPAD medium with hygromycin B, cycloheximide, anisomycin or paromomycin (20 µg/mL, 50 ng/mL, 15 µg/mL and 5 mg/mL, respectively) in two wells of a sterile 96-well plate. Yeast strains were grown in a Synergy HTX plate reader (BioTek, catalog #S1A) at 30°C, where the OD_{600} of each well was taken every 15 min for 48 h, with shaking for 10 min preceding each measurement. The average absorbance of wells containing only medium or medium with translational inhibitor was subtracted from each measurement, which were then averaged across the two triplicate wells for each strain at every time point. Non-linear regression was performed with GraphPad Prism to fit the exponential phase to an exponential growth function. Doubling time was calculated by dividing ln(2) by the rate parameter found through non-linear regression. Heat map values were generated by calculating the $\log_2$ of the FC for each variant relative to WT in the presence of each translational inhibitor, which was then subtracted from the $\log_2$(FC) for growth of corresponding variant in rich media. Experiments were repeated with three biological replicates.

Results

De novo EEF2 variants are likely deleterious

De novo missense variants in the *EEF2* gene (NM_001961.3) were identified in peripheral blood samples of three unrelated individuals presenting with NDD (**Table 3**). None of the variants were found in the individual's parents, none of whom were consanguineous, nor did any have first degree relatives with a NDD. No other likely pathogenic variants were identified in additional candidate genes. *EEF2* variants were localized throughout the gene (**Figure 20A**) and occurred in highly conserved amino acids, considering 12 species (**Figure 18**). None of the *EEF2* variants were present in the Genome Aggregation Database (gnomAD)[190]. Population data available in gnomAD indicated that the gene is highly constrained for predicted loss-of-function (pLoF) and missense variation (LOEUF = 0.172, misZ score = 4.878)[190]. Furthermore, all missense variants were predicted to be likely pathogenic by a CADD score above 20[191]. Structurally, all *de novo* missense *EEF2* variants mapped to functionally important locations within the protein (**Figure 19**). Specifically, p.(Cys388Tyr) is positioned at a critical interface between domains I and II, p.(Val28Met) is at the base of domain I where it directly contacts the SRL, and p.(His769Tyr) is located in domain V, which is known to interact with the GAC at the tip of Helix 43.

Table 3: *De novo* missense variants in *EEF2*

Individual	cDNA change [a]	Amino acid change [b,c]	Protein domain	CADD score	Corresponding yeast variant [d]
1	c.82G>A	p.(Val28Met)	G domain (Domain I)	28.5	V28M
2	c.1163G>A	p.(Cys388Tyr)	Domain II	33	C372Y
3	c.2305C>T	p.(His769Tyr)	Domain V	24.2	Q753Y

[a] GenBank: NM_001961.3
[b] GenBank: NP_001952.1
[c] None of these variants is present in the Genome Aggregation Database (gnomAD).
[d] For complete description of the eEF2 yeast variants, please see Appendix 2

```
P13639|Human          MVNFTVDQIR AIMDKKANIR NMSVIAHVDH GKSTLTDSLV CKAGIIASAR AGETRFTDTR  60
P58252|Mouse          MVNFTVDQIR AIMDKKANIR NMSVIAHVDH GKSTLTDSLV CKAGIIASAR AGETRFTDTR  60
Q6P3J5|Zebrafish      MVNFTVDQIR AIMDKKSNIR NMSVIAHVDH GKSTLTDSLV SKAGIIASAR AGETRFTDTR  60
P13060|Fruit fly      MVNFTVDEIR GLMDKKRNIR NMSVIAHVDH GKSTLTDSLV SKAGIIAGAK AGETRFTDTR  60
P29691|Worm           MVNFTVDEIR ALMDRKRNIR NMSVIAHVDH GKSTLTDSLV SKAGIIAGSK AGETRFTDTR  60
P32324|Yeast          MVAFTVDQMR SLMDKVTNVR NMSVIAHVDH GKSTLTDSLV QRAGIISAAK AGEARFTDTR  60

P13639|Human          ALLQMITIHL PSPVTAQKYR CELLYEGPPD DEAAMGIKSC DPKGPLMMYI SKMVPTSDKG  408
P58252|Mouse          ALLQMITIHL PSPVTAQKYR CELLYEGPPD DEAAMGIKSC DPKGPLMMYI SKMVPTSDKG  408
Q6P3J5|Zebrafish      ALLQMITIHL PSPVTAQKYR CELLYEGPGD DEAAMGIKNC DPKGPLMMYI SKMVPTTDKG  408
P13060|Fruit fly      ALLQMIAIHL PSPVVAQKYR MEMLYEGPHD DEAAIAVKSC DPDGPLMMYI SKMVPTSDKG  394
P29691|Worm           TMLQMIAFHL PSPVTAQKYR MEMLYEGPHD DEAAVAIKTC DPNGPLMMYI SKMVPTSDKG  402
P32324|Yeast          ALLEMIVLHL PSPVTAQAYR AEQLYEGPAD DANCIAIKNC DPKADLMLYV SKMVPTSDKG  392

P13639|Humen          HVFEESQVAG TPMFVVKAYL PVNESFGFTA DLRSNTGGQA FPQCVFDHWQ ILPGDPFDNS  828
P58252|Mouse          HVFEESQVAG TPMFVVKAYL PVNESFGFTA DLRSNTGGQA FPQCVFDHWQ ILPGDPFDNS  828
Q6P3J5|Zebrafish      HVFEESQVMG TPMFVVKAYL PVNESFGFTA DLRSNTGGQA FPQCVFDHWQ ILPGDPKDAA  828
P13060|Fruit fly      HVFEENQVVG TPMFVVKAYL PVNESFGFTA DLRSNTGGQA FPQCVFDHWQ VLPGDPSEPS  814
P29691|Worm           HVFEESQVTG TPMFVVKAYL PVNESFGFTA DLRSNTGGQA FPQCVFDHWQ VLPGDPLEAG  822
P32324|Yeast          QVVSEEQRPG TPLFTVKAYL PVNESFGFTG ELRQATGGQA FPQMVFDHWS TLGSDPLDPT  812
```

Figure 18: Cross-species alignment by Clustal Omega[192] of the protein sequences directly surrounding the three *de novo* missense variants in *EEF2*, p.(Val28Met), p.(Cys388Try), and p.(His 769Tyr).

The changes are highlighted by the black boxes and all conserved down to the zebrafish. Protein accession numbers used for alignment are given before the sequences and include the specific species. The position of the last amino acid residue in each row is given right after the respective sequences.

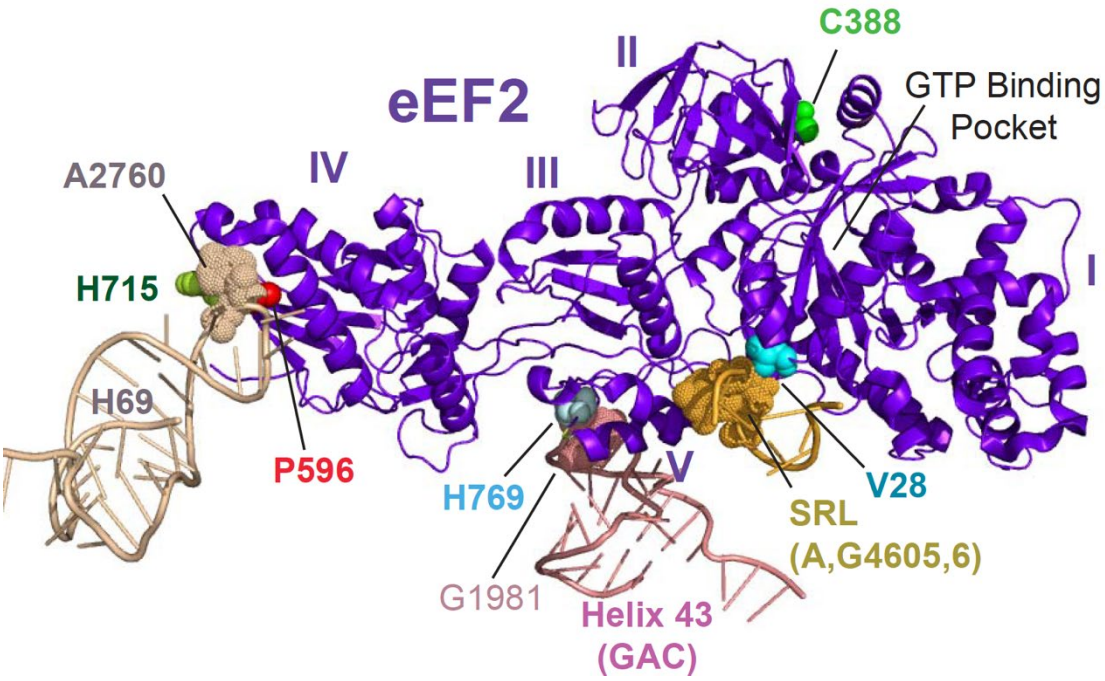

Figure 19: De novo human missense EEF2 variants mapped to the 857-amino acid human eEF2 protein [Homo sapiens protein EF2_HUMAN (P13639)] suggesting that these variants disturb the structure of eEF2, specifically at critical intermolecular interfaces between eEF2 and the ribosome (H43, H69 and the SRL), or intramolecular interfaces between Domains I and II.

eEF2 is purple, and domains are indicated as roman numerals. The amino acid residues examined in this study are shown as colored spheres: V28 (light blue), C388 (dark red) and H769 (dark blue). The amino acid residue mutated in SCA26, P596, is shown as light red spheres. Large ribosomal subunit rRNA structures (H43, H69 and the SRL) are indicated as are important rRNA bases (G1981 and A2760).

Individuals with de novo missense EEF2 variants share neurodevelopmental delay and other structural and functional nervous system abnormalities

All three male individuals of 3, 6 and 9 years of age had neurodevelopmental delays (**Table 4**). Ages of walking were 22, 24 and 26 months and ages at first words were 12, 15 and 24 months. Neurologic abnormalities (2/3) included hypotonia, gait instability, poor motor coordination and seizures. Morphological central nervous system (CNS) abnormalities were also frequent (3/3) (**Figure 20**). All individuals had some widening of cerebrospinal fluid (CSF) spaces, especially dilated lateral and third ventricles. Individual 1 had additional abnormalities of the cerebral morphology, i.e. diffuse thinning of the corpus callosum and left temporo-occipital focal dysplasia. Behavioral problems (1/3) included autistic behavior. At physical examination, all individuals had a head relatively larger than expected for height. Short stature could be observed in individual 3. Furthermore, they shared facial dysmorphisms, namely a prominent forehead with a high hairline, small and low-set ears with a prominent helix and antihelix, deep set eyes with narrow palpebral fissures, a short nose, a thin upper lip and a small (prominent) chin (**Figure 20**). Interestingly, both individuals 1 and 2 had fine and sparse scalp hair, sparse eyebrows and nail dysplasia (hypoplastic and dystrophic toenails). Individual 3 had, fast growing hair and nails, except for the toenails of the 5th toes that were hypoplastic. Minor hand abnormalities (3/3) included bilateral palmar creases, short and tapering fingers, and 5th finger clinodactyly. Mild 2–3 toe syndactyly was observed in individual 1. Ophthalmologic abnormalities (2/3) included strabismus requiring surgery and myopia.

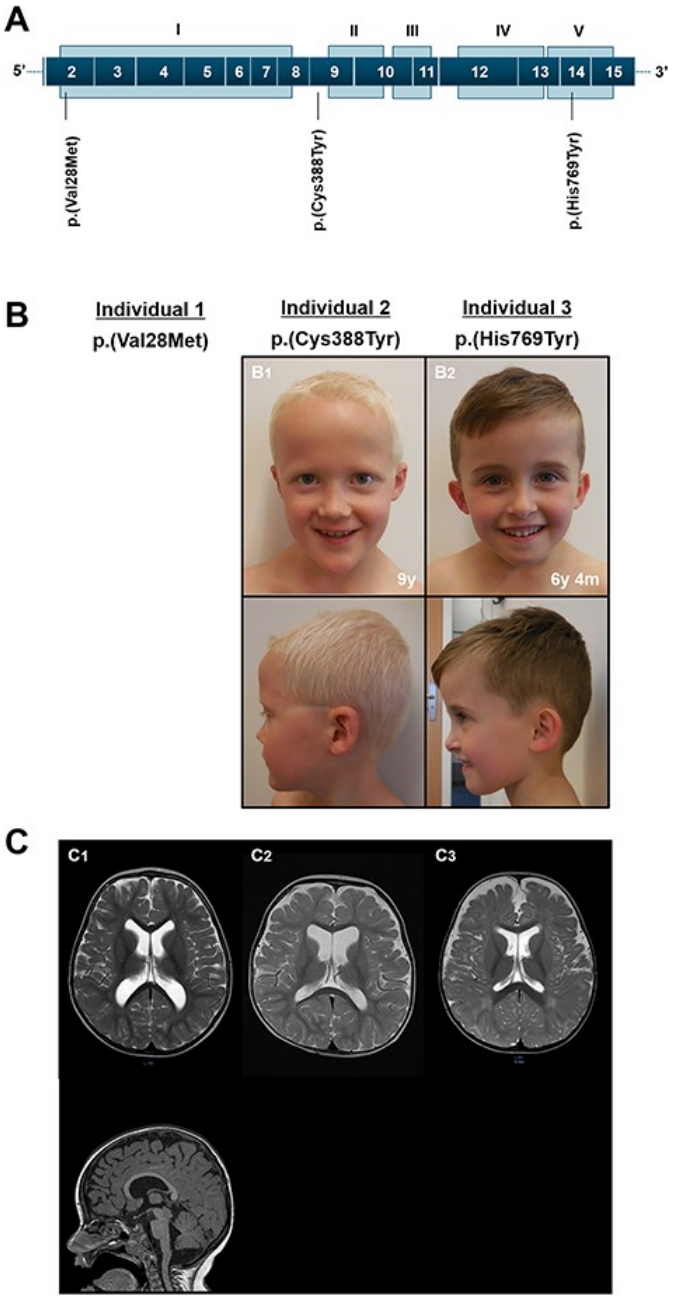

Figure 20: *De novo* pathogenic *EEF2* variants cause a NDD with minor craniofacial dysmorphisms and structural brain abnormalities

(A) EEF2 transcript (NM_001961.3) and human de novo EEF2 variants within or adjacent to specific domains of the eEF2 protein (NP_001952.1). (B) Individuals 1, 2 (B1) and 3 (B2) had a large head with a prominent forehead. (C) Axial, T2-weighted MR images of individuals 1 (C1, upper panel), 2 (C2) and 3 (C3), showing mild enlargement of lateral ventricles and external CSF spaces. Sagittal, T1-weigthed MR image of individual 1 (C1, lower panel) illustrates the diffuse thinning of the corpus callosum. This work was performed by our collaborators.

Table 4: Genotype and phenotype of individuals with *de novo* pathogenic variants in the *EEF2* gene

Individuals	**1**	**2**	**3**
Gender / Age at examination	M / 3y 10m	M / 9y	M / 6y 4m
Genotype			
cDNA change [a]	c.82G>A	c.1163G>A	c.2305C>T
Protein change [b]	p.(Val28Met)	p.(Cys388Tyr)	p.(His769Tyr)
Inheritance	*de novo*	*de novo*	*de novo*
Phenotype			
Growth [c]			
Gestational age at birth	39w	37w	38w
Length at birth (centile range)	NA	52 cm	NA
Weight at birth (centile range)	3345 g (25-50th)	3440 g	2470 g (3rd-15th)
HC at birth (centile range)	NA	35 cm	NA
Age at measurements	3y 10m	6y / 9y	6y 4m
Height (centile range) [c]	101 cm (~50th)	111 cm (~20th) / 130 cm (~30th)	102 cm (-2.5SD)
Weight (centile range) [c]	18 kg (~85th)	19 kg (~25th) / 26.4 kg (30th)	15.5 kg (-2.2SD)
HC (centile range) [c]	52 cm (85-97th)	52.7 cm (80th) / 53.4 cm (75th)	52.3 cm (~75th)
Prenatal & neonatal history			
Congenital abnormalities	periscrotal hypospadias	NA	-
Other neonatal problems	jaundice requiring phototherapy	NA	-
Psychomotor development			
Motor delay	+	+	+
Age at walking	22m	24m	26m
Speech delay	+	+	+
Age at first words	15m	24m	12m
Intellectual disability	-	-	-
Degree of intellectual disability	n.a.	n.a.	mild
Neurologic and psychiatric features			
Neurological abnormalities	+ (hypotonia, unsteady gait, high stepping)	+ (poor motor coordination)	-
Brain abnormalities (brain MRI or CT)	+ (mild-moderate enlargement of lateral and third ventricles, diffuse thinning of CC, left temporo-occipital focal dysplasia)	+ (mild-moderate enlargement of the lateral and third ventricles and external CSF spaces)	+ (mild enlargement of the lateral ventricles and external CSF spaces)
Seizures (age of onset / type)	+ (2y 6m / 2 febrile seizures)	-	-
Abnormal EEG (age / result)	- (2y 7m / normal)	n.a.	n.a.
Behavioral problems	-	+ (autistic behavior)	-
Dysmorphic features			
Craniofacial dysmorphisms	+ (minor)	+ (minor)	+ (minor)
Hands	+ (bilateral single transverse palmar creases; short fingers; clinodactyly of the 5th finger)	+ (clinodactyly of the 5th finger)	+ (tapering fingers)

Feet	+ (mild 2-3 toes syndactyly)	-	-
Other abnormalities			
Abnormal vision	+ (strabismus requiring surgery)	+ (myopia)	-
Skin / hair / nails abnormalities	+ (fine sparse scalp hair, sparse eyebrows, hypoplastic and dystrophic toenails, capillary malformations)	+ (fine sparse scalp hair, fast growing and brittle toe nails)	+ (fast growing hair and nails, hypoplastic nails of 5th toes)
Musculoskeletal system abnormalities	-	+ (mild joint laxity)	-

Abbreviations are as follows: +, present; -, absent; F, female; M, male; y, years; m, months; w, weeks; SD, standard deviation; HC, head circumference; CC, corpus callosum; CSF, cerebrospinal fluid; NA, not available; and n.a., not applicable.
[a] GenBank: NM_001961.3
[b] GenBank: NP_001952.1
c Percentile range; if the percentile is <3rd or >97th, standard deviation (SD) is indicated.

De novo EEF2 variants alter cellular growth and sensitivity to translational inhibitors

Often used as a genetic model for human diseases, the yeast *Saccharomyces cerevisiae* protein translation apparatus is highly similar to that of higher eukaryotes. The eEF2 amino acid sequence is 66% identical with 85% homology between yeast and humans at the DNA and protein levels, respectively[184,185], making this organism a viable substitute for functional analysis. Thus, a yeast model system was used to investigate the functional consequences of eEF2 variants. Yeast eEF2 mutants were constructed using a strain (generously donated by Dr Terri Kinzy) in which both endogenous copies of the paralogous eEF2 genes, *EFT1* and *EFT2*, were disrupted and replaced with a low-copy plasmid bearing the *EFT2* gene[28]. A multiple sequence alignment was used to determine equivalent codons within the *Homo sapiens* and *S. cerevisiae* eEF2 sequence. If the position of the variant was not conserved, two yeast strains were constructed: one containing the equivalent *H. sapiens* codon and the other, the allele of the affected individual. Additionally, the P580H and H699N alleles were employed as positive controls because their functional defects have been previously characterized in yeast systems[65,103,193].

Growth curves were collected in order to determine whether the sole expression of variant eEF2 would have an effect on cell growth rates. Most eEF2 variants demonstrated overall slower growth, i.e. increased doubling times, indicating disruption to normal growth but retention of viability (**Figure 21A**). Surprisingly, the V28M allele enhanced cellular growth rates relative to the wild-type (WT) eEF2.

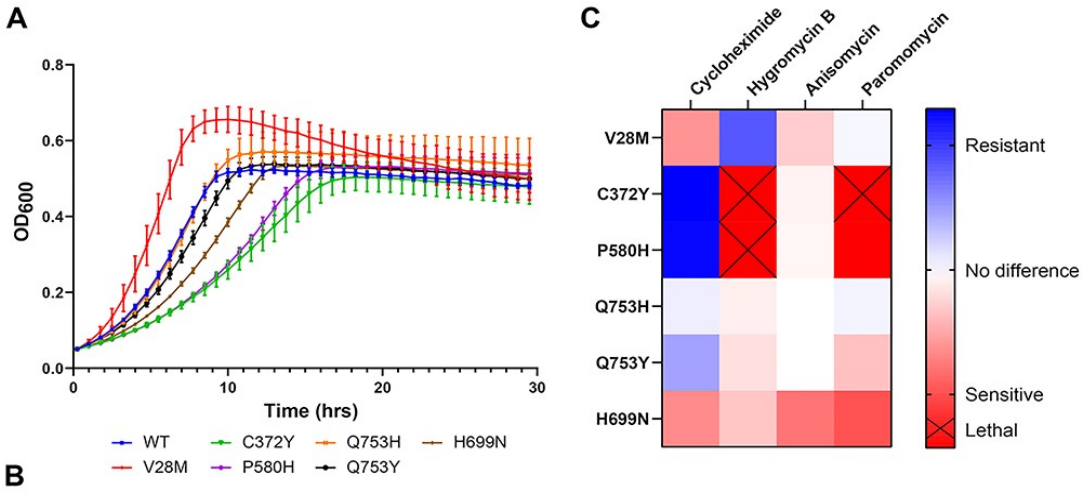

B

	Doubling time (hours)				
	YPAD	Cycloheximide	Hygromycin B	Anisomycin	Paromomycin
WT	2.28 ± 0.02	5.21 ± 0.03	3.92 ± 0.05	2.67 ± 0.02	3.25 ± 0.02
V28M	1.59 ± 0.01	4.46 ± 0.04	2.03 ± 0.02	2.04 ± 0.03	2.25 ± 0.01
C372Y	4.02 ± 0.04	5.92 ± 0.08	–	4.81 ± 0.04	–
P580H	3.92 ± 0.02	5.76 ± 0.02	–	4.67 ± 0.03	9.17 ± 0.17
Q753H	2.28 ± 0.02	5.08 ± 0.03	4.05 ± 0.05	2.66 ± 0.01	3.18 ± 0.02
Q753Y	2.58 ± 0.02	4.99 ± 0.02	4.70 ± 0.05	3.01 ± 0.02	4.14 ± 0.03
H699N	3.12 ± 0.02	8.92 ± 0.13	5.98 ± 0.03	4.77 ± 0.09	6.21 ± 0.06

Figure 21: Growth phenotypes of eEF2 model yeast strains showed altered cellular growth and sensitivity to translational inhbitors

(A) Growth curves of WT and variant yeast strains in rich media. Of the de novo variants, V28M exhibited an increased growth rate, while C372Y and Q753Y showed varying decreased growth rates. The growth rate of the control Q753H was equivalent to the WT, validating the yeast model approach. Error bars denote standard deviation. (B) Doubling times of all model strains in media with varying translational inhibitors. Doubling time was calculated by dividing ln(2) by the growth rate, which was found by non-linear regression of the exponential phase of each growth curve. Missing values indicate strains that were inviable. Errors denote 95% confidence intervals. (C) Heat map illustrating the effects of each translational inhibitor on growth of the variant yeast strains relative to WT. Cycloheximide: V28M sensitive; C372Y, Q753Y resistant. Hygromycin B: C372Y lethal; Q753Y sensitive; V28M resistant. Anisomycin: V28M sensitive; C372Y, Q753Y no change. Paromomycin: C372Y lethal; Q753Y sensitive; V28M no change. Heat map values were generated by calculating the log2 of the fold-change relative to WT for each variant's doubling time in the presence of each translational inhibitor.

This was then subtracted from the log2(FC) for growth of the corresponding variant in rich media. This work was performed by the dissertation author.

Translational inhibitors can be used as probes to indicate specific aspects of the protein synthetic process that may be altered by variants. Paromomycin is an aminoglycoside whose binding to the small subunit rRNA increases misreading by decreasing the ability of the ribosome to proofread incoming aminoacyl-tRNAs, and also by inhibiting translocation[194]. Hygromycin B is also an aminoglycoside that binds close to the decoding center near the top of helix 44 of small subunit rRNA. Although it does cause some miscoding, its major effect is to inhibit translocation by sequestering peptidyl-tRNA in the ribosomal P site through increased affinity of the A site for aminoacyl-tRNA[194]. Cycloheximide inhibits eEF2-mediated translocation by blocking the ability of deacylated tRNA to enter the E-site of the large ribosomal subunit[195]. Lastly, anisomycin binds to the A-site of the large subunit, inhibiting aa-tRNA accommodation into the A site[194].

Consistent with the central role played by eEF2 in the process of translocation, hygromycin B, paromomycin and cycloheximide all had effects on at least one of the strains, whereas anisomycin tended to have either small inhibitory (V28M and H699N) or no effects on cell growth (C372Y, Q753Y and P580H) (**Figure 21C**). In validation of the humanized strain employed as a control for Q735Y, it did not demonstrate altered growth compared with the WT (**Figure 21A**), indicating that the growth phenotypes observed were specific to the patient-derived allele. Notably, however, variant-specific phenotypes were observed. For example, the V28M variant conferred resistance to the hygromycin B; in contrast, the Q753Y and H699N variants conferred sensitivity to this drug, and the C372Y and P580H were completely inviable at the concentration employed in these experiments (**Figure 21C**). A similar profile was observed for paromomycin, consistent with its chemical similarity with hygromycin B. The

sensitivity/resistance profiles to cycloheximide tended to be the reverse of the aminoglycosides, with the exception of the H699N variant (**Figure 21C**).

De novo EEF2 variants confer allele-specific effects on translational fidelity

To further probe the function effects of the eEF2 variants, dual-luciferase assays were performed in the yeast models to determine their abilities to accurately translate the genetic code (**Figure 22A**). Analysis of programmed −1 ribosomal frameshifting (−1 PRF) recoding demonstrated that the *de novo* variants exhibited no significant change in −1 PRF frequency while recapitulating previous findings that P580H and H699N cause an increase. Furthermore, translational recoding of the programmed +1 ribosomal frameshifting (+1 PRF) signal did not appear to differ between any of the strains (**Figure 22B**) Termination codon readthrough (TCR) is also an indicator of changes in translational fidelity. As seen in **Figure 22B**, several eEF2 variants result in a decrease in the background level of TCR, including C372Y and Q753Y, with V28M exhibiting a similar rate to that of the WT strain. The previously reported P580H and H699N also decreased the amount of TCR.

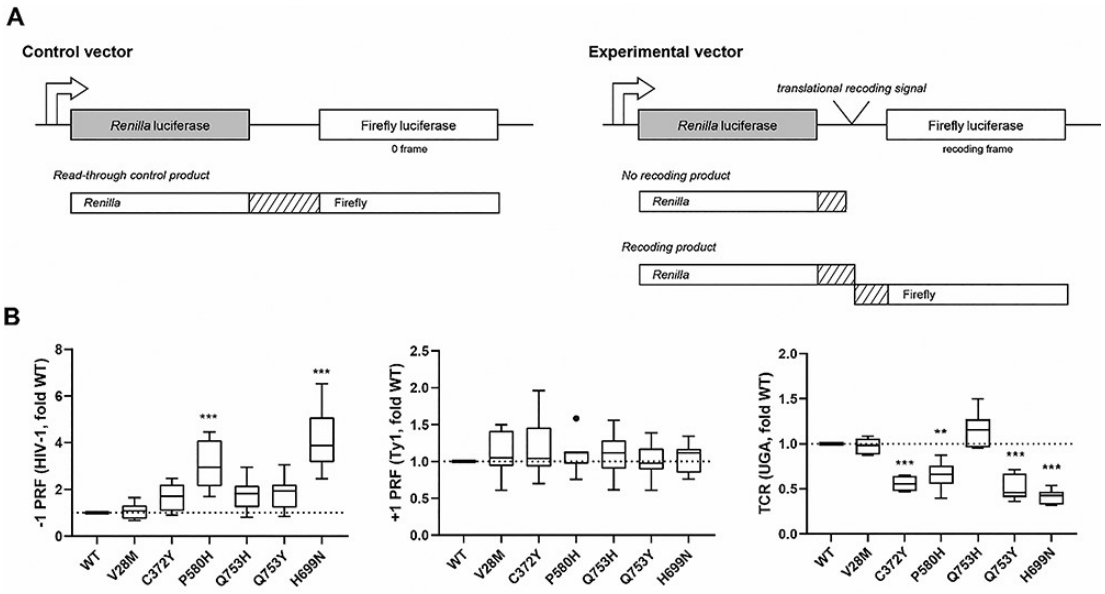

Figure 22: Translational recoding in eEF2 (yeast) model strains showed patient-derived variants alter translational fidelity

A) Control and experimental vector designs for dual-luciferase assay. Dual-luciferase reporters are bicistronic constructs that contain two luciferase genes separated by a spacer region[196]. These reporters can be easily engineered to insert different translational recoding signals within this spacer, thereby affecting the translation of the second luciferase gene. Recoding signals that can be utilized include RNA sequences that program ribosomes (PRF) to slip by one base in either the 5′ (−1 PRF) or 3′ (+1 PRF) direction. Canonical termination codons can also be used to determine the amount of TCR. The reporters are designed where the second gene is only translated if recoding occurs. The amount of both translated proteins can be assayed using chemiluminescence and their ratio can be compared with that of a control reporter containing no recoding signal. This yields the frequency of recoding events that occur during translation of that experimental reporter. The recoding signals used to determine the translational fidelity were the −1 PRF signal from the human immunodeficiency virus (HIV-1)[71] and the +1 PRF signal derived from the S. cerevisiae Ty1 retrotransposable element[77]. These sequences were employed because they have been well characterized and are frequently used to measure translational recoding. The ability of ribosomes to misread the UGA termination codon was used to measure TCR, since it is the most prone to endogenous readthrough of the three stop codons[197], thus enabling maximization of signal-to-noise ratios. Using these different recoding signals enables the analysis of the overall translational fidelity profile of each variant eEF2 model. (B) Translational recoding in eEF2 (yeast) model strains: −1 frameshifting, +1 frameshifting and termination codon read-through in yeast strains. Of the de novo variants, C372Y (ns) and Q753Y (ns) exhibited increased −1 PRF, no strains exhibited altered +1 PRF, and C372Y and Q753Y showed decreased TCR. Data represented as fold-change values relative to WT. Dotted line marks a fold-change of 1, which would indicate no difference between WT and variant. Box plots show the median, interquartile range and range of data. P-values were calculated by Tukey's multiple comparisons tests between the WT and each variant. ns: non-significant, *P<0.05, **P<0.01, ***P<0.001. This work was performed by the dissertation author.

Discussion

We identified *de novo* pathogenic *EEF2* variants in three unrelated children with a NDD and structural brain anomalies. Here, we propose that the *EEF2* gene, so far exclusively associated with the autosomal dominant adult-onset SCA26, is involved in a broader spectrum of NDDs.

Firstly, *in vitro* and *in vivo* findings support a deleterious effect of the *de novo* *EEF2* variants. Bioinformatic analyses indicated that the substitution of the three conserved amino acids are likely damaging and all *de novo* variants were not previously reported in healthy population-based cohorts[190], supporting the low frequency of these missense variants in *EEF2*. Furthermore, this gene is highly intolerant to pLoF variation[190]. Additionally, investigation of yeast models of eEF2 patient-derived mutants showed these *EEF2* variants confer growth and translational fidelity defects. The observation of variant-specific differences in both translational fidelity and sensitivity/resistance to translational inhibitors points to differences in the effects of the variants on different aspects of eEF2 functions. For example, the p.(Cys388Tyr) and p.(His769Tyr) variants promoted better recognition of stop codons (TCR) than even WT cells. This may be explained by decreased ability of eEF2 to compete with the elongation termination factors eRF1/eRF3, either by decreased affinity for the ribosome or by decreased GTPase activity. In contrast, the p.(Val28Met) mutant did not affect the aspects of translational fidelity assayed in this study. Of particular interest, the p.(Val28Met) variant is located at a critical site of interaction with the SRL which plays a central role in the translocation process. Phenotypically, it is unique in that it grows faster than WT and shows altered sensitivities to translational inhibitors that are very different than the other mutants. The p.(Cys388Tyr) variant is positioned at an important interface between domains I and II. It may affect folding of the GTP

binding pocket and/or the structural flexibility of the molecule[198]. The p.(Cys372Tyr) variant, which corresponds to p.(Cys388Tyr) of individual 2, conferred the most pronounced phenotypic defects in yeast. The p.(His769Tyr) substitution is located at a critical interaction between eEF2 and the distal tip of the large subunit ribosomal RNA Helix 43, the GAC. This variant conferred altered sensitivities to translational inhibitors and decreased termination codon misreading. It may affect the affinity of eEF2 for the ribosome, and/or ribosomal stimulation of the eEF2 GTPase activity by the ribosome. Lastly, the SCA26 p.(Pro596His) substitution maps to the critical interaction between domain IV and H69. This variant stimulated −1 PRF and conferred increased fidelity at termination codons, suggesting that it inhibits eEF2 function, perhaps by decreasing the affinity of the protein for the ribosome.

Secondly, individuals with *de novo EEF2* variants present with a childhood-onset, variable phenotype consisting of developmental delay/intellectual disability, non-specific craniofacial dysmorphisms and abnormalities of the brain morphology, including benign external hydrocephalus. *EEF2* is associated with diverse neurodevelopmental presentations, ranging from psychomotor developmental delay with normal intelligence (individuals 1 and 2) to mild ID (individual 3). In these individuals, motor delay was more pronounced than speech delay. The three individuals also shared structural brain abnormalities, in particular a mild to moderate enlargement of the lateral and third ventricles and external CSF spaces. Interestingly, individual 1 manifested additional cerebral morphology abnormalities, such as cortical dysplasia and an abnormal corpus callosum. Craniofacial dysmorphisms included relative macrocephaly due to benign external hydrocephalus with a prominent forehead, low-set ears with a prominent helix, deep set eyes, short nose and thin upper lip. Ectodermal abnormalities included fine sparse scalp hair and nail dysplasia in individuals 1 and 2 and fast growing hair and nails in individual 3.

Although the number of patients identified so far is limited, overlapping mild clinical features in three patients seems to exemplify the variable expressivity of *EEF2*-related disorders, because the phenotype of these children differs substantially from that of previously reported adults presenting with SCA26[103], in particular due to the childhood age of onset, occurrence of the intellectual disability and distinct morphological CNS abnormalities. Remarkably, developmental delay/intellectual disability, short stature, dysmorphic facial features, abnormal head circumference (microcephaly or macrocephaly), CNS malformations and ectodermal abnormalities were previously described in individuals carrying biallelic variants in the *DPH1*[105,199,200] or *DPH2* genes[201], which result in a deficiency in the biosynthesis of diphthamide, a critical post-translational modification in eEF2 that enables the regulation of its function.

Altogether, the fundamental role of eEF2 in gene expression, the abnormal cell growth pattern, translation inhibitors sensitivity and translation fidelity in yeast, and the observed delayed neurodevelopment and brain structure anomalies, support the pathogenicity of the three *de novo EEF2* variants. As described above, we hypothesize that these missense variants result in distinct functional effects, based on allele-specific phenotypes in yeast. Since *de novo* variants in *EEF2* result a childhood-onset, more severe and more variable phenotype than the autosomal dominant late-onset SCA26, we propose that the phenotype of the *EEF2*-related disorders is a consequence of the specific pathogenic variants that distort the different eEF2 intrinsic functions and its interactions with the ribosome, which differently influence the ability to accurately translate the transcriptome and subsequently disrupts growth on various organ levels. A multicenter effort to further clinically and molecularly characterize a growing number of individuals with an *EEF2*-related disorder will shed light on the predictable broad spectrum of

these disorders. In order to facilitate this, a website will be available for collection of in-depth phenotypic data of individuals carrying likely pathogenic *EEF2* variants, which aims to corroborate the observed phenotypic heterogeneity and establish firm genotype–phenotype correlations.

Acknowledgements

We are grateful to all the families for participating in this study. We are thankful to Erin Torti (GeneDx, Inc.) for bringing us in contact with the clinicians of individual 1.

Conflict of Interest statement. Francisca Millan is an employee of GeneDx, Inc. The remaining authors declare no competing interests.

Funding

Dutch Organization for Health Research and Development (ZON-MW grants 917-86-319 and 912-12-109 to B.B.A.d.V.) and the National Institutes of Health (R01 GM 117177 to J.D.D.).

Chapter 4: Deep mutational analysis of eEF2 residues implicated in human disease

Introduction

In the previous work, mutations in eEF2 were implicated in translational fidelity loss and neurological disorders[183]. Structural analysis revealed that these pathogenic amino acid substitutions map to the three main points of contact between eEF2 and critical rRNA elements of the ribosome. Specifically, the eEF2 mutants mapped to contacts with H69, the sarcin-ricin loop (SRL, H95), and H43 of the GTPase associated center (GAC) all of the LSU (**Figure 23**). In order to further investigate the contributions of these eEF2-ribosome interactions to translational fidelity, mutants with distinct biochemical characteristics were generated corresponding to the eEF2 residues at each site based on their proximity to these functionally important rRNA elements. The targeted residues were constructed as to test the biochemical contributions of amino acid side chains, including acidic, basic, nonpolar, and deletion (alanine) residues, excluding the category to which the endogenous residue belonged.

Materials and methods

Yeast strains and media

For the construction of *EFT2*-6xHis mutational analysis strains, site-directed mutagenesis of pJD2490 (YCp*EFT2-LEU2*) was performed using Q5 high-fidelity DNA polymerase (NEB) per the manufacturer's instructions with the following adjustments. The final reaction volume was 15 µL and 4 mM $MgCl_2$ was added to the reaction mixture. Touchdown cycling was used to

eliminate the need for different cycling parameters for each oligo pair, where the annealing temperature started at 70°C and decreased 1°C each cycle for 15 cycles, then remained at 54°C for the remaining 20 cycles. Template DNA was then digested in concert with phosphorylation and circularization of PCR product. 1 µL of PCR reaction mixture was incubated with 5U of T4 DNA ligase (NEB), 200U of T4 polynucleotide kinase (NEB), and 10U of DpnI (NEB) in T4 DNA ligase buffer (NEB) at a final volume of 10 µL. The reaction mixture was incubated at RT for 2 hours then at 30°C for 30 minutes. 5 µL of the final reaction mixture was transformed into 25 µL NEB 5-alpha competent *E. coli* (high efficiency) per manufacturer's instructions and 75 µL of transformed cells were plated onto $LBCb_{50}$ plates. Mutagenesis was confirmed by diagnostic digest of the transformed plasmid by PstI-FD (Thermo) and Sanger sequencing by Genewiz.

EFT2 mutant plasmids were transformed into yJD995 (MATa *ade2 ura3 his3 leu2 trp1 eft::HIS3 eft2::TRP1* +YCp*EFT1-URA3*) as previously described[183] except confirmation of successful transformation was determined by colony PCR. Briefly, 50 µL of transformed yeast culture was pelleted and resuspended in 50 µL of water, which was then incubated at 99°C for 5 minutes. 5 µL of "heat popped" yeast were then used as template DNA for PCR using DreamTaq MasterMix (Thermo) and appropriate primers. PCR product was purified with DNA Clean & Concentrator kit (Zymo) and sequenced by Genewiz using Sanger sequencing to confirm incorporation of mutant *EFT2*.

Yeast strain growth analysis

Yeast strains were grown to logarithmic phase then diluted to an OD_{600} = 0.05 in 400 µL of media (either YPAD only or YPAD with translation inhibitor). Diluted cultures were split into 100 µL in 3 wells of a clear 96-well plate which was then sealed with a Breathe Easy sealing

membrane (Electron Microscopy Sciences). Yeast were grown in a Synergy HTX plate reader (BioTek) at 30°C for 48 hours. The OD_{600} of each well was taken ever 15 minutes, with shaking for 10 minutes preceding each measurement. Concentrations of translation inhibitors were determined by an approximate 50% reduction in growth rate of WT *EFT2* yeast. These concentrations were: 15 μg/mL anisomycin, 5 mg/mL paromomycin, 20 μg/mL hygromycin B, and 50 ng/mL cycloheximide.

Translational fidelity assays

The killer maintenance assay was performed by growing *EFT2* strains to mid log phase overnight in YPAD, then diluting each culture to an OD_{600} of 1 in YPAD with 30% glycerol. 5x47 was used as the killer sensitive strain and was grown and diluted the same, except without the presence of glycerol. 300 μL of diluted 5x47 were spread onto 4.7MB plates and allowed to fully dry. 2 μL of *EFT2* strains were spotted onto lawn plates and were incubated at RT (~20°C) for 5 days. Dual-luciferase assays were performed as previously described[183].

Purification of histidine-tagged eEF2

Yeast cultures were grown in 1L of YPAD to an OD of 1.5. Cells were harvested by centrifugation and washed twice with equilibration buffer (20 mM sodium phosphate pH = 7.4, 500 mM NaCl, 20 mM imidazole). Cells were lysed by addition of 2.5-3 mL of lysis buffer (Yeast Protein Extraction Reagent (Thermo), 1X Halt protease inhibitor (Thermo), 1 mM DTT) per gram of cells (wet weight) and mixed gently at room temperature for 20m. Lysate was clarified by centrifugation at 4,000 x g for 25 minutes at 4°C then combined with an equal amount of 2X equilibration buffer (40 mM sodium phosphate pH = 7.4, 1 M NaCl, 40 mM

imidazole). Lysate was filtered through a 0.22 μm syringe filter then purified on a 1 mL HisTrap HP column (Cytivia) using an AKTA FPLC instrument. The column washed with 10 volumes of equilibration buffer then 5 volumes of 10% elution buffer. Protein was eluted with elution buffer (20 mM sodium phosphate pH = 7.4, 500 mM NaCl, 250 mM imidazole) and fractions containing eEF2-6xHis were concentrated with an Amicon Ultra-15 50K centrifugal filter. The concentrated protein was then loaded onto a HiPrep 16/60 S-200 HR column (Cytiva) and isocratically eluted with 20 mM Tris-HCl pH = 7.5, 150 mM NaCl, 0.1 mM EDTA. Fractions containing eEF2-6xHis were again concentrated by centrifugal filtration and stored in HiPrep buffer with 10% glycerol at -80°C. Purification was evaluated by SDS-PAGE (**Supplemental figure 32A**) and concentration was measured using Coomassie Plus Bradford assay (ThermoFisher).

Circular dichroism spectroscopy

Purified eEF2 was buffer exchanged into 20 mM Tris-HCl pH=7.5, 1 mM EDTA and diluted to a final concentration of 0.15 mg/mL in 200 μL. CD spectra were taken in a 0.1 cm quartz cuvette with a JASCO J810 spectro-polarimeter at room temperature from 250-200nm with a scanning speed of 20nm/min. CD of a blank run containing only buffer was subtracted from each data set and molar ellipticity was calculated using the exact concentration as measured by Bradford assay.

GTPase activity measurements

GTPase activity of purified eEF2 was carried out using the GTPase-Glo Assay (Promega) as described[202,203]. A 10 μL reaction containing 0.1 μM 80S ribosomes, 0.5 μM GTP, 1 mM DTT, 0.5 mg/mL polyU and varying amounts of eEF2 (4 - 0.125 μM) in GAP/GTPase buffer

were incubated at 30°C for 90m and remaining [GTP] was converted to luminescence as per the manufacturer's instructions. Luminescence was measured in a white 384 well plate (Corning) with the Promega GloMax Multi+ Detection system. RLU values were normalized to each data set and GTPase activity was calculated as described[203].

Results

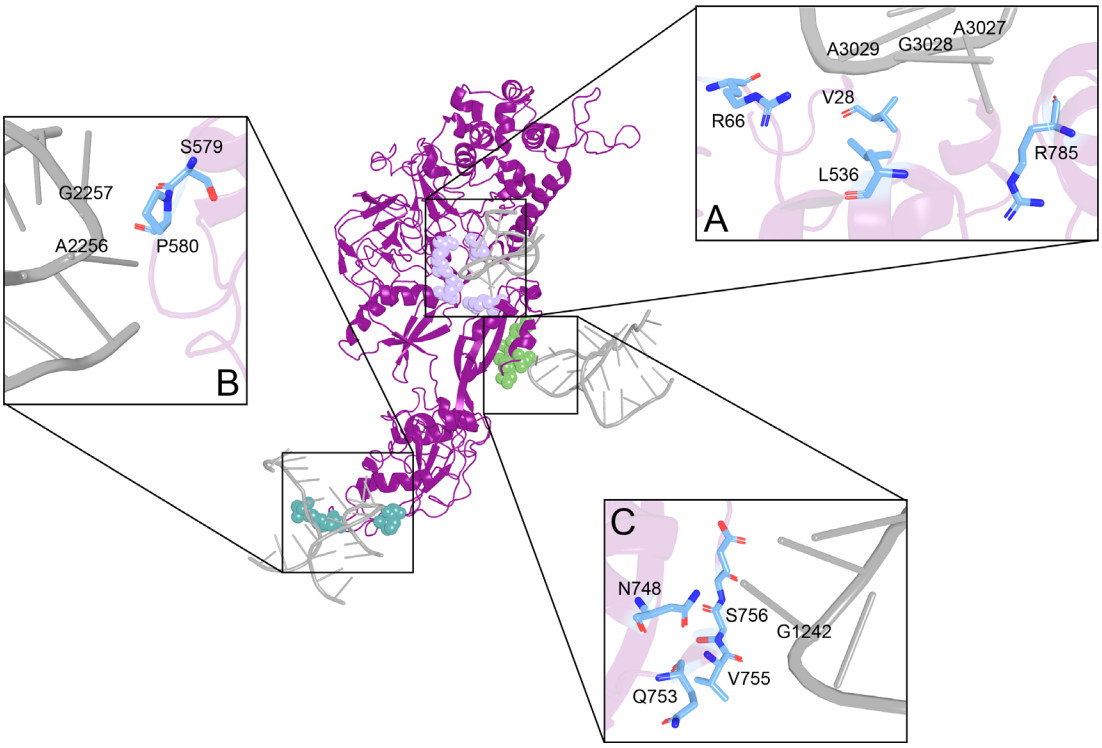

Figure 23: eEF2 interaction sites with the ribosome

Structure of *Saccharomyces cerevisiae* bound to the ribosome (modified from PDB 6GQV[204]) eEF2 shown in purple, eEF2 residues in light purple, green, teal, and blue, and rRNA in light grey. A) Residues proximal to the sarcin-ricin loop of the GAC. B) Residues proximal to H69 in the A site of the SSU. C) Residues proximal to H43 in the GAC

Alterations to eEF2 sites of ribosome interaction are lethal and confer growth defects in yeast models

EFT2 mutant yeast strains were generated from a parent strain in which the endogenous *EFT1* and *EFT2* genes were disrupted and replaced by a centromeric plasmid encoding either wild-type or mutant *EFT2* under control of its endogenous promoter. Standard auxotrophic and 5-FOA driven plasmid shuffle methods were used to select for cells expressing the eEF2 mutants. This method also enabled the identification of lethal mutants of this essential protein (**Figure 24**). For each interaction site there appeared to be one amino acid to which substitutions were particularly deleterious. For the H69 residues, all substitutions of S579 were lethal. In the SRL site, 3 out of the 4 V28 substitutions created for this research were lethal, including V28F, V28K, and V28D. Mutations of amino acids that interact with H43 interactions appeared to be less deleterious overall, but 2 substitutions at S756 were inviable. Other residues were able to tolerate all but one substitution, including R66D and R785A of the SRL-proximal residues and P580T of the H69 group.

Growth rates of the viable yeast strains were first determined to begin characterizing the global effects of these eEF2 mutations (**Figure 24**). Most mutations conferred small decreases in growth rates, resulting in a marginally longer doubling time. Several positions proximal to the SRL appeared to increase the doubling times to a greater extent, including R66A, R66F, and L536A. Of the single remaining H69 position, only P580F exhibited more than a 2 fold increase in doubling time. Of the amino acids that interact with H43, only Q753A significantly affected doubling time.

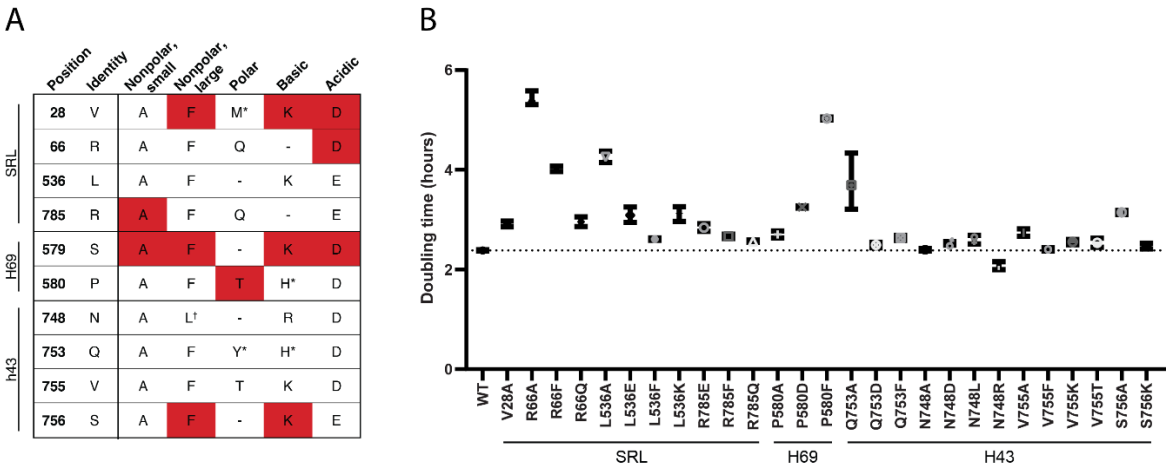

Figure 24: eEF2 interaction sites are necessary for cell viability and normal growth

A) Rational design approach to eEF2 mutational analysis. Target residues are listed along with the variants made according to their chemical properties. Shaded cells indicate strains found to be inviable. Dashes represent mutations which would recapitulate the original residue and were therefore excluded. *Mutants described in previous research. †Nonpolar variant of equivalent size to original residue. B) Doubling times of viable eEF2 mutant strains. Doubling times were calculated by nonlinear regression of the exponential phase of growth of n=3 experiments for each strain. Error bars represent 95% C.I. Dashed line indicates doubling time of the WT strain (2.38 hours).

Rationally designed eEF2 variants demonstrate sensitivity to decoding center inhibitors

In order to probe the effect of eEF2 mutations on critical sites of interaction between eEF2 and the ribosome, cellular growth in the presence of sub-lethal concentrations ribosome-targeting translational inhibitors were assayed (**Figure 25**). Hygromycin B and paromomycin are aminoglycosides that bind to rRNA near the DC in the A site of the SSU (**Figure 25A**). Specifically, paromomycin stabilizes the binding of tRNA in the A site, inducing missense incorporation and inhibiting translocation while hygromycin B also stabilizes A site tRNA as well as interfering with the conformational changes associated with rotation of the ribosome[205,206]. Anisomycin binds the PTC in the A site of the LSU (**Figure 25A**), where it destabilizes aa-tRNA binding and inhibits peptidyl transfer[207,208]. Cycloheximide binds to the

LSU (**Figure 25A**) and competes with deacylated tRNA for binding to the E site, inhibiting the movement of the P site tRNA into the E site during translocation[208]. By measuring the doubling time of the eEF2 variants in the presence of these translation inhibitors, the degree to which the difference between the WT and mutant changes between normal and inhibited growth can be compared, indicating how specific mutations may alter the functional interactions between eEF2 and the ribosome. As shown in **Figure 25B**, inhibitors hygromycin B and paromomycin tended to slow the growth rate of the mutant strains, with some being unable to survive at the concentrations used indicating that most of the mutants functionally perturb the interactions between eEF2 and the DC. Anisomycin had little to no effects, consistent with the lack of interactions between eEF2 and the LSU A site. Most of the mutants conferred at least conferred at least some degree of resistance to cycloheximide. The ribosome interaction sites also tended to confer distinct profiles, with the residues that interact with the SRL and H69 showing the strongest differences. For the SRL proximal site, all R66 mutants were inviable in the presence of paromomycin, and R66F and L536A were inviable with both aminoglycosides. V28A also demonstrated sensitivity to both while the L536 mutants had moderate, variable responses and some of the strongest resistance to cycloheximide. At the H69 interaction region, P580 residues exhibited the same patterns of growth, with the strength of the phenotype increasing from P580A to D to F, the latter of which was also inviable in the presence of both aminoglycosides. Interestingly, residues near H43 showed little to no growth alterations in the presence of translation inhibitors, with the notable exceptions of Q753A, which conferred resistance to all four antibiotics, and S756A promoting strong resistance to cycloheximide.

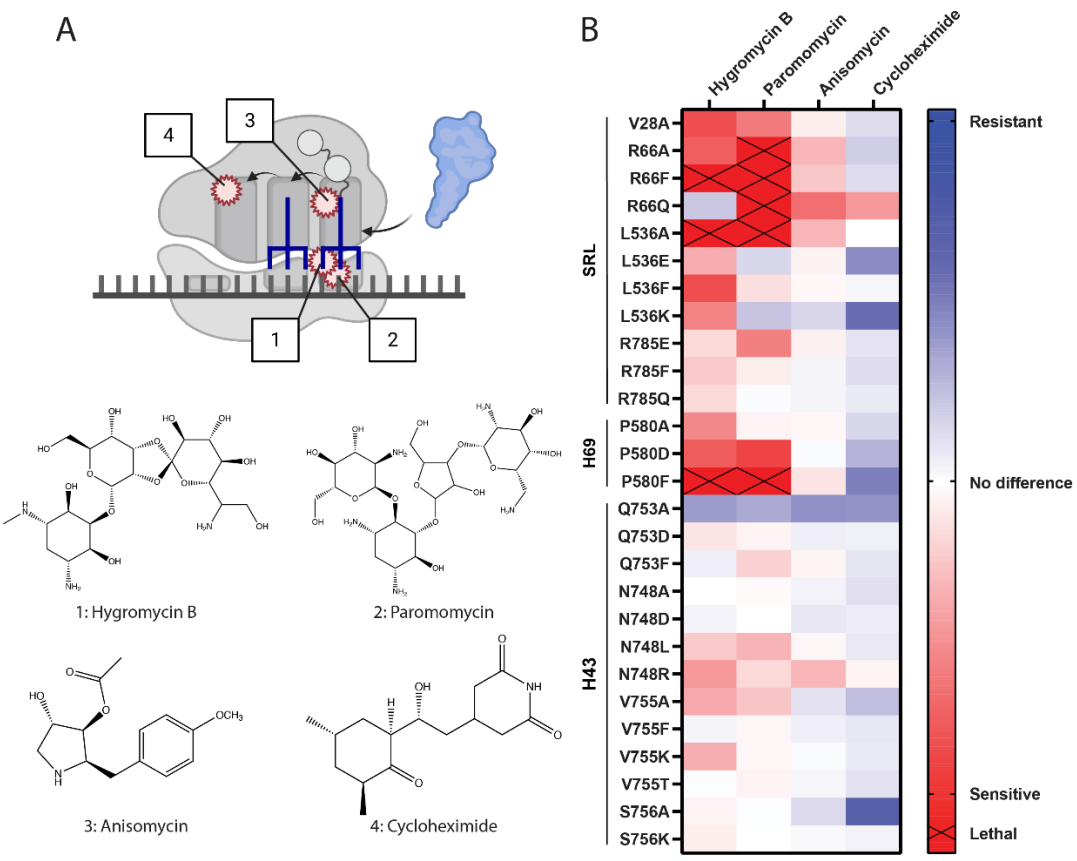

Figure 25: eEF2 mutations to ribosome interaction sites confer sensitivity to aminoglycosides

A) Diagram of antibiotic interactions with the ribosome and their structures. Hygromycin B (1) and paromomycin (2) bind to the A site of the SSU. Anisomycin (3) binds to the A site of the LSU. Cycloheximide (4) binds to the LSU in the E site. B) Heat map of eEF2 mutant strain growth in the presence of translational inhibitors. Color saturation indicates strength of the phenotype indicated. Xs indicate strains that were unable to grow at the concentration of inhibitor used. Heat map values calculated by the $\log_2$ of the ratio of mutant doubling time to WT doubling time in presence of translational inhibitor (n = 3), minus the $\log_2$ of the ratio of mutant doubling time to WT doubling time in rich media. Positive values indicate resistance, negative values indicate sensitivity, and 0 indicates no difference in growth due to translational inhibitor.

Mutations in eEF2-ribosome interactions sites cause translational fidelity loss in yeast cells

The effects of the mutants on programmed translational recoding were measured using dual luciferase assays of HIV-1 mediated -1 PRF, and Ty1 driven +1 PRF as previously described[183]. Briefly, production of the downstream firefly luceriferase enzymes is reliant on successful ribosomal frameshifting while upstream *Renilla* luciferase functions as an internal

control for any effects on general translation conferred by the mutants. Therefore, the ratio between the two luciferase activities, as measured by luminescence, is reflective of the fraction of times frameshifting occurs along this message. As shown in **Figure 26**, the H69 mutants have the strongest effects on -1 PRF, with P580D and P580F demonstrating a significant increases. Conversely, the R66Q and N748R mutants conferred moderate but significant decreases on -1 PRF. The L536E, L536K, and Q753A strains of the SRL and H43 regions promoted increases in +1 PRF, while the H69 mutations had no effects. We note, however, that the data tended to show a bimodal distribution, with clusters of high and low frameshift values. Therefore, only the Q753A strain had a statistically significant increase in frameshifting, although the portion of high frameshifting seen in the indicated L536 strains could still be biologically significant.

Many commercial and research yeast strains are carriers of the L-A totivirus, a dsRNA virus that supports the M1 satellite virus, which encodes for the "killer toxin" which is lethal to non-carrier strains. The L-A virus genome contains a -1 PRF signal at the *Gag/gag-pol* juncture necessary for viral replication. Maintenance of the Killer phenotype is highly dependent on -1 PRF efficiency[209], therefore, defects in frameshifting will materialize as reduction or loss of viral persistence and killer toxin production. The parental strain used in these studies (yJD995) has the Killer$^+$ (K^+) phenotype, thus enabling us to determine the effects of the eEF2 mutants on viral maintenance (**Figure 26C**). To monitor this, yeast strains are grown on a lawn of a diploid k^- indicator strain that is sensitive to the toxin and the size of the zone of growth inhibition around the strain being tested is indicative of cellular Killer viral load. The R66A mutant was completely unable to maintain the Killer virus, and the R66F and L536A showed partial decreases in killer activity, suggesting partial defects on virus maintenance.

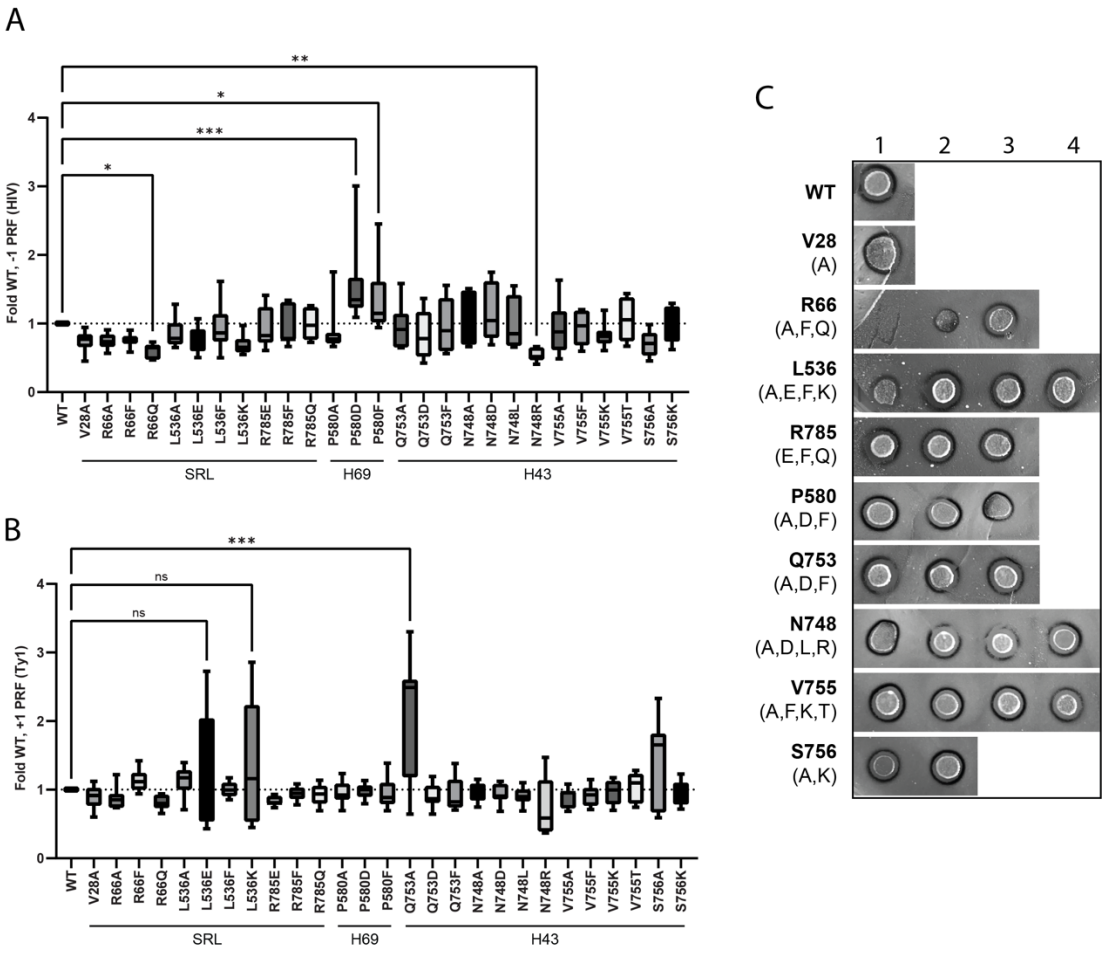

Figure 26: Translational fidelity defects resulting from eEF2 mutations to ribosome interaction sites

A-B) Dual luciferase assay of -1 PRF (A) and +1 PRF (B) translation in eEF2 variants. Data represented as fold-change values relative to WT. Dotted line marks a fold-change of 1, which would indicate no difference between WT and variant. Box plots show the median, interquartile range, and range of data. *P*-values were calculated by Tukey's multiple comparisons tests between the WT and each variant (n=8) ns: non-significant, $^{*}P<0.05$, $^{**}P<0.01$, $^{***}P<0.001$. C) Killer maintenance assay of eEF2 mutant strains. Killer activity exhibited by a zone of inhibition surrounding the spot and precipitation of the methylene blue, resulting in a dark ring. Loss of killer activity indicates translational fidelity loss rendering L-A virus replication, and therefore toxin production, inviable. Representative results from n=4 shown.

Mutant eEF2 confers translocation defects in vitro

Based on the phenotypes displayed in the growth and translational fidelity assays, one mutation was selected from each cluster for deeper biophysical and biochemical characterization.

R66A, P580H, and Q753A were chosen from the SRL, H69, and H43 regions, respectively. P580H, which was previously described in greater detail[103], is the original eEF2 mutation found to be causative for SCA26 and has previously demonstrated phenotypes similar to those expressed by P580D and P580F. Therefore, due to its known biological significance and characterization by several groups, P580H was chosen to represent the H69 interacting region.

Circular dichroism spectra were obtained for purified wild-type and three mutant eEF2s to determine whether the mutations imparted biophysical effects on eEF2 folding (**Figure 28A**). The mutants all exhibited similar CD spectra to the WT protein, indicating that none conferred gross defects on eEF2 maturation. This is consistent with their ability to support cell viability as the sole form of the protein. However, an increase in lower molecular weight contaminants was noticed during purification of R66A and P580H. These appeared in middle stages of purification and were subsequently removed during the final preparation step (**Figure 27B**). This could indicate higher amounts of eEF2 degradation, potentially as a result of folding defects. However, since these lower MW species were removed during purification, they were not represented in the CD spectra.

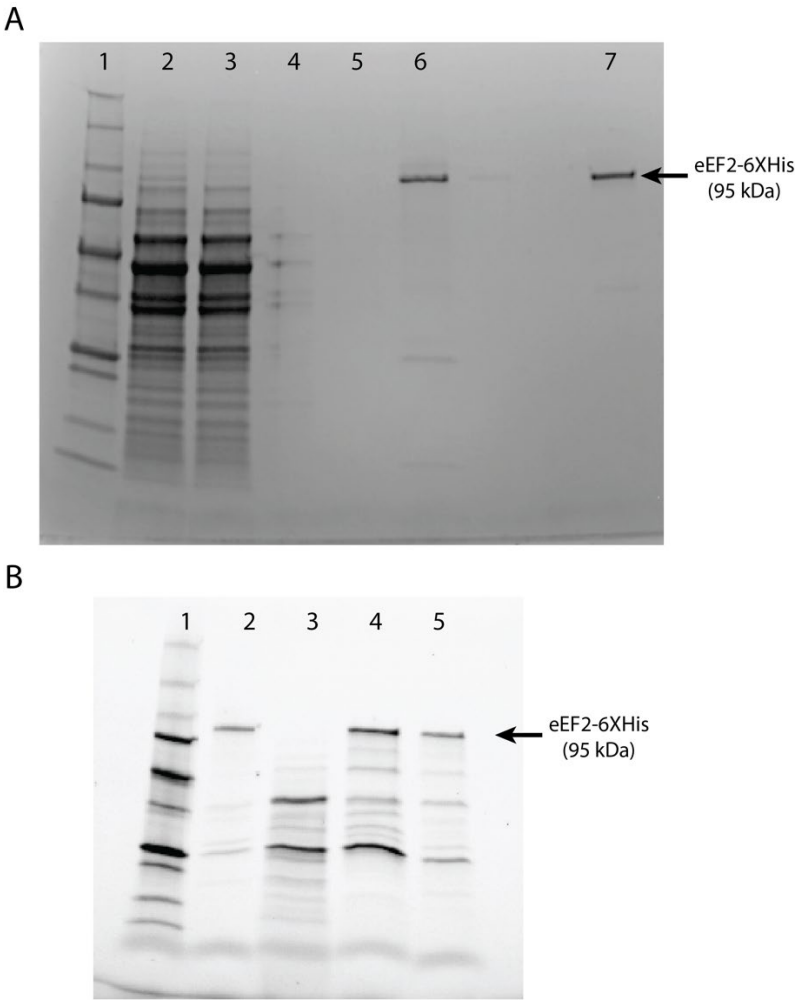

Figure 27: Purification of eEF2-6XHis variants

A) Representative gel of eEF2 purification process, WT shown. Lanes: 1. Precision plus unstained protein standard (Bio-Rad), 2. Cell lysate, 3. Ni-NTA column flowthrough, 4. Ni-NTA column wash 1, 5. Ni-NTA column wash 2, 6. Ni-NTA purified protein, 7. SEC purified protein
B) Ni-NTA purified eEF2 variants. Lanes: 1. Precision plus unstained protein standard, 2. WT, 3. R66A, 4. P580H, 5. Q753A

To examine the functional effects of the eEF2 mutations on its function, the ability of the purified eEF2 samples to hydrolyze GTP was measured in the presence of 80S ribosomes (**Figure 28B**). R66A and Q753A showed moderate reductions in GTPase activity, while P580H showed a marked decrease in GTP hydrolysis. This indicates that in the absence of folding

differences, mutations of eEF2 that map to sites of interaction with the ribosome can directly impact the enzymatic activity of this protein, suggesting that they may impair translocation rates.

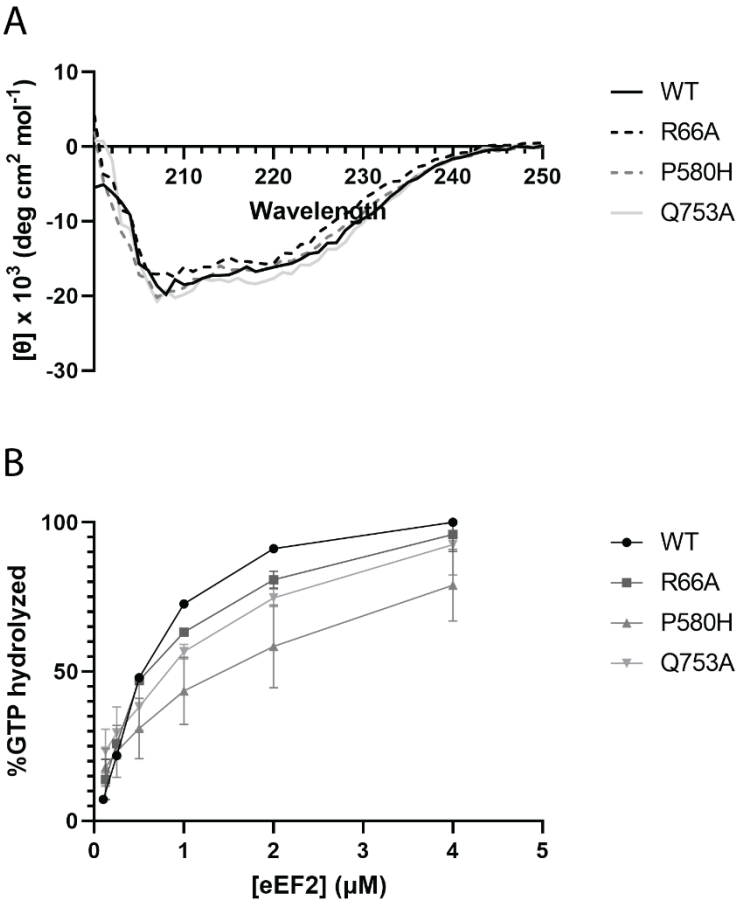

Figure 28: *In vitro* characterization of mutant eEF2

A) Circular dichroism spectra of WT and mutant eEF2. B) *In vitro* GTPase activity of WT and mutant eEF2. Luminescence data was normalized to concurrently measured positive and negative controls. WT n=1, all mutants n=2.

Discussion

The work in this study investigates the importance of eEF2-ribosome interactions implicated on neurological disorders to cellular fitness and translational fidelity. A panel of rationally designed mutations were introduced to eEF2 at these interaction sites in order to probe their effects in yeast model strains and *in vitro* experiments.

The SRL is a highly conserved region of the 28S rRNA that works with the GAC, the ribosomal center for activating GTP hydrolysis, to ensure coordination of GTPase activity by translation factors with various ribosomal functions including delivery of cognate aa-tRNAs by the eEF1A-tRNA-GTP ternary complex, translocation by eEF2, termination by the eRF1/eRF3 complex, and interactions with a growing list of factors involved in the ribosome quality control mechanism[210]. The SRL has previously been implicated as a key site for EF-G and eEF2 function; though it has been demonstrated that it is not necessary for GTP hydrolysis, it is thought to serve as an anchoring point for EF-G to the ribosome during translocation[210]. This is supported by data obtained in eukaryotic systems as well, with structural studies showing that dissociation of eEF2 from the ribosome is mediated by contacts with the SRL[211]. Here, we have demonstrated that eEF2 residues V28, R66, and L536 are important sites of interaction with the SRL. In particular, alterations to V28 were almost always lethal, with the exceptions of substitution with alanine, an amino acid that is similarly small and nonpolar, and the previously investigated methionine substitution (which causes congenital defects and intellectual disability in humans, see chapter 3) that, while having different charge properties, is similar in size to valine. Viable substitutions to the SRL-interacting region promoted sensitivity to aminoglycosides and moderate translational fidelity defects, and *in vitro* characterization of R66A revealed a slight reduction of GTPase activity. Together, these findings support the idea that SRL contacts are important to eEF2 function and reading frame maintenance.

Helix 43 of the 28S rRNA is part of the GTPase associated center. Along with H44, it is involved in activating GTPase activity of translation factors. eEF2 residues proximal to this region did not generally promote strong phenotypes, with the exceptions of Q753A and S756A. Q753 is also a position that was previously shown to be linked to neurological disorders, though

it is not as well conserved between yeast and human eEF2 as the other residues in this study. Q753A exhibited growth defects and slight resistance to all translational inhibitors, as well as increased +1 frameshifting. S756A also had mild growth defects, and conferred strong resistance to cycloheximide, but did not alter translational fidelity. In this way, it appears that these two variants have similar phenotypes, with the Q753A defects being more pronounced, indicating that they share a common mechanistic effect. Q753A also showed a similar decrease in GTPase activity similar to the R66A mutant, which is expected as interaction with the GAC is important for GTPase activation.

The final region of eEF2 interaction investigated was with H69 of the LSU. This helix is part of the B2a intersubunit bridge and has been implicated in the "unlocking" mechanism of the decoding center from the tRNA-mRNA complex. Particularly, rearrangement of A2256 (**Figure 23B**) in H69 has been shown to be part of the conformational change that destabilizes the contacts between h44 of the DC and the codon-anticodon interaction[212]. Mutations of the two residues close to H69 in this work further underscore the importance of this function to reading frame maintenance. The mutations attempted at position S579 in this work were all lethal, indicating essential nature of this amino acid residue. P580 is the location of the original SCA26 allele and the additional variants generated in this work recapitulated its effects from previous research to varying extents. P580H was also characterized in terms of its GTPase activity, which showed the largest defect overall, potentially due to decreased binding affinity with the A site or defects in the allosteric network to trigger GTP hydrolysis. The necessity of S579 and translational fidelity loss seen with several P580 mutations indicate these two residues as an important interaction site with A2256 and the subsequent unlocking mechanism that coordinates reading frame maintenance.

Overall, several original residues recapitulate the phenotypes of yeast strains modeled after alleles implicated in neurological translationopathies, supporting the hypothesis that alterations of these eEF2-ribosome contacts are part of the disease mechanism. This, combined with the data on translational fidelity, indicates that not only is translational infidelity a likely contributor to these genetics disorders, but also defines the importance of eEF2-ribosome contacts to reading frame maintenance.

Chapter 5: Discussion and conclusions

With this work, I have investigated the role of translational fidelity in novel genetic disorders resulting from mutations in two essential components of the cellular protein translation apparatus. Chapter 2 describes mutations in a ribosomal protein, *RPL9*, that lead to largely different variant-specific clinical presentations: one causes DBA due to ribosome biogenesis defects and the other confers increased risk for specific cancers with an accompanying decrease in translational fidelity. Chapter 3 presents *de novo* variants in *EEF2* that are associated with congenital defects and neurological disorders resulting from translational fidelity loss. Finally, chapter 4 further explores the function of eEF2-ribosome contacts by leaning on the knowledge gained from the preceding work and exploring the three major sites of interaction between eEF2 and the ribosome hypothesized critical for eEF2 function. Together, this work highlights salient points about the relevance of translational fidelity to human health.

The contrast between the two *RPL9* ribosomopathies presented in chapter 2 is also broadly relevant to the divide between ribosomopathies and translationopathies. On one hand, the 5'UTR variant presents as a classical ribosomopathy: haploinsufficiency of RPs impairs ribosome biogenesis, resulting in the clinical presentation of DBA. On the other, although the missense variant also affected pre-rRNA processing, it is not associated with haploinsufficiency as the mutant RP is incorporated into the mature ribosome. Importantly, the missense variant was shown to decrease translational fidelity, potentially caused by changes in uL6 folding which impact the interaction of the SRL with translation factors. Due to this, the *RPL9* missense variant joins several atypical ribosomopathies that do not replicate the usual hematopoietic phenotypes, e.g. mutations in *RPS23*[101] and *RPL10*[100]. Interestingly, *RPS23* mutations were also shown to result in translational fidelity defects[101], indicating a potential common link between these

atypical presentations. In this way, these ribosomopathies share more in common with translationopathies, which are characterized by translational fidelity defects. However, as illustrated by *RPL9*, these differences are not solely based on the identity of the RP affected, as the specific downstream consequences can differ between variants within the same RP.

In chapters 3 and 4, focus turned from the ribosome to the essential translation factor, eEF2. Chapter 3 explored links between neurodevelopmental disorders caused by several *de novo* mutations in eEF2 and defects in translational fidelity. Evidence from yeast models showed that cellular fitness was altered by the patient mutations and probing with translational fidelity inhibitors demonstrated altered sensitivity to aminoglycosides hygromycin B and paromomycin in the C373Y strain. This sensitivity is likely caused by perturbations of eEF2 interactions with the DC of the ribosome, which is an important point of contact for the "unlocking" mechanism vital to reading frame maintenance. C372Y and Q753Y also demonstrated resistance to cycloheximide, indicating that these mutants allow more time for the spontaneous movement of the 3' end of the deacylated tRNA to move from the P- to the E- site. In contrast, V28M exhibited opposite effects, with resistance to hygromycin B and sensitivity to cycloheximide, potentially an indication of "promiscuous" translation. Interestingly, despite having nearly identical binding site with hygromycin B[213], paromomycin did not affect V28M growth at all. As hygromycin B is also known to interfere with ribosome rotation during translocation, this indicates the DC interaction is not affected by V28M while the ribosome rearrangements induced by eEF2 are.

Importantly, it was noticed that several of the *de novo* mutations as well as previously described eEF2 variants mapped to three distinct sites of interaction with the ribosome. As several of these mutants demonstrated changes to translational fidelity, it was hypothesized that

these sites of eEF2-ribosome contact are necessary for proper translational fidelity. To test this hypothesis, a panel of mutations were introduced to eEF2 at residues determined to be proximal to these sites by structural analysis. This work is described in chapter 4, where it was also shown that interactions with the SRL and H69 are important to reading frame maintenance as mutations to these regions of eEF2 demonstrated sensitivity to aminoglycosides and altered translational fidelity. Both H69 and the SRL are known to be important to eEF2 function, with A2256 of H69 being vital to mRNA-tRNA "unlocking" and the SRL to controlling eEF2 binding to the ribosome. Mutations to H43 were less impactful, indicating that the specific interactions between eEF2 and this site are less important. However, two mutants demonstrated altered phenotypes, specifically Q753A and S756A. Biochemical analysis indicated that folding of the purified mature proteins was not altered, but increased degradation of mutant eEF2 was observed, suggesting that they may affect specific eEF2 folding processes resulting in a subset of misfolded protein. Further investigation will be needed to determine the biological relevance of this observation. Analysis of GTPase activity showed that the selected mutants from each region demonstrated defects in GTP hydrolysis. While this experiment was not able to deconvolute the rates of ribosome binding with catalysis, it is still evident that eEF2 function is inhibited by these mutations, indicating that interactions with the SRL, H69, and H43 of the ribosome are central to eEF2-catalyzed translocation.

As a whole, this work provides valuable insight into human disorders that result from ribosome and translation defects. The advent of affordable whole genome sequencing has made genetic testing more accessible than ever, revealing causes of genetic disorders that may have previously gone unknown. In particular, it has led to the discovery of ribosomopathies and their commonalities, including ribosome biogenesis defects and hematopoietic consequences. An

outgrowth of this medical research has been into mutations found in other factors that also affect translation. Though they do not strictly follow the same hallmarks as ribosomopathies, these translationopathies have their own set of overlapping presentations, including neurological disorders, congenital abnormalities, and translational fidelity defects.

Though they both affect protein synthesis, the unique effects of ribosomopathies and translationopathies implicate different aspects of translation in cellular and tissue function. However, both disease classes frequently present with congenital abnormalities. During development, translation is highly controlled in spatiotemporal aspects as part of the precise programs that differentiate cells and give rise to distinct tissues. Aberrations in translational control are likely to disrupt the sequences that control development, resulting in birth defects. This can result from both haploinsufficiency and translational infidelity as inadequate ribosome concentration can cause an imbalance in initiation while translational fidelity can also cause discrepancies in translation ratios. Therefore, that both ribosomopathies and translationopathies frequently present with congenital abnormalities is no surprise.

The tissue specificities typically seen in these two disease types are also distinct, with ribosomopathies typically presenting as hematopoietic disorders and translationopathies as neurological and developmental ones. Red blood cells are one of the most abundant cell types in the body and are constantly being regenerated by the bone marrow. It is estimated that 2 million blood cells are produced in the human body every second[214], representing a large protein synthetic metabolic demand. Though aberrant translation of specific transcripts such as *GATA1* is likely a contributing factor to anemia, the reduction in overall translation rates demonstrated in most ribosomopathies is also predicted to more detrimentally affect rapidly proliferating cells (compared to terminally differentiated cells), as their ribosomes cannot keep up with the demand.

As there are a number of tissues with similar cellular production, reduced translation capacity cannot be the only contributing factor to these hematopoietic disorders, but likely pre-sensitizes erythropoiesis to be susceptible to further molecular disfunction. This is also evident in certain ribosomopathies such as X-linked dyskeratosis congenita that also present with skin abnormalities, a tissue that with a similarly high cell production and protein synthesis demand.

In contrast, translationopathies frequently present as neurological disorders. Neurogenesis occurs primarily during embryonic development, with most neurons persisting the entire lifespan. Therefore, a decrease in protein synthesis rate is unlikely to chronically affect brain tissue. However, neurons are some of the largest cells in the body and also feature a vast network of branch-like dendrites. These morphological characteristics present a unique challenge to proteostasis, with the presence of the proteostasis network including translation machinery, chaperones, and degradative pathways necessary in all parts of the cell. Neurons have evolved specific mechanisms to overcome these challenges, but they consequently remain particularly susceptible to defects in proteostasis. One such defect is that of translational infidelity, which can result in the accumulation of unfolded or misfolded protein products. In the case of translationopathies, neurons potentially function as a canary in a coal mine, exhibiting cellular stress and degeneration due to translational fidelity loss that is endemic to all cells in the body.

Though the past two decades have seen the emergence and growth of research into ribosomopathies and translationopathies, much work is needed to be done to understand their unique features and paradoxes. In terms of the research presented in this work, structural and functional characterization of uL6 L20P ribosomes could reveal the basis for translational fidelity defects observed in chapter 2. For the *de novo* eEF2 mutations discussed in chapter 3, their effects on cellular stress response pathways could be investigated to establish a link

between observed translational fidelity defects and disease and an animal model could be used to definitively show that these novel mutations are causative for neurodevelopmental disorders. Additional biochemical characterizations of the panel of eEF2 mutations developed in chapter 4 could further elucidate the precise effect of eEF2-ribosome interactions on translational fidelity, including denaturation curves, ribosome binding equilibria, translocation rates, and even kinetic determinations of the translocation pathway using smFRET (single molecule fluorescence resonance energy transfer). As a whole, future research into these disorders should focus on the potential for therapeutic intervention, as well as harnessing the knowledge gained to deepen our understanding of the relationships between ribosome homeostasis, protein synthesis, translational fidelity, and cellular fitness, stress, and disease.

Appendices

Appendix 1: Plasmids

Table 5: List of plasmids used in this study

Plasmid	Description
pJD375	pYDL 0-frame control
pJD377	pYDL +1 PRF (Ty1)
pJD378	pYDL -1 PRF (HIV)
pJD433	pYDL TCR (UGA)
pJD2257	pSGDmod 0-frame control
pJD2337	pSGDmod PEG10 (-1 PRF)
pJD2349	pSGDmod OAZ1 (-1 PRF)
pJD2443	pSGDmod UAA
pJD2444	pSGDmod UGA
pJD2445	pSGDmod UAG
pJD2490	pyJD1334 (S.c.*EFT2*-6xHis, see yJD1334)
pJD2419	S.c.*EFT2* in pyJD1334::V28M
pJD2422	S.c.*EFT2* in pyJD1334**::**C372Y
pJD2423	S.c.*EFT2* in pyJD1334**::**P580H
pJD2424	S.c.*EFT2* in pyJD1334**::**Q753Y
pJD2425	S.c.*EFT2* in pyJD1334**::**Q753H
pJD2497	S.c.*EFT2* in pyJD1334**::**H699N
pJD2533	S.c.*EFT2* in pyJD1334::V28A
pJD2534	S.c.*EFT2* in pyJD1334::V28D
pJD2535	S.c.*EFT2* in pyJD1334::V28F
pJD2536	S.c.*EFT2* in pyJD1334::V28K
pJD2537	S.c.*EFT2* in pyJD1334::R66A
pJD2538	S.c.*EFT2* in pyJD1334::R66E
pJD2539	S.c.*EFT2* in pyJD1334::R66F
pJD2540	S.c.*EFT2* in pyJD1334::R66Q
pJD2541	S.c.*EFT2* in pyJD1334::R785A
pJD2542	S.c.*EFT2* in pyJD1334::R785E
pJD2543	S.c.*EFT2* in pyJD1334::R785F
pJD2544	S.c.*EFT2* in pyJD1334::R785Q
pJD2545	S.c.*EFT2* in pyJD1334::L536A
pJD2546	S.c.*EFT2* in pyJD1334::L536E
pJD2547	S.c.*EFT2* in pyJD1334::L536F
pJD2548	S.c.*EFT2* in pyJD1334::L536K

pJD2549	S.c.*EFT2* in pyJD1334::S579A
pJD2550	S.c.*EFT2* in pyJD1334::S579C
pJD2551	S.c.*EFT2* in pyJD1334::S579D
pJD2552	S.c.*EFT2* in pyJD1334::S579K
pJD2553	S.c.*EFT2* in pyJD1334::S579V
pJD2554	S.c.*EFT2* in pyJD1334::P580A
pJD2555	S.c.*EFT2* in pyJD1334::P580D
pJD2556	S.c.*EFT2* in pyJD1334::P580F
pJD2557	S.c.*EFT2* in pyJD1334::P580T
pJD2561	S.c.*EFT2* in pyJD1334::Q753A
pJD2562	S.c.*EFT2* in pyJD1334::Q753D
pJD2563	S.c.*EFT2* in pyJD1334::Q753F
pJD2564	S.c.*EFT2* in pyJD1334::N748A
pJD2565	S.c.*EFT2* in pyJD1334::N748D
pJD2566	S.c.*EFT2* in pyJD1334::N748L
pJD2567	S.c.*EFT2* in pyJD1334::N748R
pJD2568	S.c.*EFT2* in pyJD1334::V755A
pJD2570	S.c.*EFT2* in pyJD1334::V755F
pJD2571	S.c.*EFT2* in pyJD1334::V755K
pJD2572	S.c.*EFT2* in pyJD1334::V755T
pJD2573	S.c.*EFT2* in pyJD1334::S756A
pJD2574	S.c.*EFT2* in pyJD1334::S756E
pJD2575	S.c.*EFT2* in pyJD1334::S756F
pJD2576	S.c.*EFT2* in pyJD1334::S756K

Appendix 2: Yeast strains

Table 6: List of yeast strains used in this study

Strain	Genotype
yJD995	(YEFD12h[215]) MATa *ade2 ura3 his3 leu2 trp1 eft1::HIS3 eft2::TRP1* +YCp*EFT1-URA3* (*EFT2* parent strain, generously provided by Dr. Terri Kinzy)
yJD1334	(TKy675[28]) MATα *ade2 leu2 ura3 his3 trp1 eft::HIS3 eft2::TRP1* pEFT2-*LEU2*-CEN (*EFT2*-6xHis plasmid isolated and used for mutagenesis (pJD2490), strain generously provided by Dr. Terri Kinzy)
yJD1923	yJD995 + pJD2490_*EFT2*-WT
yJD1924	yJD995 + pJD2419_*EFT2*-V28M
yJD1927	yJD995 + pJD2422_*EFT2*-C372Y
yJD1928	yJD995 + pJD2423_*EFT2*-P580H
yJD1929	yJD995 + pJD2423_*EFT2*-Q753Y
yJD1930	yJD995 + pJD2425_*EFT2*-Q753H
yJD1958	yJD995 + pJD2497_*EFT2*-H699N
yJD2026	yJD995 + pJD2533_*EFT2*-V28A
yJD2027	yJD995 + pJD2537_*EFT2*-R66A
yJD2028	yJD995 + pJD2539_*EFT2*-R66F
yJD2029	yJD995 + pJD2540_*EFT2*-R66Q
yJD2030	yJD995 + pJD2542_*EFT2*-R785E
yJD2031	yJD995 + pJD2543_*EFT2*-R785F
yJD2032	yJD995 + pJD2544_*EFT2*-R785Q
yJD2033	yJD995 + pJD2545_*EFT2*-L536A
yJD2034	yJD995 + pJD2546_*EFT2*-L536E
yJD2035	yJD995 + pJD2547_*EFT2*-L536F
yJD2036	yJD995 + pJD2548_*EFT2*-L536K
yJD2037	yJD995 + pJD2554_*EFT2*-P580A
yJD2038	yJD995 + pJD2555_*EFT2*-P580D
yJD2039	yJD995 + pJD2556_*EFT2*-P580F
yJD2040	yJD995 + pJD2561_*EFT2*-Q753A
yJD2041	yJD995 + pJD2562_*EFT2*-Q753D
yJD2042	yJD995 + pJD2563_*EFT2*-Q753F
yJD2043	yJD995 + pJD2564_*EFT2*-N748A
yJD2044	yJD995 + pJD2565_*EFT2*-N748D
yJD2045	yJD995 + pJD2566_*EFT2*-N748L
yJD2046	yJD995 + pJD2567_*EFT2*-N748R
yJD2047	yJD995 + pJD2568_*EFT2*-V755A
yJD2048	yJD995 + pJD2570_*EFT2*-V755F
yJD2049	yJD995 + pJD2571_*EFT2*-V755K
yJD2050	yJD995 + pJD2572_*EFT2*-V755T
yJD2051	yJD995 + pJD2573_*EFT2*-S756A
yJD2052	yJD995 + pJD2576_*EFT2*-S756K

Appendix 3: Cell lines

Table 7: List of cell lines used in this study

Cell line name	Description	Clinical phenotype
NhnF	Control LCL	Healthy
NhnM	Control LCL	Healthy
F.T.	Control LCL	Healthy
RPL9 c. -2+1	Chr4(GRCh37):g.39460510C>G	DBA
RPL9 L20P (C.I.)	uL6 L20P (c.59C>T)	Cervical cancer

All cell lines generously provided by Dr. Alyson MacInnes from the European Diamond Blackfan Anemia Foundation (euroDBA). Cell lines were deidentified by the provider.

Appendix 4: Oligonucleotides

Table 8: List of oligonucleotides used for sequencing

Name	Sequence
Sc_EFT1_F1	CACTGTTGACCAAATGCGTTC
Sc_EFT1_F2	GAGCTTTGTTGGAATTGCAAG
Sc_EFT1_F3	GAGAAAGTTCTTGCCAGCTGC
Sc_EFT1_F4	CTCTCCAGTTGTGCAAGTCGC
Sc_EFT1_F5	GCTTTCCAATGGGCTACCAAG
Sc_EFT1_F6	TCTGACCCATTGGACCCAACC
Sc_EFT1_R1	TTGTGGGAAAGCTTGACCACC
Sc_EFT1_R2	GCCATGATTCTAGCTCTGGCC
Sc_EFT1_R3	GTGAGCAGTTTCACTGGTGGTC
Sc_EFT1_R4	TCCAAGTCCTTTTCGTCACCC
Sc_EFT1_R5	TTCGGTTTGGACACAGACACC
Sc_EFT1_R6	GCAATAACGGACATGTTACGC

Table 9: List of oligonucleotides used for site-directed mutagenesis

Name	Sequence
V28M-fwd	GTCCGTTATTGCTCACatgGATCATGGTAAGTCCAC
V28M-rev	GTGGACTTACCATGATCcatGTGAGCAATAACGGAC
C372Y-fwd	CTGTATTGCTATCAAGAACtatGATCCAAAGGCTGATTTGATG
C372Y-rev	CATCAAATCAGCCTTTGGATCATAGTTCTTGATAGCAATACAG
P580H-fwd	CTCAAACTGCTTTGTCCAAGTCTcatAACAAGCATAACAGAATC
P580H-rev	GATTCTGTTATGCTTGTTATGAGACTTGGACAAAGCAGTTTGAG
Q753Y-fwd	CGTCTTAAACAAGAAGAGAGGTtatGTCGTTTCTGAAGAACAAAG
Q753Y-rev	CTTTGTTCTTCAGAAACGACATAACCTCTCTTCTTGTTTAAGACG
Q753H-fwd	CGTCTTAAACAAGAAGAGAGGTcacGTCGTTTCTGAAGAACAAAG
Q753H-rev	CTTTGTTCTTCAGAAACGACGTGACCTCTCTTCTTGTTTAAGACG
H699N-fwd	CATGCCGATGCTATCaacAGAGGTGGTGGTC
H699N-rev	GACCACCACCTCTGttgATAGCATCGGCATG
V28A_fwd	TATTGCTCACgccGATCATGGTAAG
V28F_fwd	TATTGCTCACttcGATCATGGTAAG
V28D_fwd	TATTGCTCACgacGATCATGGTAAG
V28AFD_rev	ACGGACATGTTACGCACA
V28K_fwd	TATTGCTCACaagGATCATGGTAAGTCCACTTTG
V28K_rev	ACGGACATGTTACGCAC
R66A_fwd-2	TAGTGATACCtgcTTCTTGTTCATCC
R66E_fwd-2	TAGTGATACCttcTTCTTGTTCATCC
R66F_fwd-2	TAGTGATACCaaaTTCTTGTTCATCCTTTC
R66Q_fwd-2	TAGTGATACCttgTTCTTGTTCATCC

R66AEFQ_rev-2	TCAAGTCTACCGCTATTTC
R785A_fwd	TGGTGAATTGgcaCAAGCTACTG
R785E_fwd	TGGTGAATTGgaaCAAGCTACTG
R785Q_fwd	TGGTGAATTGcaaCAAGCTACTG
R785F_fwd	TGGTGAATTGtttCAAGCTACTGGTG
R785AEQF_rev	GTGAAACCGAAAGATTCG
L536A_fwd	TACCGGTGAAgctCATTTGGAAATTTGTTTG
L536F_fwd	TACCGGTGAAtttCATTTGGAAATTTG
L536K_fwd	TACCGGTGAAaagCATTTGGAAATTTG
L536AFK_rev	CCAGCAACGATATGTTCAC
L536E_fwd-2	TTTCCAAATGTTCTTCACCGGTACCAG
L536E_rev-2	TTTGTTTGCAAGATTTGG
S579A_fwd	TTTGTCCAAGgctCCAAACAAGC
S579A_rev	GCAGTTTGAGAAGATTCACTTTC
S579D_fwd	TTTGTCCAAGgatCCAAACAAGC
S579K_fwd	TTTGTCCAAGaaaCCAAACAAGC
S579V_fwd	TTTGTCCAAGgttCCAAACAAGCATAAC
S579C_fwd	TTTGTCCAAGtgtCCAAACAAGC
S579DKVC_rev	GCAGTTTGAGAAGATTCAC
P580A_fwd	GTCCAAGTCTgcaAACAAGCATAAC
P580F_fwd	GTCCAAGTCTtttAACAAGCATAAC
P580D_fwd	GTCCAAGTCTgatAACAAGCATAAC
P580T_fwd	GTCCAAGTCTacaAACAAGCATAAC
P580AT_rev	AAAGCAGTTTGAGAAGATTCAC
P580FD_rev	AAAGCAGTTTGAGAAGATTC
Q753A_fwd	GAAGAGAGGTgctGTCGTTTCTGAAG
Q753F_fwd	GAAGAGAGGTtttGTCGTTTCTGAAG
Q753D_fwd	GAAGAGAGGTgatGTCGTTTCTG
Q753AFD_rev	TTGTTTAAGACGGAGTAG
N748A_fwd	CTCCGTCTTAgctAAGAAGAGAGGTCAAGTCG
N748D_fwd	CTCCGTCTTAgacAAGAAGAGAGG
N748L_fwd	CTCCGTCTTActaAAGAAGAGAGGTCAAGTCGTTTC
N748R_fwd	CTCCGTCTTAagaAAGAAGAGAGGTCAAGTC
N748ADLR_rev	TAGATACCACCGACGGCT
V755A_fwd	AGGTCAAGTCgctTCTGAAGAAC
V755A_rev	CTCTTCTTGTTTAAGACGGAG
V755F_fwd	AGGTCAAGTCtttTCTGAAGAAC
V755T_fwd	AGGTCAAGTCactTCTGAAGAACAAAG
V755K_fwd	AGGTCAAGTCaagTCTGAAGAACAAAGAC
V755FTK_rev	CTCTTCTTGTTTAAGACGG
S756E_fwd	TCAAGTCGTTgagGAAGAACAAAGAC
S756A_fwd	TCAAGTCGTTgctGAAGAACAAAG

S756F_fwd	TCAAGTCGTTtttGAAGAACAAAG
S756K_fwd	TCAAGTCGTTaaaGAAGAACAAAGACC
S756EAFK_rev	CCTCTCTTCTTGTTTAAGAC

Table 10: List of oligonucleotides used for colony PCR

Mutations	Name	Sequence
V28, R66	EFT2-A fwd	CTGAAGATTGGGTCCAAGATGA
	EFT2-A rev	CTTTCAGCACTGAAGAGTCCA
L536, S579, P580, N748, Q753, V755, S756	EFT2-C fwd	CCAACAAGAAACCAGCGTAAG
	EFT2-C rev	CAAACTACGTTCCAGGTAAGA
R785	EFT2-D fwd	GTCCAATGGGTCAGAACCTAAA
	EFT2-D rev	CCAAGTCTCCAAACAAGCATAAC

Bibliography

1. Harris, J. K., Kelley, S. T., Spiegelman, G. B. & Pace, N. R. The Genetic Core of the Universal Ancestor. *Genome Research* **13**, 407–412 (2003).
2. Koonin, E. v. Comparative genomics, minimal gene-sets and the last universal common ancestor. *Nature Reviews Microbiology* **1**, 127–136 (2003).
3. Buttgereit, F. & Brand, M. D. A hierarchy of ATP-consuming processes in mammalian cells. *Biochemical Journal* **312**, 163–167 (1995).
4. Russell, J. B. & Cook, G. M. Energetics of bacterial growth: balance of anabolic and catabolic reactions. *Microbiological Reviews* **59**, 48–62 (1995).
5. Lafontaine, D. L. J. & Tollervey, D. The function and synthesis of ribosomes. *Nature Reviews Molecular Cell Biology* **2**, 514–520 (2001).
6. Gerbi, S. A. Expansion segment: regions of variable size that interrupt the universal core secondary structure of ribosomal RNA. in *Ribosomal RNA: structure, evolution, processing, and function in protein synthesis.* (eds. Zimmermann, R. A. & Dahlberg, A. E.) 71–87 (CRC Press, 1996).
7. Bowman, J. C., Petrov, A. S., Frenkel-Pinter, M., Penev, P. I. & Williams, L. D. Root of the Tree: The Significance, Evolution, and Origins of the Ribosome. *Chemical Reviews* **120**, 4848–4878 (2020).
8. Schmeing, T. M. & Ramakrishnan, V. What recent ribosome structures have revealed about the mechanism of translation. *Nature* **461**, 1234–1242 (2009).
9. Cech, T. R. The Ribosome Is a Ribozyme. *Science (1979)* **289**, 878–879 (2000).
10. Moore, P. B. & Steitz, T. A. The involvement of RNA in ribosome function. *Nature* **418**, 229–235 (2002).
11. Brodersen, D. E. & Nissen, P. The social life of ribosomal proteins. *FEBS J.* **272**, 2098–2108 (2005).
12. Fujii, K., Susanto, T. T., Saurabh, S. & Barna, M. Decoding the Function of Expansion Segments in Ribosomes. *Molecular Cell* **72**, 1013-1020.e6 (2018).
13. Wilson, D. N. & Nierhaus, K. H. Ribosomal proteins in the spotlight. *Crit Rev.Biochem.Mol Biol* **40**, 243–267 (2005).
14. Bhavsar, R. B., Makley, L. N. & Tsonis, P. A. The other lives of ribosomal proteins. *Human Genomics* **4**, 327 (2010).
15. Sergiev, P. v, Aleksashin, N. A., Chugunova, A. A., Polikanov, Y. S. & Dontsova, O. A. Structural and evolutionary insights into ribosomal RNA methylation. *Nature Chemical Biology* **14**, 226–235 (2018).
16. Hinnebusch, A. G. & Lorsch, J. R. The Mechanism of Eukaryotic Translation Initiation: New Insights and Challenges. *Cold Spring Harbor Perspectives in Biology* **4**, a011544–a011544 (2012).
17. Cigan, A. M., Feng, L. & Donahue, T. F. tRNA $_{i}^{met}$ Functions in Directing the Scanning Ribosome to the Start Site of Translation. *Science (1979)* **242**, 93–97 (1988).
18. Zhouravleva, G. *et al.* Termination of translation in eukaryotes is governed by two interacting polypeptide chain release factors, eRF1 and eRF3. *EMBO J.* **14**, 4065–4072 (1995).
19. Hellen, C. U. T. Translation Termination and Ribosome Recycling in Eukaryotes. *Cold Spring Harbor Perspectives in Biology* **10**, a032656 (2018).

20. Schuller, A. P. & Green, R. Roadblocks and resolutions in eukaryotic translation. *Nature Reviews Molecular Cell Biology* **19**, 526–541 (2018).
21. Dever, T. E., Dinman, J. D. & Green, R. Translation Elongation and Recoding in Eukaryotes. *Cold Spring Harbor Perspectives in Biology* **10**, a032649 (2018).
22. Ogle, J. M. *et al.* Recognition of cognate transfer RNA by the 30S ribosomal subunit. *Science (1979)* **292**, 897–902 (2001).
23. Demeshkina, N., Jenner, L., Westhof, E., Yusupov, M. & Yusupova, G. A new understanding of the decoding principle on the ribosome. *Nature* **484**, 256–259 (2012).
24. Shao, S. *et al.* Decoding Mammalian Ribosome-mRNA States by Translational GTPase Complexes. *Cell* **167**, 1229-1240.e15 (2016).
25. Leung, E. K., Suslov, N., Tuttle, N., Sengupta, R. & Piccirilli, J. A. The mechanism of peptidyl transfer catalysis by the ribosome. *Annu.Rev.Biochem.* **80**, 527–555 (2011).
26. Sievers, A., Beringer, M., Rodnina, M. v. & Wolfenden, R. The ribosome as an entropy trap. *Proceedings of the National Academy of Sciences* **101**, 7897–7901 (2004).
27. Gavrilova, L. P., Kostiashkina, O. E., Koteliansky, V. E., Rutkevitch, N. M. & Spirin, A. S. Factor-free ("Non-enzymic") and factor-dependent systems of translation of polyuridylic acid by Escherichia coli ribosomes. *Journal of Molecular Biology* **101**, 537–552 (1976).
28. Jørgensen, R., Carr-Schmid, A., Ortiz, P. A., Kinzy, T. G. & Andersen, G. R. Purification and crystallization of the yeast elongation factor eEF2. *Acta Crystallographica Section D Biological Crystallography* **58**, 712–715 (2002).
29. CARLBERG, U., NILSSON, A. & NYGARD, O. Functional properties of phosphorylated elongation factor 2. *European Journal of Biochemistry* **191**, 639–645 (1990).
30. Schaffrath, R., Abdel-Fattah, W., Klassen, R. & Stark, M. J. R. The diphthamide modification pathway from <scp> *S* </scp> *accharomyces cerevisiae* – revisited. *Molecular Microbiology* **94**, 1213–1226 (2014).
31. Goodsell, D. S. Elongation Factors. *RCSB Protein Data Bank* (2006) doi:10.2210/rcsb_pdb/mom_2006_9.
32. Jørgensen, R., Merrill, A. R. & Andersen, G. R. The life and death of translation elongation factor 2. *Biochemical Society Transactions* **34**, 1–6 (2006).
33. Noller, H. F., Lancaster, L., Zhou, J. & Mohan, S. The ribosome moves: RNA mechanics and translocation. *Nature Structural & Molecular Biology* **24**, 1021–1027 (2017).
34. Frank, J. & Agrawal, R. K. A ratchet-like inter-subunit reorganization of the ribosome during translocation. *Nature* **406**, 318–322 (2000).
35. Spiegel, P. C., Ermolenko, D. N. & Noller, H. F. Elongation factor G stabilizes the hybrid-state conformation of the 70S ribosome. *RNA* **13**, 1473–1482 (2007).
36. Ratje, A. H. *et al.* Head swivel on the ribosome facilitates translocation by means of intra-subunit tRNA hybrid sites. *Nature* **468**, 713–716 (2010).
37. Blanchard, S. C., Kim, H. D., Gonzalez Jr., R. L., Puglisi, J. D. & Chu, S. tRNA dynamics on the ribosome during translation. *Proc.Natl.Acad.Sci.U.S.A* **101**, 12893–12898 (2004).
38. Mohan, S., Donohue, J. P. & Noller, H. F. Molecular mechanics of 30S subunit head rotation. *Proc Natl Acad Sci U S A* **111**, 13325–30 (2014).
39. Rodnina, M. v., Peske, F., Peng, B.-Z., Belardinelli, R. & Wintermeyer, W. Converting GTP hydrolysis into motion: versatile translational elongation factor G. *Biological Chemistry* **401**, 131–142 (2019).

40. Rodnina, M. v, Savelsbergh, A., Katunin, V. I. & Wintermeyer, W. Hydrolysis of GTP by elongation factor G drives tRNA movement on the ribosome. *Nature* **385**, 37–41 (1997).
41. Savelsbergh, A. *et al.* An elongation factor G-induced ribosome rearrangement precedes tRNA-mRNA translocation. *Molecular Cell* **11**, 1517–1523 (2003).
42. Lin, J., Gagnon, M. G., Bulkley, D. & Steitz, T. A. Conformational Changes of Elongation Factor G on the Ribosome during tRNA Translocation. *Cell* **160**, 219–227 (2015).
43. Chen, C. *et al.* Elongation factor G initiates translocation through a power stroke. *Proceedings of the National Academy of Sciences* **113**, 7515–7520 (2016).
44. Ermolenko, D. N. & Noller, H. F. mRNA translocation occurs during the second step of ribosomal intersubunit rotation. *Nature Structural & Molecular Biology* **18**, 457–462 (2011).
45. Chen, J., Petrov, A., Tsai, A., O'Leary, S. E. & Puglisi, J. D. Coordinated conformational and compositional dynamics drive ribosome translocation. *Nature Structural & Molecular Biology* **20**, 718–727 (2013).
46. Li, W. *et al.* Activation of GTP hydrolysis in mRNA-tRNA translocation by elongation factor G. *Science Advances* **1**, (2015).
47. Cunha, C. E. *et al.* Dual use of GTP hydrolysis by elongation factor G on the ribosome. *Translation* **1**, e24315 (2013).
48. Carbone, C. E. *et al.* Time-resolved cryo-EM visualizes ribosomal translocation with EF-G and GTP. *Nature Communications* **12**, 7236 (2021).
49. Ibba, M. & Söll, D. Aminoacyl-tRNA Synthesis. *Annual Review of Biochemistry* **69**, 617–650 (2000).
50. Schmidt, E. & Schimmel, P. Mutational Isolation of a Sieve for Editing in a Transfer RNA Synthetase. *Science (1979)* **264**, 265–267 (1994).
51. Ling, J., Reynolds, N. & Ibba, M. Aminoacyl-tRNA Synthesis and Translational Quality Control. *Annual Review of Microbiology* **63**, 61–78 (2009).
52. Kramer, E. B. & Farabaugh, P. J. The frequency of translational misreading errors in E. coli is largely determined by tRNA competition. *RNA.* **13**, 87–96 (2007).
53. Cochella, L. & Green, R. Fidelity in protein synthesis. *Curr.Biol* **15**, R536–R540 (2005).
54. Pape, T., Wintermeyer, W. & Rodnina, M. Induced fit in initial selection and proofreading of aminoacyl-tRNA on the ribosome. *EMBO J.* **18**, 3800–3807 (1999).
55. Parker, J. Errors and Alternatives in Reading the Universal Genetic-Code. *Microbiological Reviews* **53**, 273–298 (1989).
56. Losson, R. & Lacroute, F. Interference of nonsense mutations with eukaryotic messenger RNA stability. *Proceedings of the National Academy of Sciences* **76**, 5134–5137 (1979).
57. Karamyshev, A. L. & Karamysheva, Z. N. Lost in Translation: Ribosome-Associated mRNA and Protein Quality Controls. *Frontiers in Genetics* **9**, (2018).
58. Doma, M. K. & Parker, R. Endonucleolytic cleavage of eukaryotic mRNAs with stalls in translation elongation. *Nature* **440**, 561–564 (2006).
59. Frischmeyer, P. A. *et al.* An mRNA surveillance mechanism that eliminates transcripts lacking termination codons. *Science (1979)* **295**, 2258–2261 (2002).
60. Shoemaker, C. J. & Green, R. Translation drives mRNA quality control. *Nature Structural & Molecular Biology* **19**, 594–601 (2012).
61. Yang, Q. *et al.* eRF1 mediates codon usage effects on mRNA translation efficiency through premature termination at rare codons. *Nucleic Acids Research* **47**, 9243–9258 (2019).

62. Svidritskiy, E., Demo, G. & Korostelev, A. A. Mechanism of premature translation termination on a sense codon. *Journal of Biological Chemistry* **293**, 12472–12479 (2018).
63. Roy, B., Leszyk, J. D., Mangus, D. A. & Jacobson, A. Nonsense suppression by near-cognate tRNAs employs alternative base pairing at codon positions 1 and 3. *Proceedings of the National Academy of Sciences* **112**, 3038–3043 (2015).
64. Paushkin, S. v., Kushnirov, V. v., Smirnov, V. N. & Ter-Avanesyan, M. D. Propagation of the yeast prion-like [psi+] determinant is mediated by oligomerization of the SUP35-encoded polypeptide chain release factor. *The EMBO Journal* **15**, 3127–3134 (1996).
65. Ortiz, P. A., Ulloque, R., Kihara, G. K., Zheng, H. & Kinzy, T. G. Translation elongation factor 2 anticodon mimicry domain mutants affect fidelity and diphtheria toxin resistance. *J.Biol.Chem.* **281**, 32639–32648 (2006).
66. Pellegrino, S. *et al.* Structural Insights into the Role of Diphthamide on Elongation Factor 2 in mRNA Reading-Frame Maintenance. *Journal of Molecular Biology* **430**, 2677–2687 (2018).
67. Zhou, J., Lancaster, L., Donohue, J. P. & Noller, H. F. Spontaneous ribosomal translocation of mRNA and tRNAs into a chimeric hybrid state. *Proceedings of the National Academy of Sciences* **116**, 7813–7818 (2019).
68. Flis, J. *et al.* tRNA Translocation by the Eukaryotic 80S Ribosome and the Impact of GTP Hydrolysis. *Cell Reports* **25**, 2676-2688.e7 (2018).
69. Allan Drummond, D. & Wilke, C. O. The evolutionary consequences of erroneous protein synthesis. *Nature Reviews Genetics* **10**, 715–724 (2009).
70. Dinman, J. D. Mechanisms and implications of programmed translational frameshifting. *Wiley Interdiscip.Rev.RNA* **3**, 661–673 (2012).
71. Jacks, T. *et al.* Characterization of ribosomal frameshifting in HIV-1 gag-pol expression. *Nature* **331**, 280–283 (1988).
72. Hung, M., Patel, P., Davis, S. & Green, S. R. Importance of ribosomal frameshifting for human immumodeficiency virus type 1 assembly and replication. *J.Virol.* **72**, 4819–4824 (1998).
73. Clark, M. B. *et al.* Mammalian gene PEG10 expresses two reading frames by high efficiency -1 frameshifting in embryonic-associated tissues. *J.Biol Chem.* **282**, 37359–37369 (2007).
74. Belew, A. T., Hepler, N. L., Jacobs, J. L. & Dinman, J. D. PRFdb: a database of computationally predicted eukaryotic programmed -1 ribosomal frameshift signals. *BMC.Genomics* **9**, 339 (2008).
75. Plant, E. P. E. P., Wang, P., Jacobs, J. L. J. L. & Dinman, J. D. J. D. A programmed -1 ribosomal frameshift signal can function as a cis-acting mRNA destabilizing element. *Nucleic Acids Res.* **32**, 784–790 (2004).
76. Belew, A. T. *et al.* Ribosomal frameshifting in the CCR5 mRNA is regulated by miRNAs and the NMD pathway. *Nature* **512**, 265–269 (2014).
77. Belcourt, M. F. & Farabaugh, P. J. Ribosomal frameshifting in the yeast retrotransposon Ty: tRNAs induce slippage on a 7 nucleotide minimal site. *Cell* **62**, 339–352 (1990).
78. Ivanov, I. P., Matsufuji, S., Murakami, Y., Gesteland, R. F. & Atkins, J. F. Conservation of polyamine regulation by translational frameshifting from yeast to mammals. *EMBO J.* **19**, 1907–1917 (2000).

79. Palanimurugan, R., Scheel, H., Hofmann, K. & Dohmen, R. J. Polyamines regulate their synthesis by inducing expression and blocking degradation of ODC antizyme. *EMBO J.* **23**, 4857–4867 (2004).
80. Murakami, Y., Tanaka, K., Matsufuji, S., Miyazaki, Y. & Hayashi, S. I. Antizyme, a protein induced by polyamines, accelerates the degradation of ornithine decarboxylase in Chinese-hamster ovary-cell extracts. *Biochemical Journal* **283**, 661–664 (1992).
81. Wang, X. *et al.* Regulation of HIV-1 Gag-Pol Expression by Shiftless, an Inhibitor of Programmed -1 Ribosomal Frameshifting. *Cell* **176**, 625-635.e14 (2019).
82. Costa-Mattioli, M. & Walter, P. The integrated stress response: From mechanism to disease. *Science* **368**, (2020).
83. Fulda, S., Gorman, A. M., Hori, O. & Samali, A. Cellular Stress Responses: Cell Survival and Cell Death. *International Journal of Cell Biology* **2010**, 1–23 (2010).
84. Francisco, S., Ferreira, M., Moura, G., Soares, A. R. & Santos, M. A. S. Does proteostasis get lost in translation? Implications for protein aggregation across the lifespan. *Ageing Research Reviews* **62**, 101119 (2020).
85. Draptchinskaia, N. *et al.* The gene encoding ribosomal protein S19 is mutated in Diamond-Blackfan anaemia. *Nat.Genet.* **21**, 169–175 (1999).
86. Narla, A. & Ebert, B. L. Ribosomopathies: human disorders of ribosome dysfunction. *Blood* **115**, 3196–3205 (2010).
87. de Keersmaecker, K., Sulima, S. O. & Dinman, J. D. Ribosomopathies and the paradox of cellular hypo- to hyperproliferation. *Blood* **125**, 1377–82 (2015).
88. Dameshek, W. Riddle: what do aplastic anemia, paroxysmal nocturnal hemoglobinuria (PNH) and "hypoplastic" leukemia have in common? *Blood* **30**, 251–4 (1967).
89. Tahmasebi, S., Khoutorsky, A., Mathews, M. B. & Sonenberg, N. Translation deregulation in human disease. *Nature Reviews Molecular Cell Biology* **19**, 791–807 (2018).
90. Shi, Z. *et al.* Heterogeneous ribosomes preferentially translate distinct subpools of mRNAs genome-wide. *Molecular Cell* **67**, 71–83 (2017).
91. Lodish, H. F. Model for the regulation of mRNA translation applied to haemoglobin synthesis. *Nature* **251**, 385–8 (1974).
92. Mills, E. W. & Green, R. Ribosomopathies: There's strength in numbers. *Science (1979)* **358**, eaan2755 (2017).
93. Choesmel, V. *et al.* Impaired ribosome biogenesis in Diamond-Blackfan anemia. *Blood* **109**, 1275–1283 (2007).
94. Ebert, B. L. *et al.* Identification of RPS14 as a 5q- syndrome gene by RNA interference screen. *Nature* **451**, 335–339 (2008).
95. Valdez, B. C., Henning, D., So, R. B., Dixon, J. & Dixon, M. J. The Treacher Collins syndrome (*TCOF1*) gene product is involved in ribosomal DNA gene transcription by interacting with upstream binding factor. *Proceedings of the National Academy of Sciences* **101**, 10709–10714 (2004).
96. Heiss, N. S. *et al.* X-linked dyskeratosis congenita is caused by mutations in a highly conserved gene with putative nucleolar functions. *Nat.Genet.* **19**, 32–38 (1998).
97. Ruggero, D. *et al.* Dyskeratosis congenita and cancer in mice deficient in ribosomal RNA modification. *Science (1979)* **299**, 259–262 (2003).
98. Ridanpaa, M. *et al.* Mutations in the RNA component of RNase MRP cause a pleiotropic human disease, cartilage-hair hypoplasia. *Cell* **104**, 195–203 (2001).

99. Boocock, G. R. B. *et al.* Mutations in SBDS are associated with Shwachman–Diamond syndrome. *Nature Genetics* **33**, 97–101 (2002).
100. Brooks, S. S. *et al.* A novel ribosomopathy caused by dysfunction of RPL10 disrupts neurodevelopment and causes X-linked microcephaly in humans. *Genetics* **198**, 723–733 (2014).
101. Paolini, N. A. *et al.* A ribosomopathy reveals decoding defective ribosomes driving human dysmorphism. *The American Journal of Human Genetics* **100**, 506–522 (2017).
102. Nakayama, T. *et al.* Deficient activity of alanyl-tRNA synthetase underlies an autosomal recessive syndrome of progressive microcephaly, hypomyelination, and epileptic encephalopathy. *Human Mutation* **38**, 1348–1354 (2017).
103. Hekman, K. E. *et al.* A conserved eEF2 coding variant in SCA26 leads to loss of translational fidelity and increased susceptibility to proteostatic insult. *Hum.Mol.Genet.* **21**, 5472–5483 (2012).
104. Liu, S. *et al.* Diphthamide modification on eukaryotic elongation factor 2 is needed to assure fidelity of mRNA translation and mouse development. *Proceedings of the National Academy of Sciences* **109**, 13817–13822 (2012).
105. Loucks, C. M. *et al.* Matching Two Independent Cohorts Validates *DPH1* as a Gene Responsible for Autosomal Recessive Intellectual Disability with Short Stature, Craniofacial, and Ectodermal Anomalies. *Human Mutation* **36**, 1015–1019 (2015).
106. Budde, B. S. *et al.* tRNA splicing endonuclease mutations cause pontocerebellar hypoplasia. *Nature Genetics* **40**, 1113–1118 (2008).
107. Breuss, M. W. *et al.* Autosomal-Recessive Mutations in the tRNA Splicing Endonuclease Subunit TSEN15 Cause Pontocerebellar Hypoplasia and Progressive Microcephaly. *The American Journal of Human Genetics* **99**, 785 (2016).
108. Nakajima, J. *et al. De novo EEF1A2* mutations in patients with characteristic facial features, intellectual disability, autistic behaviors and epilepsy. *Clinical Genetics* **87**, 356–361 (2015).
109. Sandbaken, M. G. & Culbertson, M. R. Mutations in elongation factor EF-1 alpha affect the frequency of frameshifting and amino acid misincorporation in Saccharomyces cerevisiae. *Genetics* **120**, 923–934 (1988).
110. Lam, W. W. K. *et al.* Novel de novo *EEF1A2* missense mutations causing epilepsy and intellectual disability. *Molecular Genetics & Genomic Medicine* **4**, 465–474 (2016).
111. Shaheen, R. *et al.* A homozygous truncating mutation in PUS3 expands the role of tRNA modification in normal cognition. *Human Genetics* **135**, 707–713 (2016).
112. Thiaville, P. *et al.* Global translational impacts of the loss of the tRNA modification t6A in yeast. *Microbial Cell* **3**, 29–45 (2016).
113. Braun, D. A. *et al.* Mutations in KEOPS-complex genes cause nephrotic syndrome with primary microcephaly. *Nature Genetics* **49**, 1529–1538 (2017).
114. Edvardson, S. *et al.* tRNA N6-adenosine threonylcarbamoyltransferase defect due to KAE1/TCS3 (OSGEP) mutation manifest by neurodegeneration and renal tubulopathy. *European Journal of Human Genetics* **25**, 545–551 (2017).
115. Doherty, L. *et al.* Ribosomal protein genes RPS10 and RPS26 are commonly mutated in Diamond-Blackfan anemia. *Am J Hum Genet* **86**, 222–8 (2010).
116. Flygare, J. *et al.* Human RPS19, the gene mutated in Diamond-Blackfan anemia, encodes a ribosomal protein required for the maturation of 40S ribosomal subunits. *Blood* **109**, 980–986 (2007).

117. Sankaran, V. G. *et al.* Exome sequencing identifies GATA1 mutations resulting in Diamond-Blackfan anemia. *J Clin Invest* **122**, 2439–43 (2012).
118. Ludwig, L. S. *et al.* Altered translation of GATA1 in Diamond-Blackfan anemia. *Nat Med* **20**, 748–53 (2014).
119. Manto, M. The wide spectrum of spinocerebellar ataxias (SCAs). *Cerebellum* **4**, 2–6 (2005).
120. Lezzerini, M. *et al.* Ribosomal protein gene RPL9 variants can differentially impair ribosome function and cellular metabolism. *Nucleic Acids Research* **48**, (2020).
121. Vlachos, A. *et al.* Diagnosing and treating Diamond Blackfan anaemia: results of an international clinical consensus conference. *British Journal of Haematology* **142**, 859 (2008).
122. Ball, S. E., Mcguckin, C. P., Jenkins, G. & Gordon-Smith, E. C. Diamond-Blackfan anaemia in the U.K.: analysis of 80 cases from a 20-year birth cohort. *Br J Haematol* **94**, 645–653 (1996).
123. Lipton, J. M., Atsidaftos, E., Zyskind, I. & Vlachos, A. Improving clinical care and elucidating the pathophysiology of Diamond Blackfan anemia: an update from the Diamond Blackfan Anemia Registry. *Pediatr Blood Cancer* **46**, 558–564 (2006).
124. Vlachos, A., Rosenberg, P. S., Atsidaftos, E., Alter, B. P. & Lipton, J. M. Incidence of neoplasia in Diamond Blackfan anemia: a report from the Diamond Blackfan Anemia Registry. *Blood* **119**, 3815–3819 (2012).
125. Vlachos, A. *et al.* Increased risk of colon cancer and osteogenic sarcoma in Diamond-Blackfan anemia. *Blood* **132**, 2205 (2018).
126. Boria, I. *et al.* The ribosomal basis of Diamond-Blackfan Anemia: mutation and database update. *Hum.Mutat.* **31**, 1269–1279 (2010).
127. Ban, N. *et al.* A new system for naming ribosomal proteins. *Curr Opin Struct Biol* **24**, 165–9 (2014).
128. Cmejla, R., Cmejlova, J., Handrkova, H., Petrak, J. & Pospisilova, D. Ribosomal protein S17 gene (RPS17) is mutated in Diamond-Blackfan anemia. *Human Mutation* **28**, 1178–1182 (2007).
129. Farrar, J. E. *et al.* Abnormalities of the large ribosomal subunit protein, Rpl35a, in Diamond-Blackfan anemia. *Blood* **112**, 1582–92 (2008).
130. Gazda, H. T. *et al.* Ribosomal protein S24 gene is mutated in Diamond-Blackfan anemia. *Am J Hum Genet* **79**, 1110–8 (2006).
131. Gazda, H. T. *et al.* Frameshift mutation in p53 regulator RPL26 is associated with multiple physical abnormalities and a specific pre-ribosomal RNA processing defect in diamond-blackfan anemia. *Hum Mutat* **33**, 1037–44 (2012).
132. Gazda, H. T. *et al.* Ribosomal protein L5 and L11 mutations are associated with cleft palate and abnormal thumbs in Diamond-Blackfan anemia patients. *Am J Hum Genet* **83**, 769–80 (2008).
133. Landowski, M. *et al.* Novel deletion of RPL15 identified by array-comparative genomic hybridization in Diamond-Blackfan anemia. *Hum Genet* **132**, 1265–74 (2013).
134. Wang, R. *et al.* Loss of function mutations in RPL27 and RPS27 identified by whole-exome sequencing in Diamond-Blackfan anaemia. *Br J Haematol* **168**, 854–864 (2015).
135. Mirabello, L. *et al.* Whole-exome sequencing and functional studies identify RPS29 as a novel gene mutated in multicase Diamond-Blackfan anemia families. *Blood* **124**, 24–32 (2014).

136. Gripp, K. W. *et al.* Diamond-Blackfan anemia with mandibulofacial dystostosis is heterogeneous, including the novel DBA genes TSR2 and RPS28. *Am J Med Genet A* **164A**, 2240–9 (2014).
137. Ikeda, F. *et al.* Exome sequencing identified RPS15A as a novel causative gene for Diamond-Blackfan anemia. *Haematologica* **102**, e93 (2017).
138. Mirabello, L. *et al.* Novel and known ribosomal causes of Diamond-Blackfan anaemia identified through comprehensive genomic characterisation. *J Med Genet* **54**, 417–425 (2017).
139. Wlodarski, M. W. *et al.* Recurring mutations in RPL15 are linked to hydrops fetalis and treatment independence in Diamond-Blackfan anemia. *Haematologica* **103**, 949 (2018).
140. Borsi, E. *et al.* Somatic reversion events point towards RPL4 as a novel disease gene in a condition resembling Diamond-Blackfan anemia. *Haematologica* **103**, e607 (2018).
141. Dutt, S. *et al.* Haploinsufficiency for ribosomal protein genes causes selective activation of p53 in human erythroid progenitor cells. *Blood* **117**, 2567 (2011).
142. Jaako, P. *et al.* Mice with ribosomal protein S19 deficiency develop bone marrow failure and symptoms like patients with Diamond-Blackfan anemia. *Blood* **118**, 6087–6096 (2011).
143. Moniz, H. *et al.* Primary hematopoietic cells from DBA patients with mutations in RPL11 and RPS19 genes exhibit distinct erythroid phenotype in vitro. *Cell Death & Disease* **3**, e356 (2012).
144. Toki, T. *et al.* De Novo Mutations Activating Germline TP53 in an Inherited Bone-Marrow-Failure Syndrome. *American Journal of Human Genetics* **103**, 440 (2018).
145. Bourque, D. K. *et al.* A de novo mutation in RPL10 causes a rare X-linked ribosomopathy characterized by syndromic intellectual disability and epilepsy: A new case and review of the literature. *Eur J Med Genet* **61**, 89–93 (2018).
146. Thevenon, J. *et al.* RPL10 mutation segregating in a family with X-linked syndromic Intellectual Disability. *Am J Med Genet A* **167A**, 1908–1912 (2015).
147. Zanni, G. *et al.* A Novel Mutation in RPL10 (Ribosomal Protein L10) Causes X-Linked Intellectual Disability, Cerebellar Hypoplasia, and Spondylo-Epiphyseal Dysplasia. *Hum Mutat* **36**, 1155–1158 (2015).
148. de Keersmaecker, K. *et al.* Exome sequencing identifies mutation in CNOT3 and ribosomal genes RPL5 and RPL10 in T-cell acute lymphoblastic leukemia. *Nat.Genet.* **45**, 186–190 (2013).
149. Fancello, L., Kampen, K. R., Hofman, I. J. F., Verbeeck, J. & de Keersmaecker, K. The ribosomal protein gene RPL5 is a haploinsufficient tumor suppressor in multiple cancer types. *Oncotarget* **8**, 14462–14478 (2017).
150. Ferreira, A. *et al.* High Frequency of RPL22 Mutations in Microsatellite-Unstable Colorectal and Endometrial Tumors. *Human Mutation* **35**, 1442–1445 (2014).
151. Landau, D. A. *et al.* Mutations driving CLL and their evolution in progression and relapse. *Nature* **526**, 525–30 (2015).
152. Nieminen, T. T. *et al.* Germline Mutation of RPS20, Encoding a Ribosomal Protein, Causes Predisposition to Hereditary Nonpolyposis Colorectal Carcinoma Without DNA Mismatch Repair Deficiency. *Gastroenterology* **147**, 595 (2014).
153. Sulima, S. O. . *et al.* Bypass of the pre-60S ribosomal quality control as a pathway to oncogenesis. *Proceedings of the National Academy of Sciences* **111**, 5640–5645 (2014).

154. Patchett, S., Musalgaonkar, S., Malyutin, A. G. & Johnson, A. W. The T-cell leukemia related rpl10-R98S mutant traps the 60S export adapter Nmd3 in the ribosomal P site in yeast. *PLoS Genetics* **13**, e1006894 (2017).
155. Hui-Yuen, J., McAllister, S., Koganti, S., Hill, E. & Bhaduri-Mcintosh, S. Establishment of Epstein-Barr Virus Growth-transformed Lymphoblastoid Cell Lines. *Journal of Visualized Experiments : JoVE* (2011) doi:10.3791/3321.
156. Paganin-Gioanni, A. *et al.* Direct visualization at the single-cell level of siRNA electrotransfer into cancer cells. *Proc Natl Acad Sci U S A* **108**, 10443–10447 (2011).
157. Pereboom, T. C., van Weele, L. J., Bondt, A. & MacInnes, A. W. A zebrafish model of dyskeratosis congenita reveals hematopoietic stem cell formation failure resulting from ribosomal protein-mediated p53 stabilization. *Blood* **118**, 5458–5465 (2011).
158. Loughran, G., Howard, M. T., Firth, A. E. & Atkins, J. F. Avoidance of reporter assay distortions from fused dual reporters. *RNA* **23**, 1285–1289 (2017).
159. Wilson, W. *et al.* HIV expression strategies: ribosomal frameshifting is directed by a short sequence in both mammalian and yeast systems. *Cell* **55**, 1159–1169 (1988).
160. Shigemoto, K. *et al.* Identification and characterisation of a developmentally regulated mammalian gene that utilises -1 programmed ribosomal frameshifting. *Nucleic Acids Res.* **29**, 4079–4088 (2001).
161. Manktelow, E., Shigemoto, K. & Brierley, I. Characterization of the frameshift signal of Edr, a mammalian example of programmed -1 ribosomal frameshifting. *Nucleic Acids Res.* **33**, 1553–1563 (2005).
162. Matsufuji, S. *et al.* Autoregulatory frameshifting in decoding mammalian ornithine decarboxylase antizyme. *Cell* **80**, 51–60 (1995).
163. Penzo, M., Carnicelli, D., Montanaro, L. & Brigotti, M. A reconstituted cell-free assay for the evaluation of the intrinsic activity of purified human ribosomes. *Nat Protoc* **11**, 1309–1325 (2016).
164. Penzo, M. *et al.* Human ribosomes from cells with reduced dyskerin levels are intrinsically altered in translation. *FASEB J* **29**, 3472–3482 (2015).
165. Salvetti, A. *et al.* Nuclear Functions of Nucleolin through Global Proteomics and Interactomic Approaches. *J Proteome Res* **15**, 1659–1669 (2016).
166. Perez-Riverol, Y. *et al.* The PRIDE database and related tools and resources in 2019: improving support for quantification data. *Nucleic Acids Research* **47**, D442 (2019).
167. Voorhees, R. M., Fernández, I. S., Scheres, S. H. W. & Hegde, R. S. Structure of the Mammalian Ribosome-Sec61 Complex to 3.4 Å Resolution. *Cell* **157**, 1632–1643 (2014).
168. Diets, I. J. *et al.* High Yield of Pathogenic Germline Mutations Causative or Likely Causative of the Cancer Phenotype in Selected Children with Cancer. *Clin Cancer Res* **24**, 1594–1603 (2018).
169. Ball, S. Diamond Blackfan anemia. *Hematology Am Soc Hematol Educ Program* **2011**, 487–491 (2011).
170. Gamalinda, M. *et al.* A hierarchical model for assembly of eukaryotic 60S ribosomal subunit domains. *Genes & Development* **28**, 198–210 (2014).
171. Amsterdam, A. *et al.* A large-scale insertional mutagenesis screen in zebrafish. *Genes & Development* **13**, 2713 (1999).
172. Antunes, A. T. *et al.* Ribosomal Protein Mutations Result in Constitutive p53 Protein Degradation through Impairment of the AKT Pathway. *PLoS Genetics* **11**, (2015).

173. Taylor, A. M. *et al.* Hematopoietic defects in rps29 mutant zebrafish depend upon p53 activation. *Experimental Hematology* **40**, 228-237.e5 (2012).
174. Amsterdam, A. *et al.* Many ribosomal protein genes are cancer genes in zebrafish. *PLoS Biol.* **2**, E139 (2004).
175. Lai, K. *et al.* Many Ribosomal Protein Mutations Are Associated With Growth Impairment and Tumor Predisposition in Zebrafish. *Dev Dyn* **238**, 76 (2009).
176. Boultwood, J., Pellagatti, A. & Wainscoat, J. S. Haploinsufficiency of ribosomal proteins and p53 activation in anemia: Diamond-Blackfan anemia and the 5q- syndrome. *Adv Biol Regul* **52**, 196–203 (2012).
177. Chong, J. & Xia, J. MetaboAnalystR: an R package for flexible and reproducible analysis of metabolomics data. *Bioinformatics* **34**, 4313 (2018).
178. Graham, T. E. & MacLean, D. A. Ammonia and amino acid metabolism in human skeletal muscle during exercise. *Can J Physiol Pharmacol* **70**, 132–141 (1992).
179. Rakauskaite, R. & Dinman, J. D. An arc of unpaired "hinge bases" facilitates information exchange among functional centers of the ribosome. *Molecular and Cellular Biology* **26**, (2006).
180. Itahana, Y. & Itahana, K. Emerging Roles of p53 Family Members in Glucose Metabolism. *International Journal of Molecular Sciences* **19**, (2018).
181. Jamar, N. H., Kritsiligkou, P. & Grant, C. M. The non-stop decay mRNA surveillance pathway is required for oxidative stress tolerance. *Nucleic Acids Research* **45**, 6881 (2017).
182. Gutteridge, J. M. C. & Professor Halliwell, B. Free radicals in disease processes: a compilation of cause and consequence. *Free Radic Res Commun* **19**, 141–158 (1993).
183. Nabais Sá, M. J. *et al. De Novo* variants in *EEF2* cause a neurodevelopmental disorder with benign external hydrocephalus. *Human Molecular Genetics* **29**, 3892–3899 (2021).
184. RAPP, G., KLAUDINY, J., HAGENDORFF, G., LUCK, M. R. & SCHEIT, K. H. Complete Sequence of the Coding Region of Human Elongation Factor 2 (EF-2) by Enzymatic Amplification of cDNA from Human Ovarian Granulosa Cells. *Biological Chemistry Hoppe-Seyler* **370**, 1071–1076 (1989).
185. Perentesis, J. P. *et al.* Saccharomyces cerevisiae elongation factor 2. *J.Biol.Chem.* **267**, 1190–1197 (1992).
186. Ling, C. & Ermolenko, D. N. Structural insights into ribosome translocation. *Wiley Interdiscip Rev RNA* **7**, 620–636 (2016).
187. Sobreira, N., Schiettecatte, F., Valle, D. & Hamosh, A. GeneMatcher: A Matching Tool for Connecting Investigators with an Interest in the Same Gene. *Human Mutation* **36**, 928–930 (2015).
188. Retterer, K. *et al.* Clinical application of whole-exome sequencing across clinical indications. *Genetics in Medicine* **18**, 696–704 (2016).
189. Neveling, K. *et al.* A Post-Hoc Comparison of the Utility of Sanger Sequencing and Exome Sequencing for the Diagnosis of Heterogeneous Diseases. *Human Mutation* **34**, 1721–1726 (2013).
190. Karczewski, K. J. *et al.* The mutational constraint spectrum quantified from variation in 141,456 humans. *Nature* **581**, 434–443 (2020).
191. Rentzsch, P., Witten, D., Cooper, G. M., Shendure, J. & Kircher, M. CADD: predicting the deleteriousness of variants throughout the human genome. *Nucleic Acids Research* **47**, D886–D894 (2019).

192. Sievers, F. *et al.* Fast, scalable generation of high-quality protein multiple sequence alignments using Clustal Omega. *Mol Syst Biol* **7**, (2011).
193. Kimata, Y. & Kohno, K. Elongation factor 2 mutants deficient in diphthamide formation show temperature-sensitive cell growth. *Journal of Biological Chemistry* **269**, 13497–13501 (1994).
194. Wilson, D. N. The A-Z of bacterial translation inhibitors. *Crit Rev.Biochem.Mol.Biol.* **44**, 393–433 (2009).
195. Schneider-Poetsch, T. *et al.* Inhibition of eukaryotic translation elongation by cycloheximide and lactimidomycin. *Nat.Chem.Biol.* **6**, 209–217 (2010).
196. Harger, J. W. & Dinman, J. D. An in vivo dual-luciferase assay system for studying translational recoding in the yeast Saccharomyces cerevisiae. *RNA* **9**, 1019–1024 (2003).
197. Dabrowski, M., Bukowy-Bieryllo, Z. & Zietkiewicz, E. Translational readthrough potential of natural termination codons in eucaryotes – The impact of RNA sequence. *RNA Biology* **12**, 950–958 (2015).
198. Jørgensen, R. *et al.* Two crystal structures demonstrate large conformational changes in the eukaryotic ribosomal translocase. *Nature Structural & Molecular Biology* **10**, 379–385 (2003).
199. Alazami, A. M. *et al.* Accelerating Novel Candidate Gene Discovery in Neurogenetic Disorders via Whole-Exome Sequencing of Prescreened Multiplex Consanguineous Families. *Cell Reports* **10**, 148–161 (2015).
200. Urreizti, R. *et al.* DPH1 syndrome: two novel variants and structural and functional analyses of seven missense variants identified in syndromic patients. *European Journal of Human Genetics* **28**, 64–75 (2020).
201. Hawer, H. *et al.* Diphthamide-deficiency syndrome: a novel human developmental disorder and ribosomopathy. *European Journal of Human Genetics* **28**, 1497–1508 (2020).
202. Mondal, S., Hsiao, K. & Goueli, S. A. A Homogenous Bioluminescent System for Measuring GTPase, GTPase Activating Protein, and Guanine Nucleotide Exchange Factor Activities. *Assay and Drug Development Technologies* **13**, 444–455 (2015).
203. Koripella, R. K. *et al.* Distinct mechanisms of the human mitoribosome recycling and antibiotic resistance. *Nature Communications* **12**, 3607 (2021).
204. Pellegrino, S. *et al.* Structural Insights into the Role of Diphthamide on Elongation Factor 2 in mRNA Reading-Frame Maintenance. *Journal of Molecular Biology* **430**, 2677–2687 (2018).
205. Belardinelli, R., Sharma, H., Peske, F. & Rodnina, M. v. Perturbation of ribosomal subunit dynamics by inhibitors of tRNA translocation. *RNA* **27**, 981–990 (2021).
206. Wintermeyer, W. Translocation on the Ribosome. in *Encyclopedia of Biophysics* 2650–2655 (Springer Berlin Heidelberg, 2013). doi:10.1007/978-3-642-16712-6_628.
207. Hansen, J. L., Moore, P. B. & Steitz, T. A. Structures of five antibiotics bound at the peptidyl transferase center of the large ribosomal subunit. *J.Mol.Biol.* **330**, 1061–1075 (2003).
208. Garreau de Loubresse, N. *et al.* Structural basis for the inhibition of the eukaryotic ribosome. *Nature* **513**, 517–522 (2014).
209. Dinman, J. D. & Wickner, R. B. Ribosomal frameshifting efficiency and Gag/Gag-pol ratio are critical for yeast M1 double-stranded RNA virus propagation. *J.Virology* **66**, 3669–3676 (1992).

210. Shi, X., Khade, P. K., Sanbonmatsu, K. Y. & Joseph, S. Functional Role of the Sarcin–Ricin Loop of the 23S rRNA in the Elongation Cycle of Protein Synthesis. *Journal of Molecular Biology* **419**, 125–138 (2012).
211. Spahn, C. M. *et al.* Domain movements of elongation factor eEF2 and the eukaryotic 80S ribosome facilitate tRNA translocation. *EMBO J.* **23**, 1008–1019 (2004).
212. Djumagulov, M. *et al.* Accuracy mechanism of eukaryotic ribosome translocation. *Nature* **600**, 543–546 (2021).
213. Jasiński, M., Kulik, M., Wojciechowska, M., Stolarski, R. & Trylska, J. Interactions of 2'-O-methyl oligoribonucleotides with the RNA models of the 30S subunit A-site. *PLOS ONE* **13**, e0191138 (2018).
214. Palis, J. Primitive and definitive erythropoiesis in mammals. *Frontiers in Physiology* **5**, (2014).
215. Phan, L. D., Perentesis, J. P. & Bodley, J. W. Saccharomyces cerevisiae elongation factor 2. Mutagenesis of the histidine precursor of diphthamide yields a functional protein that is resistant to diphtheria toxin. *Journal of Biological Chemistry* **268**, 8665–8668 (1993).